UNIVERSITY OF KWAZULU-NATAL

ENHANCED PERFORMANCE AND EFFICIENCY SCHEMES FOR GENERALISED SPATIAL MODULATION

Nigel Reece Naidoo

Supervised by:

Professor Hongjun Xu

2017

ENHANCED PERFORMANCE AND EFFICIENCY SCHEMES FOR GENERALISED SPATIAL MODULATION

Nigel Reece Naidoo

Supervised by:

Professor Hongjun Xu

Submitted in fulfilment of the academic requirements
for the degree of Doctor of Philosophy in Electronic Engineering
in the Faculty of Engineering
at the University of KwaZulu-Natal, Durban, South Africa

May 2017

As the candidate's supervisor I have approved the submission of this thesis.

Signed: _____

Name: Professor Hongjun Xu

Date: 19 May 2017

Plagiarism Declaration

I, Nigel Reece Naidoo, declare that

i. The research reported in this thesis, except where otherwise indicated, is my original work.
ii. This thesis has not been submitted for any degree or examination at any other university.
iii. This thesis does not contain other persons' data, pictures, graphs or other information, unless specifically acknowledged as being sourced from other persons.
iv. This thesis does not contain other persons' writing, unless specifically acknowledged as being sourced from other researchers. Where other written sources have been quoted, then:
    a. their words have been re-written but the general information attributed to them has been referenced;
    b. where their exact words have been used, their writing has been placed inside quotation marks, and referenced.
v. Where I have reproduced a publication of which I am an author, co-author or editor, I have indicated in detail which part of the publication was actually written by myself alone and have fully referenced such publications.
vi. This thesis does not contain text, graphics or tables copied and pasted from the Internet, unless specifically acknowledged, and the source being detailed in the thesis and in the References sections.

Signed: _____

Publication Declaration

Details of contributions to publications that form part and/or include research presented in this thesis are as follows:

Paper A – N. Naidoo, H. Xu and N. Pillay, "Generalised spatial modulation with constellation reassignment," [under second review *IET Communications Journal*], Aug. 2016.

Paper B – N. Naidoo and H. Xu, "A low complexity detection scheme for generalized spatial modulation with constellation reassignment," [prepared for submission to *IET Communications Journal*]

Paper C – N. Naidoo and H. Xu, "Generalised spatial modulation with dual constellation reassignment," [prepared for submission to *IET Communications Journal*]

Signed: _____

Abstract

Generalised spatial modulation (GSM) is a relatively new multiple-input multiple-output (MIMO) technique, which conveys information via a spatial constellation, comprising groupings of active transmit antenna, and a conventional M-ary quadrature amplitude modulation (MQAM) or M-ary phase shift keying (MPSK) signal constellation.

The first objective of this thesis is to propose a GSM scheme with improved bit error rate (BER) performance, termed generalised spatial modulation with constellation reassignment (GSM-CR). A framework for the design of GSM-CR systems is presented. An analytical bound for the average BER of GSM-CR over independent and identically distributed (i.i.d.) Rayleigh flat fading channels is also derived and the accuracy of this bound is verified by Monte Carlo simulation results. Moreover, Monte Carlo simulation results demonstrate that for 9 bits/s/Hz transmission, GSM-CR achieves gains of 5 dB and 4 dB, at a BER of 10^{-5}, when compared to GSM and spatial modulation (SM), respectively.

The maximum likelihood (ML) GSM-CR detector offers optimal BER performance at the expense of high computational complexity, particularly when high order digital modulation techniques are employed. The second objective of this thesis is to propose a new GSM-CR detector, termed zero-forcing maximum likelihood (ZF-ML). The proposed ZF-ML detector is characterised by low computational complexity, complexity that is independent of the order of digital modulation technique utilised and BER performance similar to that obtained by the ML detector. Performance and complexity comparisons between the ZF-ML GSM-CR detector and popular GSM and GSM-CR detection schemes reveal that for the $N_t \times 4$ 64QAM configuration, where N_t refers to the number of transmit antennas and 4 is the number of receive antennas: i) the ZF-ML GSM-CR detector reduces computational complexity at the receiver by up to 60% and exhibits similar BER performance when compared to the ML GSM-CR detection scheme; ii) ZF-ML configured with two candidate symbols per initial symbol estimate reduces the receiver complexity by up to 60% whilst ZF-ML configured with eight candidate symbols per initial symbol estimate achieves gains of up to 5 dB, at a BER of 10^{-5}, when compared to the ML GSM detector; iii) for systems that encode more than one information bit in the spatial domain, certain ZF-ML configurations operate at a higher computational complexity of up to 235% when compared to the SV GSM detector. However, the higher

computational complexity imposed by the ZF-ML GSM-CR detector is traded-off by significant gains of up to 5 dB, at a BER of 10^{-5}, when compared to the SV GSM detection scheme.

The GSM-CR scheme only permits two active transmit antennas during a particular timeslot. This limits the number of bits that can be encoded in the spatial domain and therefore the overall spectral efficiency attainable. The third objective of this thesis is to propose a generalised spatial modulation with dual constellation reassignment (GSM-DCR) technique, which is geared towards improving the overall spectral efficiency of GSM-CR. A framework for the design of GSM-DCR is presented. Moreover, an analytical bound for the average BER of GSM-DCR over i.i.d. Rayleigh flat fading channels is derived, and the accuracy of this bound is verified by Monte Carlo simulation results. A comparison between various GSM-DCR, GSM-CR and GSM schemes, which employ equivalent system configurations, reveals the following: i) for all configurations, GSM-DCR improves spectral efficiency by 1 bits/s/Hz as compared to both GSM-CR and GSM; ii) for the 6×4 64QAM configuration, GSM-DCR exhibits reduced performance of 2 dB, at a BER of 10^{-5}, as compared to GSM-CR. However, the degraded performance is traded-off by the enhanced spectral efficiency of 1 bit/s/Hz offered by the GSM-DCR scheme; iii) for the 6×4 64QAM configuration, GSM-DCR can achieve gains of 2.5 dB, at a BER of 10^{-5}, when compared to GSM.

To Crystal and Bailee

Acknowledgements

I would like to extend my deepest gratitude to God almighty through whom all things are possible.

To Prof. Xu, Dr. Pillay and Dr. Quazi, my sincere thanks for the countless hours spent guiding and supporting this research initiative. It has truly been a humbling experience working with a team of such high calibre.

To my family: Ronny; Melvin; Daisy; Letticia and Ma, I am forever grateful for the kind support and motivation. Your prayers have carried me through the most difficult of times.

A special thanks to my wife Crystal and daughter Bailee for always believing in me and supporting my endeavours with full faith and confidence. You both have served as a constant source of love, tranquillity and inspiration. This thesis is dedicated to you.

Table of Contents

List of Figures ..... **xii**

List of Tables ..... **xiii**

Notation ..... **xiv**

List of Acronyms ..... **xvi**

Part I **1**

1. Introduction **2**

1.1 GSM Research Developments **3**

1.1.1 Enhanced BER and Spectral Efficiency Schemes 3

1.1.2 Analytical Frameworks 4

1.1.3 Detection Schemes 5

1.1.4 Optical Systems 6

1.2 Motivation and Contributions **7**

1.2.1 Paper A: Generalised Spatial Modulation with Constellation Reassignment 7

1.2.2 Paper B: A Low Complexity Detection Scheme for Generalised Spatial Modulation with Constellation Reassignment 8

1.2.3 Paper C: Generalised Spatial Modulation with Dual Constellation Reassignment 9

1.3 Organisation of Thesis **10**

References **11**

Part II **18**

Paper A **19**

Abstract **20**

1. Introduction **21**

1.1 Notation **23**

2. System Model **23**

2.1 Transmission **24**

2.2 Maximum Likelihood Detector **26**

3. System Design **27**

3.1 Spatial Constellation Optimisation **27**

3.2 MQAM Signal Constellation Optimisation 28
3.3 Rotation Angle Optimisation 30
4. BER Performance Analysis 31
4.1 Analytical BER of Symbol Pair Estimation 32
4.2 Analytical BER of Transmit Antenna Pair Index Estimation 34
5. Simulation Results 35
5.1 Analytic and Simulated Average BER Comparison 35
5.2 Performance Comparison 36
6. Conclusion 38
Appendix A-1 39
Appendix A-2 41
Appendix A-3 42
Appendix A-4 43
Appendix A-5 45
Appendix A-6 48
References 49
Paper B 52
Abstract 53
1. Introduction 54
1.1 Notation 57
2. System Models 58
2.1 Generalised Spatial Modulation with Constellation Reassignment 58
2.2 Generalised Spatial Modulation 59
3. Current Detection Schemes 60
3.1 Maximum Likelihood GSM and GSM-CR Detector 60
3.2 Signal Vector GSM Detector 60
4. Proposed Zero-Forcing Maximum Likelihood Detector 62

4.1 Stage One: Zero-Forcing 62
4.2 Stage Two: Maximum Likelihood Detection 65
5. Computational Complexity Analysis 66
5.1 Maximum Likelihood GSM-CR Detector 66
5.2 Maximum Likelihood GSM Detector 67
5.3 Signal Vector GSM Detector 67
5.4 Zero-Forcing Maximum Likelihood GSM-CR Detector 68
6. Performance and Computational Complexity Comparison 70
6.1 Computational Complexity 70
6.2 Performance Comparison 72
7. Conclusion 75
References 76
Paper C 78
Abstract 79
1. Introduction 80
1.1 Notation 82
2. System Model 82
2.1 Transmission 83
2.2 Maximum Likelihood Detector 85
3. System Design 85
3.1 Spatial Constellation Optimisation 86
3.2 MQAM Signal Constellation Optimisation 87
3.3 Rotation Angle Optimisation 90
4. BER Performance Analysis 90
4.1 Analytical BER of Symbol Pair Estimation 91
4.2 Analytical BER of Transmit Antenna Pair Index Estimation 91
5. Simulation Results 92

5.1 Analytic and Simulated Average BER Comparison 93
5.2 Performance Comparison 94
6. Conclusion 96
Appendix C-1 98
Appendix C-2 100
Appendix C-3 103
References 104
Part III 106
1. Conclusion and Future Work 107
1.1 Conclusion 107
1.2 Future Work 108

List of Figures

Figure A.1 GSM-CR System Model 25

Figure A.2 16QAM GSM Signal Constellation 29

Figure A.3 16QAM GSM-CR Signal Constellations 30

Figure A.4 Analytic and Simulated Average BER 36

Figure A.5 Average BER - 6 bits/s/Hz and 8 bits/s/Hz Configurations 37

Figure A.6 Average BER - 7 bits/s/Hz and 9 bits/s/Hz Configurations 38

Figure B.1 Generating Candidate Symbols Based on the Initial Symbol Estimate 64

Figure B.2 Computational Complexity of Various Detection Schemes 70

Figure B.3 Average BER - 4x4 64QAM GSM and GSM-CR Configurations 73

Figure B.4. Average BER - 6x4 64QAM GSM and GSM-CR Configurations 73

Figure C.1 GSM-DCR System Model 83

Figure C.2a 16QAM Primary Signal Constellation 89

Figure C.2b 16QAM Secondary and Dual Signal Constellations 89

Figure C.3 Analytic and Simulated Average BER – 4x4 GSM-DCR 93

Figure C.4 Analytic and Simulated Average BER – 6x4 GSM-DCR 94

Figure C.5 Average BER – 4x4 Configuration 95

Figure C.6 Average BER – 6x4 Configuration 96

List of Tables

Table B.1: Computational Complexity of Various Detection Schemes……..72

Notation

x	Scalar quantity x
$\|x\|$	Absolute value of x
x^*	Complex conjugate of x
$\boldsymbol{x}$	Vector $\boldsymbol{x}$
$\boldsymbol{x}^T$	Transpose of $\boldsymbol{x}$
$\|\boldsymbol{x}\|_F$	Frobenius norm of $\boldsymbol{x}$
$\boldsymbol{x}^H$	Hermitian (conjugate transpose) of $\boldsymbol{x}$
$*$	Convolution operator
$\approx$	Approximately equal to
$arccos(x)$	Arccosine of x
$\binom{n}{r}$	n choose r
$\lfloor \cdot \rfloor$	Floor operation
$E[A]$	Statistical expectation of A
$Re\{\cdot\}$	Real part of a complex variable
$\underset{x}{argmin} \ f(x)$	Value of x that minimizes the function $f(x)$
$\underset{x}{argmax} \ f(x)$	Value of x that maximizes the function $f(x)$
$\mathcal{N}(\mu, \sigma^2)$	Gaussian distribution with mean μ and variance σ^2

$\mathcal{CN}(\mu,\sigma^2)$	Complex Gaussian distribution with mean μ and variance σ^2. Note the real and imaginary components of the random variable are independent and are distributed according to $\mathcal{N}\left(\mu,\frac{\sigma^2}{2}\right)$

List of Acronyms

3GPP	Third generation partnership project
AJM-GSM	Adaptive joint mapping generalised spatial modulation
AWGN	Additive white Gaussian noise
BER	Bit error rate
CR	Constellation reassignment
CSI	Channel state information
dB	Decibels
EBCS	Enhanced Bayesian compressive sensing
DGSM	Distributed generalised spatial modulation
GOSM	Generalised optical spatial modulation
GRV	Gaussian random variable
GSM	Generalised spatial modulation
GSM-CR	Generalised spatial modulation with constellation reassignment
GSM-DCR	Generalised spatial modulation with dual constellation reassignment
HR-GSM	High-rate generalised spatial modulation
IAS	Inter-antenna synchronization
ICI	Inter-channel interference
IEEE	Institute of electrical and electronic engineers
i.i.d.	Independent and identically distributed
I-ZF	Iterative zero-forcing

LAN	Local area network
LOS	Line-of-sight
MGF	Moment generating function
MIMO	Multiple-input multiple-output
ML	Maximum likelihood
MPSK	M-ary phase shift keying
MQAM	M-ary quadrature amplitude modulation
MRRC	Maximum receive ratio combining
OB-MMSE	Ordered block minimum mean square error
PDF	Probability density function
PEP	Pairwise error probability
RF	Radio frequency
SER	Symbol error rate
SIMO	Single-input multiple-output
SM	Spatial modulation
SNR	Signal-to-noise ratio
STBC	Space-time block code
SV	Signal vector
V-BLAST	Vertical-bell layered space-time
VLC	Visible light communication
VGSM	Variable generalised spatial modulation

WiFi	Wireless fidelity
ZF	Zero-forcing
ZF-ML	Zero-forcing maximum likelihood

Part I

Introduction

1. Introduction

Multiple-input multiple-output (MIMO) techniques are an effective means to fulfil the high quality of service and enhanced data rate requirements of next generation wireless communication systems [1]-[5]. MIMO techniques may be categorised into the two broad classes of multiplexing and diversity schemes. Multiplexing schemes such as the vertical-bell layered space-time (V-BLAST) system [6], achieve high date rates by allowing the simultaneous transmission of multiple independent data streams. Furthermore, diversity schemes such as Alamouti [7], improve link reliability by transmitting multiple redundant copies of data to a receiver over independent channels.

Despite their benefits, MIMO techniques have the common pitfalls of inter-channel interference (ICI) and inter-antenna synchronisation (IAS) [8]-[11]. Spatial modulation (SM) is a relatively new MIMO technique proposed in [12]-[14], which employs a single active transmit antenna within a particular timeslot. SM is therefore not prone to the ICI and IAS issues that plague MIMO schemes.

SM has ushered in a novel approach to MIMO transmission, where both the location of the active transmit antenna (spatial domain) and a conventional M-ary quadrature amplitude modulation (MQAM) or M-ary phase shift keying (MPSK) symbol (signal domain) are used to convey information. The use of the active transmit antenna location as an information bearing unit is a key feature of SM, which increases the overall spectral efficiency by the base-two logarithm of the number of transmit antennas [12]. A comprehensive analysis of the state of the art of SM for generalised MIMO technologies is presented in [15], with particular emphasis on the benefits of SM, research challenges encountered and real world implementation of SM MIMO systems. Moreover, an SM MIMO design framework is presented in [16], where issues such as, *inter alia*, transceiver design, signal constellation optimisation, link adaptation techniques and distributed/cooperative protocol design are addressed.

The single active transmit antenna architecture of SM poses a limitation to the number of information bits that can be encoded in the spatial domain and ultimately the achievable spectral efficiency. Generalised spatial modulation (GSM) [17] is an extension of SM, which permits the transmission of the same data symbol from

multiple active transmit antennas. GSM differs from SM in that the spatial domain now comprises combinations of transmit antennas that may be activated in a particular timeslot. GSM therefore overcomes the spectral efficiency constraint of SM by increasing the overall spectral efficiency by the base–two logarithm of the number of antenna combinations [17]. However, for identical system configurations, the bit error rate (BER) performance of GSM is limited and degraded compared to SM [17];

1.1 GSM Research Developments

Numerous research initiatives have been undertaken since the inception of the GSM scheme in 2010. In general, research into GSM has been conducted under four broad thematic areas, namely: enhanced BER performance and spectral efficiency, analytical frameworks, detection schemes and optical systems. A survey of relevant literature covering aforementioned thematic areas is presented next.

1.1.1 Enhanced BER and Spectral Efficiency Schemes

Several approaches spanning, *inter alia*, coding and optimised spatial and signal constellation architectures have been employed to enhance the BER performance or/and the spectral efficiency of GSM schemes.

Notable research developments in respect of GSM techniques employing coding include, *inter alia*: i) space-time block code GSM (STBC-GSM) in [18], which exploits the advantages of space-time block coding in order to deliver improved BER performance as compared to conventional GSM; ii) trellis coding is employed in conjunction with GSM in [19], with a view of combating the degraded BER performance encountered when operating under correlated fading channel conditions; iii) a high-rate generalized spatial modulation (HR-GSM) scheme that is tailored for use with MPSK signal constellations is proposed in [20]. The HR-GSM scheme achieves high data rates by encoding information in two modulated symbols and the indices of two active transmit antennas [20]; iv) Coded GSM for structured large-scale MIMO systems is explored in [21], which employs a GSM architecture with turbo coding and erasure declarations in order to provide improved error correction and detection capabilities.

Notable research developments in respect of GSM techniques employing optimised signal and spatial constellation architectures include, *inter alia*: i) an adaptive joint mapping GSM scheme in [22], which employs a dynamic signal and spatial domain mapping based on the present channel state information in order to deliver improved BER performance; ii) [23], where the optimal combination of the total number of transmit antenna elements and number of transmit radio frequency (RF) chains are formulated with a view of attaining improved throughput and BER performance; iii) an optimised signal-spatial constellation for GSM is proposed in [24]. The proposed signal-spatial constellation offers improved symbol error rate (SER) performance and energy efficiency when compared to conventional GSM. Moreover, the proposed signal-spatial constellation differs from conventional GSM in that the construction of the signal constellation part is formulated as an optimisation problem, which is subsequently solved using the gradient search algorithm [24]; iv) GSM transmit antenna schemes based on block grouping and interleaved grouping are proposed in [25] as a means to combat the degraded BER performance encountered in correlated fading channel conditions; v) GSM is used as the basis for a novel distributed MIMO system called distributed generalised spatial modulation (DGSM) in [26]. The proposed DGSM scheme increases the transmission rate by conveying additional information in the unused antenna combinations [26]. Simulation results presented in [26] show that DGSM outperforms conventional distributed MIMO systems, in terms of average BER.

1.1.2 Analytical Frameworks

Extensive research has been conducted towards the development of theoretical expressions for the BER performance and information capacity of GSM systems. Notable research developments in this regard include, *inter alia*: i) the derivation and validation of analytical bounds for the average BER and codeword error probability of GSM over independently and identically distributed (i.i.d.) Rayleigh flat fading channels in [27]; ii) an analytical bound for the average BER of multiuser GSM in the uplink channel is formulated and confirmed in [28]; iii) [29], where upper and lower bounds for the capacity of GSM MIMO systems are derived and the accuracy of these bounds are verified; iv) an analytical framework for deriving the average BER of GSM over correlated fading channels is presented and validated in [30]; v) the analytical

average BER of GSM in the presence of channel estimation errors and correlated Rayleigh and Rician fading channels is derived and verified in [31]; vi) GSM is analysed from an information theory perspective in [32], where a closed form expression for the capacity of GSM is derived. Moreover, tight upper bounds for the average BER of GSM over generalised fading channels such as Rayleigh, Rician and Nakagami-m are derived in [32]; vii) upper and lower bounds for the achievable rate of SM-based schemes, including GSM, are proposed and confirmed in [33]; viii) in [34], analytical expressions for the error probability and mutual information of GSM employing various transmitter pre-coder schemes are derived and verified.

1.1.3 Detection Schemes

A myriad of GSM detection schemes that are geared towards attaining a suitable trade-off between computational complexity and BER performance are proposed in [35]-[56]. Specific notable developments in this regard include, *inter alia*: i) the signal vector (SV) based detector in [35] that operates over two stages. In the first stage the most likely transmit antenna pair indices are determined based on the minimum Hermitian angle between the received signal vector and the combined channel vector. Thereafter in the second stage, the modulated symbol is estimated by computing the difference between the normalised projection of the received symbol in the direction of combined channel and the actual transmitted symbols [35]. The SV GSM detector was shown to operate with much lower complexity as compared to the ML GSM detector and exhibited near-ML BER performance in both the high and low signal-to-noise ratio (SNR) regions; ii) enhanced Bayesian compressive sensing (EBCS) in [36] that formulates GSM detection as a sparse recovery problem with a fixed sparsity constraint. Despite its low complexity detection properties, EBCS performs sub-optimally in the low SNR region; iii) ordered block minimum-mean-squared-error (OB-MMSE) in [37], which uses an ordering algorithm to sort possible transmit antenna combinations and then applies the minimum-mean-square-error equaliser for the recovery of the signal vector. OB-MMSE results in much lower complexity than the ML GSM detector but performs sub-optimally in the low SNR region; iv) a maximum receive ratio combining (MRRC) scheme proposed in [38] for the detection of the active transmit antenna combination and modulated symbol; v) an iterative zero forcing (I-ZF) detection scheme for GSM was proposed in [39]. The I-ZF detector

significantly reduced complexity in comparison to the ML detector but at the expense of poor BER performance [39].

1.1.4 Optical Systems

An emerging trend is the use of GSM in the optical domain, where information is conveyed through optical radiations. This may be considered a potential alternative to conventional GSM that uses the radio frequency spectrum medium. Notable research developments in optical GSM systems include, *inter alia*: i) GSM in the context of indoor wireless visible light communication (VLC) systems is studied in [57] and a tight analytical bound for the average BER is also derived. Simulation results confirm the validity of the proposed analytical framework and further demonstrate that within the VLC setting, GSM outperforms other MIMO schemes including spatial multiplexing, space-shift keying, generalized space-shift keying and SM [57]; ii) A GSM scheme for indoor optical wireless communication, termed generalised optical spatial modulation (GOSM), is presented in [58]. The use of multiple active transmit antennas affords GOSM greater flexibility in system design and improved spectral efficiencies, as compared to SM-based optical wireless communication techniques [58]. Furthermore, simulation results presented in [58] show that GOSM exhibits enhanced BER performance compared to SM-based optical wireless communications, particularly under correlated channel conditions; iii) a symbol search tree algorithm is proposed for the optimal symbol set selection in GSM MIMO VLC systems in [59]. Analysis, simulation and experiments conducted in [59] all demonstrate the low complexity and near-optimal BER performance benefits of the proposed optimal symbol set selection; iv) a variable generalised spatial modulation (VGSM) scheme for indoor line-of-sight (LOS) millimetre wave communication is proposed and analysed in [60]. The proposed VGSM scheme varies the number of active antennas in order to make more efficient use of the available transmit antennas and to achieve higher data rates [60]. Simulations conducted in [60] demonstrate the favourable capacity and BER performance characteristics of VGSM in relation to conventional indoor LOS GSM schemes; v) a novel GOSM encoding structure is formulated based on an active space collaborative constellation design technique in [61]. Simulations show that the proposed scheme improves the power efficiency when compared to conventional GOSM [61].

1.2 Motivation and Contributions

1.2.1 Paper A: Generalised Spatial Modulation with Constellation Reassignment

GSM overcomes the spectral efficiency limitation of SM schemes by permitting the use of multiple active transmit antennas [17]. However, for identical configurations, the BER performance of GSM is limited and degraded as compared to SM [17]. Moreover, the GSM scheme may be utilised in conjunction with any digital modulation technique. MQAM is a popular digital modulation technique that has been widely adopted in cable television, wireless fidelity (Wi-Fi) local-area networks (LANs), and mobile telephony systems. The popularity of MQAM coupled with the requirement to improve the BER performance of GSM, motivates for the development of a BER performance enhanced GSM technique that utilises MQAM signal constellations.

In Paper A, a novel BER performance enhanced GSM technique with MQAM signalling, termed generalised spatial modulation with constellation reassignment (GSM-CR) is proposed. This technique employs constellation reassignment (CR) [62, 63] in conjunction with GSM in order to maximise the minimum Euclidean distance between transmitted symbol pairs, thereby improving BER performance.

CR has traditionally been used to improve the error performance of systems that employ multiple transmissions of the same information bits [62, 63]. The CR technique maps the same information bits into different signal constellations for multiple transmissions, and has been employed in wireless relay networks in [62] and multiple packet transmission systems in [63]. In general, CR is utilised over multiple transmit timeslots. To the best of the author's knowledge, CR has not been discussed within the context of a single transmit timeslot system, such as GSM-CR.

The principal contributions in Paper A are as follows:

i. A novel GSM-CR technique is proposed and a detailed description of the transmission and detection aspects of the system model is presented.
ii. A design process for GSM-CR systems is presented, which covers spatial constellation design, signal constellation design and rotation angle optimisation.

iii. An analytical expression to quantify the average BER of GSM-CR over i.i.d. Rayleigh flat fading channels is derived.
iv. Monte Carlo simulations are conducted in order to verify the analytical frameworks and to demonstrate the enhanced BER performance of GSM-CR in comparison with GSM and SM schemes.

1.2.2 Paper B: A Low Complexity Detection Scheme for Generalised Spatial Modulation with Constellation Reassignment

Although the GSM-CR maximum likelihood (ML) detector is capable of achieving optimal BER performance, its exhaustive search leads to intractable computational complexity at the receiver, particularly when, *inter alia*, high order digital modulation techniques are employed. This motivates for the development of a low complexity detection scheme for GSM-CR that attains BER performance similar to that of the ML detector, and has computational complexity that is independent of the order of digital modulation technique employed.

In Paper B, a zero-forcing maximum likelihood (ZF-ML) detector for GSM-CR is proposed. The proposed ZF-ML detector is designed such that it functions with low complexity, which is independent of the order of digital modulation technique employed, and near-ML BER performance capability. ZF-ML combines the operation of both zero-forcing (ZF) and ML, with a view of inheriting the desirable properties of its constituent detectors, namely the low complexity of ZF [64] and the optimal BER performance of ML [64]. With regard to the selection of constituent detectors in the proposed scheme, ZF was specifically chosen since it is the simplest MIMO detector [64] and ML due to its ability to provide optimal BER performance.

The principal contributions in Paper B are as follows:

i. A novel ZF-ML GSM-CR detector is proposed.
ii. Computational complexity analyses of ZF-ML and various existing GSM-CR and GSM detection schemes are undertaken in order demonstrate the low complexity operation of the proposed detection scheme.

iii. Monte Carlo simulations are conducted in order to exhibit the average BER performance of ZF-ML in relation to existing GSM and GSM-CR detection schemes.

1.2.3 Paper C: Generalised Spatial Modulation with Dual Constellation Reassignment

GSM-CR only permits two active transmit antennas during a particular timeslot. This limits the number of bits that can be encoded in the spatial domain and therefore the overall spectral efficiency attainable. This motivates for the development of a GSM-CR-based scheme with enhanced spectral efficiency.

Paper C proposes a generalised spatial modulation with dual constellation reassignment (GSM-DCR) technique, which is geared towards improving the overall spectral efficiency of GSM-CR. The GSM-DCR technique can be viewed as an extension to conventional GSM-CR. Similar to the GSM-CR scheme, GSM-DCR uses the CR technique [62, 63] to maximise the minimum Euclidean distance between transmitted symbol pairs. However, a key difference between GSM-CR and GSM-DCR is that the latter embeds an additional information bit in the signal domain, thereby improving spectral efficiency by 1 bit/s/Hz, as compared to GSM-CR. In GSM-DCR systems, the additional information bit is used to select between one of two possible signal constellation pairs, which are subsequently used as the basis for generating the transmitted symbol pair.

To the best of the author's knowledge, utilising an active signal constellation pair as an information bearing unit is a novel concept, which has yet to be explored within the context of either GSM or CR systems.

The principal contributions in Paper C are as follows:

i. A novel GSM-DCR technique is proposed and a detailed description of the transmission and detection aspects of the system model is presented.
ii. A design process for GSM-DCR systems is presented, which covers spatial constellation design, signal constellation design and rotation angle optimisation.

iii. An analytical expression to quantify the average BER of GSM-DCR over i.i.d. Rayleigh flat fading channels is derived.

iv. Monte Carlo simulations are conducted in order to verify the analytical frameworks and to demonstrate the enhanced spectral efficiency and BER performance properties of GSM-DCR.

1.3 Organisation of Thesis

Part II presents the following three potential journal papers that are either currently under review or pending submission to the Institution of Engineering and Technology Journal of Communications:

i. Paper A: Generalised Spatial Modulation with Constellation Reassignment.

ii. Paper B: A Low Complexity Detection Scheme for Generalised Spatial Modulation with Constellation Reassignment.

iii. Paper C: Generalised Spatial Constellation with Dual Constellation Reassignment.

Part III concludes the thesis and recommends future potential research initiatives.

References

[1] E. Telatar, "Capacity of multi-antenna Gaussian channels," *Eur. Trans. Telecommun.*, vol. 10, no. 6, pp. 558–595, Nov. 1999.

[2] J. Mietzner, R. Schober, L. Lampe, *et al.*, "Multiple-antenna techniques for wireless communications - A comprehensive literature survey," *IEEE Commun. Surveys Tuts.*, vol. 11, no. 2, pp. 87–105, Jun. 2009.

[3] G. J. Foschini and M. J. Gans, "On limits of wireless communications in a fading environment when using multiple antennas," *Wireless Pers. Commun.*, vol. 6, no. 3, pp. 311–335, Mar. 1998.

[4] Q. Li, G. Li, W. Lee, *et al.*, "MIMO techniques in WiMAX and LTE: A feature overview," *IEEE Commun. Mag.*, vol. 48, no. 5, pp. 86–92, May 2010.

[5] F. Boccardi, B. Clerckx, A. Ghosh, *et al.*, "Multiple-antenna techniques in LTE-advanced," *IEEE Commun. Mag.*, vol. 50, no. 3, pp. 114–121, Mar. 2012.

[6] P. Wolniansky, G. Foschini, G. Golden, *et al.*, "V-BLAST: An architecture for realizing very high data rates over the richscattering wireless channel," *Proc. URSI Int. Symp. on Signals, Syst. and Electron.*, pp. 295–300, Oct. 1998.

[7] S. M. Alamouti, "A simple transmit diversity technique for wireless communications," *IEEE J. Sel. Areas Commun.*, vol.16, no. 8, pp. 1451–1458, Oct. 1998.

[8] A. Goldsmith, S. Jafar, N. Jindal, *et al.*, "Capacity limits of MIMO channels," *IEEE J. Sel. Areas Commun.*, vol. 21, no. 5, pp. 684 - 702, Jun. 2003.

[9] M. Damen, A. Abdi, and M. Kaveh, "On the effect of correlated fading on several space-time coding and detection schemes," *Proc. IEEE Veh. Technol. Conf.*, pp. 13–16. Oct. 2001.

[10] M. Chiani, M. Win, and A. Zanella, "On the capacity of spatially correlated MIMO Rayleigh-fading channels," *IEEE Trans. Inf. Theory*, vol. 49, no. 10, pp. 2363–2371, Oct. 2003.

[11] T. Svantesson and A. Ranheim, "Mutual coupling effects on the capacity of multielement antenna systems," *Proc. IEEE Int. Conf. on Acoust. Speech and Signal Process.*, vol. 4, pp. 2485–2488, May 2001.

[12] R. Mesleh, H. Haas, S. Sinanovic, *et al.*, "Spatial modulation," *IEEE Trans. Veh. Technol.*, vol. 57, no. 4, pp. 2228-2241, Jul. 2008.

[13] J. Jeganathan, A. Ghrayeb and L. Szczecinski, "Spatial modulation: Optimal detection and performance analysis," *IEEE Commun. Lett.*, vol. 12, no. 8, pp. 545-547, Aug. 2008.

[14] M. D. Renzo, H. Haas and P. M. Grant, "Spatial modulation for multiple antenna wireless systems: a survey," *IEEE Commun. Mag.*, vol. 49, no. 12, pp. 182-191, Dec. 2011.

[15] M. D Renzo, H. Haas, A. Ghrayeb, *et al.*, "Spatial modulation for generalized MIMO: Challenges opportunities and implementation," *Proc. IEEE*, vol. 102, no.1, pp. 56-103, Jan. 2014.

[16] P. Yang, M. D. Renzo, Y. Xiao, *et al.*, "Design guidelines for spatial modulation," *IEEE Commun. Surveys Tuts.*, vol. 17, no. 1, pp. 6-26, May 2014.

[17] A. Younis, N. Serafimovski, R. Mesleh, *et al.*, "Generalised spatial modulation," *Proc. Signals, Syst. Comput.*, pp. 1498–1502, Nov. 2010.

[18] K. Sundaravadivu and S. Bharathi, "STBC codes for generalized spatial modulation in MIMO systems," *Proc. Int. Conf. on Emerging Trends in Computing, Commun. and Nanotechnology*, pp. 486-490, Mar. 2013.

[19] Y. Zou, D. Yuan, X. Zhou, *et al.*, "Trellis coded generalised spatial modulation," *Proc. IEEE Veh. Technol. Conf.*, pp. 1-5, May 2014.

[20] Z. Yiğit and E. Basar, "High rate generalised spatial modulation," *Proc. IEEE. Conf. Signal Process. and Applicat.*, pp. 117-120, May 2016.

[21] D. Franz and V. Kuehn, "Coded generalized spatial modulation for structured large scale MIMO systems," *Proc. Int. Symp. On Wireless Commun. Syst.*, pp. 32-36, Sep. 2016.

[22] N. Ma, A. Wang, C. Han, *et al.*, "Adaptive joint mapping generalized spatial modulation," *Proc. IEEE Int. Conf. Commun.*, pp. 520-523, Aug. 2012.

[23] T. Datta and A. Chockalingam, "On generalized spatial modulation," *Proc. IEEE Wireless Commun. Netw. Conf.*, pp. 2716-2721, Apr. 2013.

[24] W. Wang and R. Y. Chang, "Signal-spatial constellation optimization for generalized spatial modulation," *Proc. IEEE Veh. Technol. Conf.*, pp. 1-5, May 2014.

[25] P. Ju, M. Zhang, X. Cheng, *et al.*, "Generalized spatial modulation with transmit antenna grouping for correlated channels," *Proc. IEEE Int. Conf. on Commun.*, pp. 1-6, May 2016.

[26] X. Jiang, M. Wen and J. Li, "Distributed generalized spatial modulation based on Chinese remainder theorem," *IEEE Commun. Lett.*, vol. PP, no. 99, pp. 1-4, Mar. 2017.

[27] T. L. Narasimhan, P. Raviteja and A. Chockalingam, "Generalized spatial modulation for large-scale MIMO systems: Analysis and detection," *Proc. Asilomar Conference on Signals Systems and Comput.*, pp. 1071-1075, Nov. 2014.

[28] T. L. Narasimhan, P. Raviteja and A. Chockalingam, "Generalized spatial modulation in large-scale multiuser MIMO systems," *IEEE Trans. Wireless Commun.*, vol. 24, no. 7, pp. 3764-3779, Jul. 2015.

[29] T. L. Narasimhan and A. Chockalingam, "On the capacity and performance of generalized spatial modulation," *IEEE Commun. Lett.*, vol. 20, no. 2, pp. 252-255, Feb. 2016.

[30] M. Koca and H. Sari, "Generalized spatial modulation over correlated fading channels: Performance analysis and optimization," *Proc. Int. Conf on Telecommun.*, pp. 1-5, May 2013.

[31] A. Younis, R. Mesleh, M. D. Renzo, *et al.*, "Generalised spatial modulation for large-scale MIMO," *Proc. European Signal Process. Conf.*, pp. 346-350, Sep. 2014.

[32] A. Younis, D. A. Basnayaka, and H. Haas, "Performance analysis for generalised spatial modulation," *Proc. European Wireless Conf.* pp. 1-6, May 2014.

[33] A. I. Ibrahim, T. Kim and D. J. Love, "On the achievable rate of generalized spatial modulation using multiplexing under a Gaussian mixture model," *IEEE Trans. on Commun.*, vol. 64, no. 4, pp. 1588-1599, Jan. 2016.

[34] Z. An, J. Wang, J. Wang, *et al.*, "Mutual information and error probability analysis on generalized spatial modulation system," *IEEE Trans. on Commun.*, vol. 65, no. 3, pp. 1044 – 1060, Dec. 2016.

[35] Y. Jiang, Y. Xu, Y. Xie, *et al.*, "Low complexity detection scheme for generalised spatial modulation," *J. of Commun.*, vol. 11, no. 8, pp. 726-732, Aug. 2016.

[36] C. Wang, P. Cheng, Z. Chen, *et al.* "Near-ML low-complexity detection for generalized spatial modulation" *IEEE Commun. Lett.*, vol. 20, no. 3, pp. 618–621, Jan. 2016.

[37] Y. Xiao, Z. Yang, L. Dan, *et al.*, "Low complexity signal detection for generalized spatial modulation," *IEEE Commun. Lett.*, vol. 18, no. 3, pp. 403–406, Apr. 2014.

[38] J. Fu, C. Hou, W. Xiang, *et al.*, "Generalised spatial modulation with multiple active transmit antennas," *Proc. IEEE Global Commun. Conf.*, pp. 839-844, Dec. 2010.

[39] Y. Sun, J. Wang and L. He, "Iterative zero forcing detection scheme for generalised spatial modulation," *Broadband Multimedia Systems and Broadcasting 2015 IEEE Int. Symp.*, pp. 1-4, Jun. 2016.

[40] J. A. Cal-Braz, C. A. Medina and R. Sampaio-Neto, "Group maximum likelihood detection in generalized spatial modulation," *Proc. Int. Symp. on Wireless Commun. Syst.* pp. 293-296, Aug. 2013.

[41] Y. Wang, J. Ge and J. Chen, "Low-complexity sphere decoding for generalised spatial modulation," *Proc. Int. Conf. on Wireless Commun. and Signal Process.*, pp. 1-5, Oct. 2014.

[42] J. A. Cal-Braz and R. Sampaio-Neto, "Low-complexity sphere decoding detector for generalized spatial modulation systems," *IEEE Commun. Lett.*, vol. 18, pp. 949-953, Jun. 2014.

[43] J. A Cal-Braz and R. Sampaio-Neto, "Nested maximum likelihood group detection in generalized spatial modulation MIMO systems," *IEEE Commun. Lett.*, vol. 18, no. 6, pp. 953-956, May 2014.

[44] J. A. Cal-Braz and R. Sampaio-Neto, "Projection-based list detection in generalized spatial modulation MIMO systems," *IEEE Commun. Lett.*, vol. 18, no. 6, pp. 953-956, Jun. 2014.

[45] S. Yang, L. Ma and Y. Xu, "Low-complexity geometric decoding based detector in generalized spatial modulation," *Proc. Int. Conf. Electron. Inform. and Emergency Commun*, pp. 71-75, May 2015.

[46] L. He, J. Wang, W. Ding, *et al.*, "Sparse Bayesian learning based symbol detection for generalised spatial modulation in large-scale MIMO systems," *Proc. IEEE Global Commun. Conf.*, pp. 1-6, Dec. 2015.

[47] C. Lin, W. Wu and C. Liu, "Low-complexity ML detectors for generalized spatial modulation systems," *IEEE Trans. Commun.*, vol. 63, no. 11, pp. 4214-4230, Nov. 2015.

[48] C. Chen, C. Li, and Y. Huang, "An improved ordered-block MMSE detector for generalized spatial modulation," *IEEE Commun. Lett.*, vol. 19, no. 5, pp. 707-710, May 2015.

[49] L. Xiao, L. Dan, Y. Zhang, *et al.*, "A low-complexity detection scheme for generalized spatial modulation aided single carrier systems," *IEEE Commun. Lett.*, vol. 19, no. 6, pp. 1069-1072, Jun. 2015.

[50] L. Xiaoa, P. Yanga, Y. Zhaoa, *et al.* "Low-complexity tree search-based detection algorithms for generalized spatial modulation aided single carrier systems," *Proc. IEEE Int. Conf. on Commun.*, pp. 1-6, May 2016.

[51] Y. Bao, L. Zhang, R. Xie, *et al.*, "Low-complexity lattice reduction aided detection for generalised spatial modulation," *Proc. Int. Symp. on Wireless Commun. Syst.*, pp. 253-257, Sep. 2016.

[52] Y. Sun, J. Wang and L. He, "Scalable-complexity detection for generalised spatial modulation: A polynomial expansion iterative zero forcing technique," *Proc. IEEE Int. Symp. on Broadband Multimedia Syst. and Broadcast.*, pp. 1-4, Jun. 2016.

[53] C. Li, J. Wang, W. Liu, *et al.*, "Low-complexity detection for GSM-MIMO systems via spatial constraint," *Proc. IEEE Veh. Technol. Conf.*, pp. 1-5, May 2016.

[54] L. Xiao, P. Yang, Y. Xiao, *et al.*, "An improved soft-input soft-output detector for generalized spatial modulation," *IEEE Signal Process. Lett.*, vol. 23, no. 1, pp. 30-34, Jan. 2016.

[55] L. Xiao, P. Yang, Y. Xiao, *et al.*, "Efficient compressive sensing detectors for generalized spatial modulation systems," *IEEE Trans. Veh. Technol.*, vol. 66, no. 2, pp. 1284-1298, Feb. 2017.

[56] B. Zheng, X. Wang, M. Wen, *et al.*, "Soft demodulation algorithms for generalized spatial modulation using deterministic sequential Monte Carlo," *IEEE Trans. on Wireless Commun.*, vol. PP, no. 99, pp. 1-1, Apr. 2017.

[57] K. Yang and C. Masouros, "On the optimal number of antennas for power efficient generalized spatial modulation," *Proc. IEEE Int. Workshop on Comput. Aided Modelling and Des. of Commun. Links and Networks*, pp. 38-42, Sep. 2015.

[58] L. Qiu and M. Jiang, "A generalized spatial modulation for indoor optical wireless communications," *Proc Opto-Electon. and Commun. Conf*, pp 1-3, Jul. 2015.

[59] E. Curry, D. K. Borah and J. M. Hinojo, "Optimal symbol set design for generalized spatial modulations in MIMO VLC systems," *Proc. IEEE Global Commun. Conf.*, pp. 1-7, Dec. 2016.

[60] P. Liu, M. D. Renzo and A. Springer, "Variable-Nu generalized spatial modulation for indoor LOS mmWave communication: Performance optimization and novel switching structure" *IEEE Trans. on Commun.*, vol. PP, no. 99, pp.1-16, Mar. 2017.

[61] C. R. Kumar and K. R Jeyachitra, "Power efficient generalized spatial modulation MIMO for indoor visible light communications," *IEEE Photonics Technol. Lett,*, vol. 29, no. 11, pp. 921-924, Apr. 2017.

[62] K. G Seddik, A. S Ibrahim and K. J. Liu, "Trans-modulation in wireless relay networks," *IEEE Commun. Lett.*, vol. 12, no. 3, pp. 170-73, Mar. 2008.

[63] H. Samra, Z. Ding and P. Hahn, "Symbol mapping diversity design for multiple packet transmission," *IEEE Trans. on Commun.*, vol. 53, no. 5, pp. 810-807, May 2005.

[64] S. Verdu, *Multiuser Detection*, 1st ed. United Kingdom: Cambridge University Press, 1998.

Part II

Journal Papers

Paper A

Generalised Spatial Modulation with Constellation Reassignment

Nigel Naidoo, Hongjun Xu and Narushan Pillay

Under second review by IET Communications Journal

Abstract

Generalised spatial modulation (GSM) addresses the transmit antenna constraint of spatial modulation (SM) and allows multiple active transmit antennas, thus unlocking the potential for transmit diversity in SM. However, for identical system configurations, the bit error rate (BER) performance of GSM is degraded compared to SM. On this note, in this paper, GSM employing constellation reassignment (GSM-CR) is proposed. A framework for the design of GSM-CR systems is presented. An analytical bound for the average BER of GSM-CR over independent and identically distributed (i.i.d.) Rayleigh flat fading channels is also derived, and the accuracy of the bound is verified by Monte Carlo simulation results. Moreover, Monte Carlo simulation results demonstrate that for 9 bits/s/Hz transmission, GSM-CR achieves gains of 5 dB and 4 dB, at a BER of 10^{-5}, when compared to GSM and SM, respectively.

1. Introduction

Spatial modulation (SM) is a multiple-input multiple-output (MIMO) technique proposed in [1]-[3], which improves transmission bandwidth efficiency by mapping information bits to a signal constellation and spatial constellation comprising transmit antenna indices. In SM, only a single transmit antenna remains active during a data transmission. As a result, SM is immune to the pitfalls of inter-channel interference (ICI) and inter-antenna synchronisation (IAS) that plague popular MIMO techniques such as the vertical-bell layered space-time (V-BLAST) architecture [4] and Alamouti [5]. A comprehensive analysis of the state of the art of SM for generalised MIMO technologies is presented in [6], with particular emphasis on the benefits of SM, research challenges encountered and real world implementation of SM MIMO systems. Moreover, a SM MIMO design framework is presented in [7], where issues such as, *inter alia*, transceiver design, signal constellation optimisation, link adaptation techniques and distributed/cooperative protocol design are addressed. The optimisation of the signal constellation is of particular importance in the context of SM system design, since the BER performance of SM is highly dependent on the minimum Euclidean distance between signal constellation points [7].

The single active transmit antenna architecture of SM necessitates the use of $log_2 n_t$ transmit antennas, where n_t is the number of information bits that are mapped onto the active transmit antenna. The large number of transmit antennas is considered a practical limitation for SM systems with large n_t. Generalised spatial modulation (GSM) [8] is an extension of SM, which permits the transmission of the same data symbol from multiple active transmit antennas. GSM differs from SM in that the spatial domain now comprises combinations of transmit antennas activated at each instance. Therefore, GSM overcomes the aforementioned SM limitation by increasing the overall spectral efficiency by the base–two logarithm of the number of antenna combinations, thus reducing the number of transmit antennas required to convey n_t [8]. However, for identical configurations, the BER performance of GSM is limited and degraded compared to SM [8].

Several techniques have been proposed to improve the error performance of GSM. A relevant example of a closed loop transmission system is adaptive joint mapping generalised spatial modulation (AJM-GSM) in [9], where the optimum signal space constellation diagram is selected at the receiver according to the channel state information, and fed back to the transmitter via an uplink channel. Notable developments in coded system configurations are: trellis coded generalised spatial modulation in [10], where trellis coding is applied to GSM, and GSM with space-time block codes (GSM-STBC) in [11], which utilises space-time block coding in conjunction with GSM. With regard to open loop transmission systems, a high-rate generalized spatial modulation (HR-GSM) scheme modulation scheme was recently proposed in [12]. In this scheme, high data rates and improved error performance are achieved by encoding information in two modulated symbols and the indices of two active transmit antennas. However, HR-GSM can only be utilised in conjunction with M-ary phase shift keying (MPSK) signal constellations. This is considered a practical limitation since the M-ary quadrature amplitude modulation (MQAM) scheme has found wide application in cable television, wireless fidelity (Wi-Fi) local-area networks (LANs), and mobile telephony systems.

The popularity of MQAM coupled with the requirement to improve the BER performance of GSM motivates for the development of a BER performance enhanced GSM technique that utilises MQAM signal constellations. In response to the aforementioned, a novel technique termed generalised spatial modulation with constellation reassignment (GSM-CR) is proposed. This technique employs constellation reassignment (CR) in conjunction with GSM in order to maximise the minimum Euclidean distance between transmitted symbol pairs, thereby resulting in improved BER performance.

CR has traditionally been used to improve the error performance of systems that employ multiple transmissions of the same information bits [13, 14]. The CR technique maps the same information bits into different signal constellations for multiple transmissions and has been employed in wireless relay networks in [13] and multiple packet transmission systems in [14]. In general, CR is utilised over multiple transmit

timeslots. To the best of the author's knowledge, CR has not been discussed within the context of a single transmit timeslot system.

Note, the following important differences exist between conventional GSM and the proposed GSM-CR scheme. In conventional GSM, there is only one bit-to-signal constellation mapper, whilst in GSM-CR there are two bit-to-signal constellation mappers. Moreover, in conventional GSM multiple antennas transmit the same symbol, whilst in GSM-CR a pair of active transmit antennas transmit different symbols.

The remainder of the paper is structured as follows: Section 2 presents the model of the proposed GSM-CR scheme. Section 3 presents a framework for the design of GSM-CR, which covers spatial constellation design, signal constellation design and rotation angle optimisation. Section 4 formulates an analytical average BER expression for MQAM GSM-CR over independent and identically distributed (i.i.d.) Rayleigh flat fading channels. Section 5 presents Monte Carlo simulation results and discussion. Finally, conclusions are drawn in section 6.

1.1 Notation

Bold italics upper/lower case symbols denote matrices/vectors, while regular letters represent scalar quantities. We use $\lfloor \cdot \rfloor$, $(\cdot)^T$, $(\cdot)^H$, $E[\cdot]$, $|\cdot|$ and $\|\cdot\|_F$ for the floor, transpose, Hermitian, expectation, Euclidean norm and Frobenius norm operations, respectively.

2. System Model

GSM-CR is a MIMO technique based on the GSM scheme [8]. However, unlike conventional GSM, which employs any number of active transmit antennas, GSM-CR only utilises two active transmit antennas in a particular timeslot. Moreover, GSM-CR differs from conventional GSM in that different signal constellations are associated with each transmit antenna within the active transmit antenna pair. These signal constellations are designed using a technique called CR, which ensures that the minimum Euclidean distance between transmitted symbol pairs is greater as compared to GSM.

The basic idea behind GSM-CR is to map a stream of input bits to a pair of transmit antenna (spatial domain) and a pair of symbols (signal domain). The spatial domain mapping is equivalent to that performed in a conventional GSM system with two active transmit antennas. The signal domain mapping on the other hand entails the selection of two symbols from two separate MQAM signal constellations, termed primary and secondary constellations.

The pair of MQAM symbols are then simultaneously transmitted over the wireless channel by the selected transmit antenna pair. At the receiver, a maximum likelihood (ML) detector is utilised for the joint detection of the active transmit antenna pair and transmitted symbol pair, thereby allowing for the recovery of the original input bits via a de-mapping process.

2.1 Transmission

Consider an $N_t \times N_r$ MQAM GSM-CR system shown in Figure A.1, where N_t refers to the number of transmit antennas, N_r is the number of receive antennas and M the order of the quadrature amplitude modulation scheme employed. In GSM-CR, information is conveyed in both the spatial and signal domains. The spatial domain comprises all possible combinations of transmit antenna pairs, where the indices of transmit antenna pairs correspond to spatial symbols. The number of usable transmit antenna pair combinations that can be considered must be a power of two and is given by $c = 2^{m_l}$, where $m_l = \left\lfloor log_2 \binom{N_t}{2} \right\rfloor$.

The signal domain comprises a pair of complementary primary and secondary MQAM signal constellations. The primary constellation corresponds to a Gray-coded MQAM constellation and the secondary constellation is generated by assigning symbols with adjacent constellation points in the primary constellation to non-adjacent points in the secondary constellation and *vice versa*, in accordance with the CR technique [13, 14].

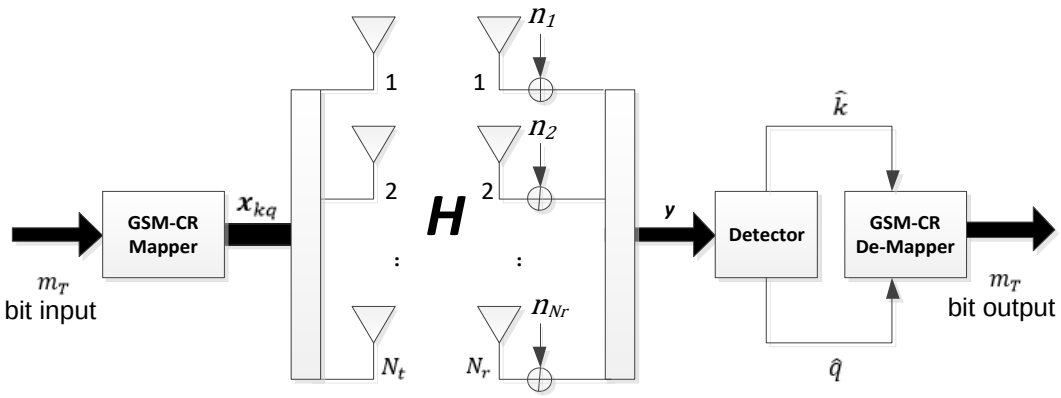

Figure A.1 GSM-CR System Model

Initially, the GSM-CR mapper assigns a stream of random $m_T = log_2 c + log_2 M$ input bits to a spatial symbol and an MQAM symbol pair in accordance with a predefined mapping table, which is known at both the transmitter and receiver. A sample mapping table for a $3 \times N_r$ 16QAM GSM-CR system is provided in Appendix A-1. The first $log_2 c$ input bits are mapped to a transmit antenna pair index k and the remaining $log_2 M$ bits are assigned to a pair of MQAM symbols x_q and $\tilde{x}_q$, where $q \in [0: M-1]$, is the decimal equivalent of the $log_2 M$ input bit sequence and the index identifying the transmitted symbol pair. The MQAM symbol x_q is obtained from the primary signal constellation $\boldsymbol{X}^{Prm}$, while the symbol $\tilde{x}_q$ is obtained from the secondary signal constellation $\boldsymbol{X}^{Sec}$. The outcome of the spatial and signal mapping processes can be expressed as follows:

$$\boldsymbol{x}_{kq} = \underset{\substack{1^{st}\ position \\ k_1{}^{th}\ position}}{\left[0 \ \ x_q \ \ldots\ldots\ \underset{\substack{k_2{}^{th}\ position \\ N_t{}^{th}\ position}}{\tilde{x}_q} \ \ldots\ldots 0 \ \ 0\right]^T} e^{j\theta_k} \tag{A.1}$$

where k_1 and $k_2 \in [1: N_t]$ are active transmit antennas from the k^{th} transmit antenna pair. $E\left\{\left|x_q\right|^2\right\} = E\left\{\left|\tilde{x}_q\right|^2\right\} = 1$. θ_k denotes the rotation angle applied to symbol pair $\left[x_q \ \tilde{x}_q\right]^T$ emitted from transmit antenna pair k. The process for the selection of appropriate rotation angles will be addressed in section 3.3.

The symbols x_q and $\tilde{x}_q$ are then simultaneously transmitted from antennas k_1 and k_2, respectively, over the $N_r \times N_t$ MIMO channel $\boldsymbol{H}$, and are subjected to N_r dimensional additive white Gaussian noise (AWGN) $\boldsymbol{n}$. The received signal vector is given by:

$$\boldsymbol{y} = \sqrt{\frac{\rho}{2}}\boldsymbol{H}\boldsymbol{x}_{kq} + \boldsymbol{n} \tag{A.2}$$

where $\boldsymbol{y}$ is the $N_r \times 1$ dimensional received signal vector. $\boldsymbol{H} = [\boldsymbol{h}_1\ \boldsymbol{h}_2 \dots \boldsymbol{h}_a \dots \boldsymbol{h}_{N_t}]$ and $\boldsymbol{h}_a$ is the $N_r \times 1$ dimensional vector corresponding to transmit antenna a. ρ is the average SNR at each receive antenna. $\boldsymbol{n}$ and $\boldsymbol{H}$ have i.i.d. entries according to the complex Gaussian distribution $CN(0,1)$.

Alternatively, the received signal vector may be represented as follows:

$$\boldsymbol{y} = \sqrt{\frac{\rho}{2}}\boldsymbol{h}'_k\boldsymbol{X}_q + \boldsymbol{n} \tag{A.3}$$

where $\boldsymbol{X}_q = \begin{bmatrix} x_q & \tilde{x}_q \end{bmatrix}^T e^{j\theta_k}$ is the transmitted symbol pair subjected to a predefined rotation angle θ_k and $\boldsymbol{h}'_k = \begin{bmatrix} \boldsymbol{h}_{k_1} \boldsymbol{h}_{k_2} \end{bmatrix}$ is an $N_r \times 2$ dimensional channel matrix corresponding to the active transmit antenna pair k.

2.2 Maximum Likelihood Detector

The receiver employs the following ML detection rule for the joint estimation of the active transmit antenna pair index and the transmitted symbol pair index:

$$\begin{aligned} [\hat{k}, \hat{q}] &= \underset{k,\boldsymbol{X}_q}{\operatorname{argmax}}\, p_y\left(\boldsymbol{y}|\boldsymbol{x}_{kq}, \boldsymbol{H}\right) \\ &= \underset{k,\boldsymbol{X}_q}{\operatorname{argmin}} \left(\sqrt{\frac{\rho}{2}}\left\|\boldsymbol{h}'_k\boldsymbol{X}_q\right\|_F^2 - 2Re\{\boldsymbol{y}^H\boldsymbol{h}'_k\boldsymbol{X}_q\}\right) \end{aligned} \tag{A.4}$$

where $p_y\left(\boldsymbol{y}|\boldsymbol{x}_{kq}, \boldsymbol{H}\right)$ is the probability density function of $\boldsymbol{y}$ conditioned on $\boldsymbol{H}$ and $\boldsymbol{x}_{kq}$. $\hat{k} \in [1:c]$ is the estimated active transmit antenna pair index of the and $\hat{q}$ is the estimated transmitted symbol pair index. The derivation of the (A.4) can be found in Appendix A-6.

3. System Design

The error performance of GSM-CR is dependent on the minimum distance between transmitted signal vectors, where larger distances yield improved BER performance. Hence, the design of GSM-CR systems is geared towards maximising the minimum distance between transmitted signal vectors.

Similar to GSM, the GSM-CR system utilises a three-dimensional constellation space comprising spatial and signal constellations. Hence, the minimum distance between transmitted signal vectors cannot be defined solely in terms of the Euclidean distance metric that is typically applied in two dimensional signal constellations. Therefore, the following hybrid minimum distance metric, which has been adapted from [15], is proposed:

$$d_{min} = \underset{\substack{k,\hat{k},q,\hat{q} \\ q \neq \hat{q}}}{\operatorname{argmin}} \left\{ \sqrt{{\delta_{k\hat{k}}}^2 + \left| x_q e^{j\theta_k} - x_{\hat{q}} e^{j\theta_{\hat{k}}} \right|^2 + \left| \tilde{x}_q e^{j\theta_k} - \tilde{x}_{\hat{q}} e^{j\theta_{\hat{k}}} \right|^2} \right\} \qquad \text{(A.5)}$$

where d_{min} is the minimum distance between transmitted between signal vectors $\boldsymbol{x}_{kq}$ and $\boldsymbol{x}_{\hat{k}\hat{q}}$ and $\boldsymbol{x}_{kq} \neq \boldsymbol{x}_{\hat{k}\hat{q}}$. $\delta_{k\hat{k}}$ is defined as the number of non-overlapping indices between transmit antenna pairs k and $\hat{k}$. For example, consider a $4 \times N_r$ GSM-CR configuration with $\binom{4}{2}$ possible transmit antenna pair groupings $\varepsilon_1 = (1\ 1\ 0\ 0), \varepsilon_2 = (1\ 0\ 1\ 0)$, $\varepsilon_3 = (1\ 0\ 0\ 1)$, $\varepsilon_4 = (0\ 1\ 1\ 0)$, $\varepsilon_5 = (0\ 1\ 0\ 1)$ and $\varepsilon_6 = (0\ \ 0\ 1\ 1)$, where 1 and 0 represent the respective active and idle state of a particular antenna. Then we have $\delta_{1,4}(\varepsilon_1, \varepsilon_4) = 2$ and $\delta_{1,6}(\varepsilon_1, \varepsilon_6) = 4$.

3.1 Spatial Constellation Optimisation

The minimum hybrid distance metric in (A.5) can be maximized by, *inter alia*, maximising the term $\delta_{k\hat{k}}$ through the selection of appropriate transmit antenna pair groupings. For example, consider the hypothetical scenario where three possible antenna pair groupings ε_1, ε_4 and ε_6 exist, and that two antenna pair groupings must be selected. Assume that ε_1 has already been selected and a choice between the two remaining pairs ε_4 and ε_6 must be made. Based on the fact that $\delta_{1,4}(\varepsilon_1, \varepsilon_4) = 2$ and $\delta_{1,6}(\varepsilon_1, \varepsilon_6) = 4$, ε_6 will be selected as it leads to the maximisation of $\delta_{k\hat{k}}$.

The maximisation of $\delta_{k\hat{k}}$ ensures that antenna groups are made to be far away from each other with the least possible number of overlapping indices. The selection of transmit antenna pairs with overlapping indices is not desirable as it leads to an increase of the linear dependence probability of channel space, which is the principal cause of active transmit antenna pair index detection error [15]. In general, there exists a trade-off between the number of transmit antennas and the extent to which overlapping of indices between transmit antenna pair groupings can be mitigated. The optimised transmit antenna pair groupings for various GSM-CR configurations are provided in Appendix A-3.

3.2 MQAM Signal Constellation Optimisation

The maximisation of the minimum hybrid distance metric in (A.5) can also be achieved by maximising the terms $\left|x_q e^{j\theta_k} - x_{\hat{q}} e^{j\theta_{\hat{k}}}\right|^2 + \left|\tilde{x}_q e^{j\theta_k} - \tilde{x}_{\hat{q}} e^{j\theta_{\hat{k}}}\right|^2$. The CR technique is employed to specifically maximise the term $\left|\tilde{x}_q e^{j\theta_k} - \tilde{x}_{\hat{q}} e^{j\theta_{\hat{k}}}\right|^2$ by reassigning symbols that have adjacent constellation points in the primary constellation to non-adjacent constellation points in the secondary constellation and *vice versa* [13]. In accordance with the approach proposed in [13], the reassignment of symbols and the subsequent construction of the secondary constellation should seek to maximise the minimum value of the product $\left|x_q - x_{\hat{q}}\right|\left|\tilde{x}_q - \tilde{x}_{\hat{q}}\right|$ over all possible pairs of transmitted symbols.

For GSM systems, a transmitted symbol pair is generated based solely on the primary signal constellation. Therefore, the minimum Euclidean distance between transmitted symbol pairs is equivalent to twice the Euclidean distance occurring between adjacent symbols in the primary signal constellation. GSM-CR on the other hand generates a transmitted symbol pair based on a primary and secondary signal constellation. The remapping of symbols in the secondary constellation yields an enhanced minimum Euclidean distance between transmitted symbol pairs as compared to GSM. It can therefore be expected that for systems with identical antenna configurations, order of modulation and spatial constellation, GSM-CR would exhibit improved BER performance when compared to GSM. The primary and secondary signal constellations for 16QAM and 64QAM GSM-CR, as proposed in [13], are presented in Figure A.3 and Appendix A-2, respectively.

An illustrative example will be used to substantiate the aforementioned claims regarding the BER performance of GSM-CR in relation to GSM. Consider the 16QAM GSM and GSM-CR configurations that use signal constellations associated with the same spatial constellation point and where no rotation angle is applied, as shown in Figures A.2 and A.3, respectively. Figure A.2 shows that in the case of GSM, the minimum Euclidean distance of $2d_{pri} = \frac{4}{\sqrt{10}}$ occurs between adjacent symbol pairs such as $[x_0\, x_0]$ and $[x_4\, x_4]$. Moreover, Figure A.3 demonstrates that the minimum Euclidean distance between the very same symbol pairs in the case of GSM-CR is $d_{pri} + d_{sec} = \frac{6}{\sqrt{10}}$. Based on the minimum Euclidean distance values obtained, we can conclude that for identical system configurations, GSM-CR will exhibit improved BER performance when compared to GSM.

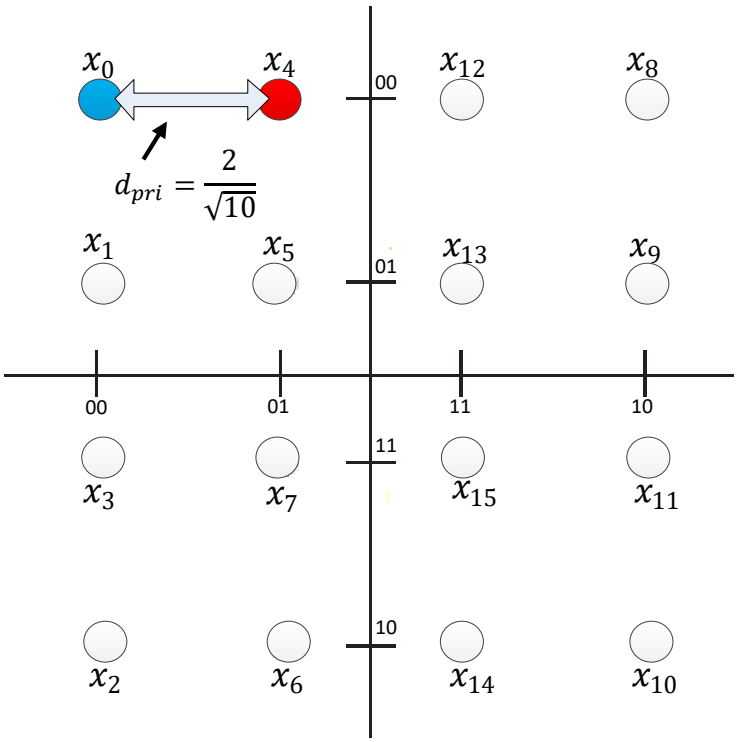

Figure A.2 16QAM GSM Signal Constellation

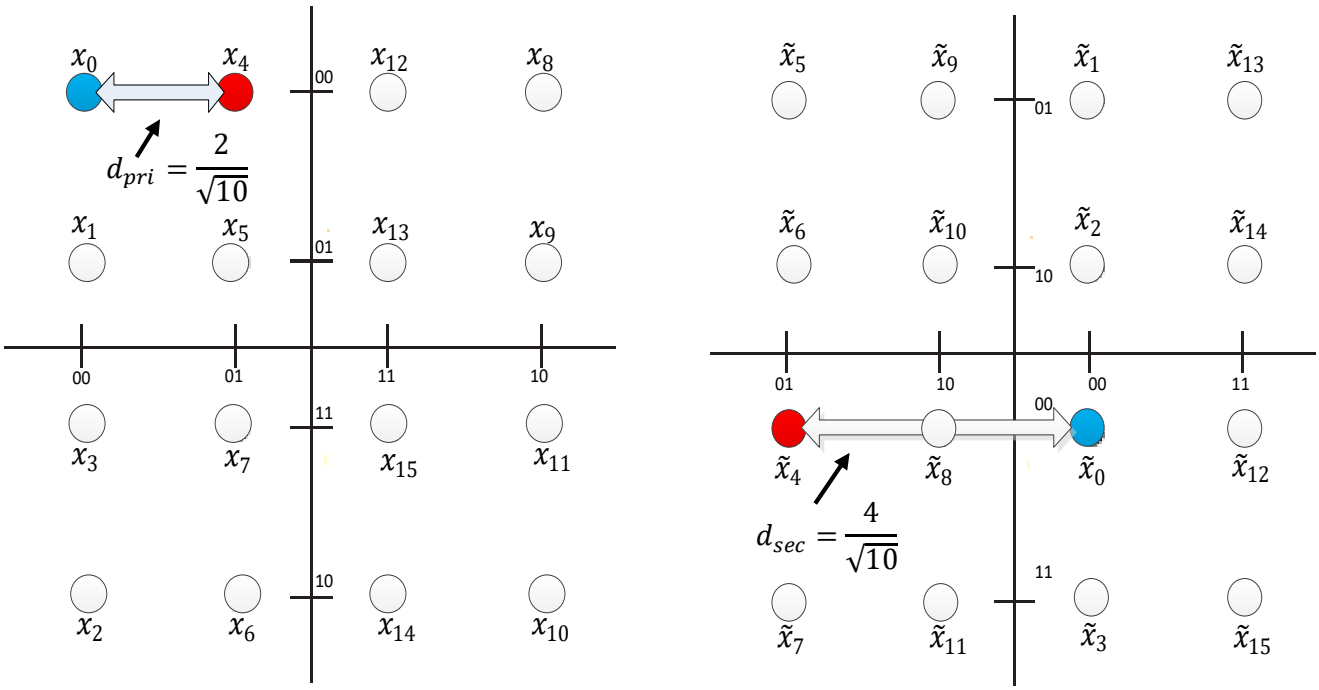

Figure A.3 16QAM GSM-CR Signal Constellations

3.3 Rotation Angle Optimisation

It can be observed from (A.5), that the minimum hybrid distance metric may be further maximised through the application of suitable rotation angles to the primary and secondary signal constellations associated with a particular transmit antenna pair. The presence of the term $\delta_{k\hat{k}}$ in (A.5) suggests that that the minimum distance will occur under conditions where transmit antenna pairs k and $\hat{k}$ have overlapping antenna indices. In light of this, rotation angles will be specifically applied to signal constellations that correspond to transmit antenna pair groupings with overlapping indices.

A high level process for generating the rotation angles is presented below**.** Note that the selection of transmit antenna pair groupings in accordance with section 3.1 and the formulation of primary and secondary signal constellations as per section 3.2 must be performed prior to generating the rotation angle.

i. Given that c possible transmit antenna pair groupings have been generated, select a subset $\boldsymbol{c}_{nov}$ of transmit antenna pairs that contain non-overlapping

entries. Note that transmit antenna pairs contained in $\boldsymbol{c}_{nov}$ should satisfy the criterion $\delta_{k\hat{k}}{}^2 = 4$.

ii. Set the rotation angle $\theta_i = 0$ for $i \in \boldsymbol{c}_{nov}$.

iii. Generate a subset $\boldsymbol{c}_{ov}$ comprising all valid transmit antenna pairs not contained in $\boldsymbol{c}_{nov}$.

iv. Determine the rotation angles θ_i for $i \in \boldsymbol{c}_{ov}$ by computing the maximisation problem $d_{max} = \underset{0 < \boldsymbol{\theta}_{cov} < 2\pi}{argmax\{d_{min}\}}$, where $\boldsymbol{\theta}_{\boldsymbol{c}_{ov}}$ is the set of rotation angles to be optimised and d_{min} has been defined in (A.5). It is not possible to derive rotation angles for MQAM signal constellation with $M > 4$ [15] and therefore an exhaustive search via computer simulation may be employed to solve the abovementioned maximisation problem. In light of the fact that all possible rotation angles within a prescribed precision are considered, the rotation angles obtained will be local optimal values with respect to the particular level of precision utilised in the computer simulation process. Due to the computationally intensive nature of the aforementioned computer simulation process, a precision of 10^{-2} was adopted in this paper.

The rotation angles for various GSM-CR configurations are shown in Appendix A-3.

4. BER Performance Analysis

In this section, an analytical bound for the average BER of GSM-CR over i.i.d. Rayleigh flat fading channels is derived. Following the approach adopted in [1, 16, 21], the transmit antenna pair index and transmitted symbol pair estimation processes are considered to be independent. Based on this assumption the average BER of GSM-CR may be approximated by [21, (9)]:

$$P_e \cong 1 - P_c = P_a + P_d - P_a P_d \tag{A.6}$$

where $P_c = (1 - P_a)(1 - P_d)$ is the probability that correct input bits are detected, P_a is the bit error probability of estimating the active transmit antenna pair index given that the transmitted symbol pair is correctly detected. P_d is the bit error probability of

symbol pair estimation given that the active transmit antenna pair index is correctly detected.

The formulation of the analytic average BER expression in (A.6), based on the assumption of independent transmit antenna pair index and symbol pair estimation processes, is in general not correct, as indicated in [16]. Nevertheless, this assumption simplifies the derivation of the analytic expression in (A.6) and has been adopted widely in literature [1, 16, 21]. Moreover, the assumption of independent estimation processes yields a fairly accurate estimation of simulated average BER og GSM-CR, which will be demonstrated in section 5.1.

A comprehensive analytical framework for computing the average BER of SM over generic fading channels was introduced in [17]. The analytical framework in [17] differs from the approach adopted in [1, 16, 21] and this paper in that the inter-relation between the transmit antenna and symbol estimation processes is specifically taken into account by utilising what is termed the improved union bound. Moreover, the analytical expressions in [17] are tailored towards SM schemes, which transmit a single symbol from a single active antenna and are therefore not directly applicable in the context of GSM-CR schemes, which simultaneously transmit two different symbols from an active transmit antenna pair.

4.1 Analytical BER of Symbol Pair Estimation

The bit error probability of symbol pair estimation is derived using the well-known union bound technique [18]. Given that the transmit antenna pair index is perfectly detected, the average BER of symbol pair estimation is bounded by:

$$P_d \leq E\left[\sum_{\hat{q}} N(q,\hat{q}) P\left(\boldsymbol{x}_{kq} \rightarrow \boldsymbol{x}_{k\hat{q}}\right)\right] \tag{A.7}$$

$$= \sum_{q=0}^{M-1} \sum_{\substack{\hat{q}=0 \\ \hat{q}\neq q}}^{M-1} \frac{N(q,\hat{q}) P\left(\boldsymbol{x}_{kq} \rightarrow \boldsymbol{x}_{k\hat{q}}\right)}{Mm}$$

where $N(q,\hat{q})$ is the number of bits in error between the symbol vectors $\boldsymbol{X}_q$ and $\boldsymbol{X}_{\hat{q}}$. $P(\boldsymbol{x}_{kq} \rightarrow \boldsymbol{x}_{k\hat{q}})$ denotes the pairwise error probability (PEP) of detecting $\boldsymbol{x}_{k\hat{q}}$ given that $\boldsymbol{x}_{kq}$ was transmitted and $m = log_2 M$.

The PEP conditioned on $\boldsymbol{H}$ may be expressed as follows (refer to Appendix A-4 for the complete derivation):

$$P(\boldsymbol{x}_{kq} \rightarrow \boldsymbol{x}_{k\hat{q}}|\boldsymbol{H}) = Q\left(\sqrt{\frac{\rho}{8}\left\|\boldsymbol{h}_k'(\boldsymbol{X}_{\hat{q}} - \boldsymbol{X}_q)\right\|_F^2}\right) \tag{A.8}$$

where $Q(\tau)$ is the Gaussian Q-function $Q(\tau) = \int_{\tau}^{\infty} \frac{1}{2\pi} e^{-\frac{t^2}{2}} dt$.

The conditional PEP in (A.8) may therefore be written as follows:

$$P(\boldsymbol{x}_{kq} \rightarrow \boldsymbol{x}_{k\hat{q}}|\boldsymbol{H}) = Q(\sqrt{g}) \tag{A.9}$$

where g is a central Chi-square square random variable with $2N_r$ degrees of freedom and is defined by:

$$g = \frac{\rho}{8}\left\|\boldsymbol{h}_k'(\boldsymbol{X}_{\hat{q}} - \boldsymbol{X}_q)\right\|_F^2 = \sum_{n=1}^{2N_r} {\alpha_n}^2 \tag{A.10}$$

where $\alpha_n \sim N(\mu, {\sigma_\alpha}^2)$ with $\mu = 0$ and ${\sigma_\alpha}^2 = \frac{\rho}{8}\left\|(\boldsymbol{X}_{\hat{q}} - \boldsymbol{X}_q)\right\|_F^2$.

The probability density function of g is given by [18]:

$$p_g(v) = \frac{v^{N_r - 1}\, e^{-v/2{\sigma_\alpha}^2}}{(2{\sigma_\alpha}^2)^{N_r}(N_r - 1)!} \tag{A.11}$$

The unconditioned PEP $P(\boldsymbol{x}_{kq} \rightarrow \boldsymbol{x}_{k\hat{q}})$ can therefore be formulated as:

$$P(\boldsymbol{x}_{kq} \rightarrow \boldsymbol{x}_{k\hat{q}}) = \int_0^{\infty} P(\boldsymbol{x}_{kq} \rightarrow \boldsymbol{x}_{k\hat{q}}|\boldsymbol{H})\, p_g(v)\, dv \tag{A.12}$$

$$= \int_0^{\infty} Q(\sqrt{v}) p_g(v)\, dv$$

By applying the trapezoidal approximation, the Gaussian Q-function in (A.12) may be written as [19]:

$$Q(\sqrt{v}) = \frac{1}{4n} exp\left(\frac{-v}{2}\right) + \frac{1}{2n}\sum_{c=1}^{n-1} exp\,\frac{-v}{2sin^2(c\pi/2n)} \tag{A.13}$$

where the approximation is implemented for $n > 10$ iterations for convergence. Substituting (A.13) into (A.12) and rewriting (A.12) in terms of the moment generating function (MGF) yields:

$$P(\boldsymbol{x}_{kq} \rightarrow \boldsymbol{x}_{k\hat{q}}) = \frac{1}{4n} M\left(\frac{1}{2}\right) + \frac{1}{2n}\sum_{c=1}^{n-1} M\left(\frac{1}{2sin^2(c\pi/2n)}\right) \tag{A.14}$$

where $M(\cdot)$ is the MGF defined by [20]:

$$M(s) = \int_0^\infty \frac{e^{-sv} v^{N_r-1}\, e^{-v/2{\sigma_\alpha}^2}}{(2{\sigma_\alpha}^2)^{N_r}(N_r-1)!}\, dv = \int_0^\infty e^{-sv} p_k(v)\, dv = \left(\frac{1}{1+2{\sigma_\alpha}^2 s}\right)^{N_r}$$

Therefore P_d is obtained by substituting (A.14) into (A.7), which yields:

$$P_d \leq \frac{1}{Mm}\sum_{q=0}^{M-1}\sum_{\substack{\hat{q}=0 \\ \hat{q}\neq q}}^{M-1} N(q,\hat{q})\left[\frac{1}{4n} M\left(\frac{1}{2}\right) + \frac{1}{2n}\sum_{c=1}^{n-1} M\left(\frac{1}{2\sin^2(c\pi/2n)}\right)\right] \tag{A.15}$$

4.2 Analytical BER of Transmit Antenna Pair Index Estimation

The bit error probability of transmit antenna pair index estimation given that the transmitted symbol is perfectly detected was derived for SM systems in [21, (19)]. This analytical BER expression may be adapted to predict the P_a performance of GSM-CR as follows:

$$P_a \leq \sum_{k=1}^{c}\sum_{q=0}^{M-1}\sum_{\hat{k}=1}^{c} \frac{N(k,\hat{k})\mu_\alpha^{N_r}\sum_{w=0}^{N_r-1}\binom{N_r-1+w}{w}[1-\mu_\alpha]^w}{cM} \tag{A.16}$$

where $N(k, \hat{k})$ is the number of bits in error between antenna pair k and $\hat{k}$ and $\mu_\alpha = \frac{1}{2}\left(1 - \sqrt{\frac{\sigma_\alpha{}^2}{1+\sigma_\alpha{}^2}}\right)$ with $\sigma_\alpha{}^2 = (\rho/8)\left|\boldsymbol{X}_q\right|^2$. Appendix A-5 provides further detail as to how A.16 was tailored for the GSM-CR scheme.

5. Simulation Results

In this section, the analytical framework developed in section 4 is validated by comparing the theoretical average BER to the simulated average BER obtained from Monte Carlo simulations. Moreover, a BER performance comparison between various SM, GSM and GSM-CR systems, with equivalent spectral efficiencies, is presented.

Identical spatial domain mappings were employed in order to ensure a fair comparison between GSM and GSM-CR. In particular, the following antenna pair groupings were used for the $4 \times N$r and $6 \times N_r$ configurations. Note that these antenna pair groupings were constructed based on the spatial constellation optimisation guidelines presented in section 3.1, which aim to reduce the number of overlapping indices across transmit antenna pairs.

- $4 \times N_r$ – (1,3) ; (1,4); (2,3) and (2,4)
- $6 \times N_r$ – (1,2); (3,4); (5,6); (2,3); (4,5); (1,6); (1,3) and (2 4)

where the numbers within brackets denote transmit antenna indices.

The Monte Carlo simulations were performed over an i.i.d. Rayleigh flat fading channel with AWGN, where the parameters pertaining to the channel and AWGN are consistent with those defined in section 2. Furthermore, Monte Carlo simulations were conducted under the following assumptions: full channel knowledge at the receiver; antennas at the transmitter and receiver are separated wide enough to avoid correlation; system model for GSM is consistent with [8], system model for SM is consistent with [2] and the total transmit power is the same for all transmissions.

5.1 Analytic and Simulated Average BER Comparison

The analytic and simulated average BER for various GSM-CR configurations are shown in Figure A.4. For all configurations, the theoretical bounds are observed to

closely estimate the average BER performance in the high SNR region. Moreover, the average BER for 6×4 and 4×4 64QAM configurations are seen to converge at high values of SNR. This can be attributed to the fact that the transmitted symbol pair estimation error P_d dominates BER performance in configurations, where $log_2 M > log_2 c$.

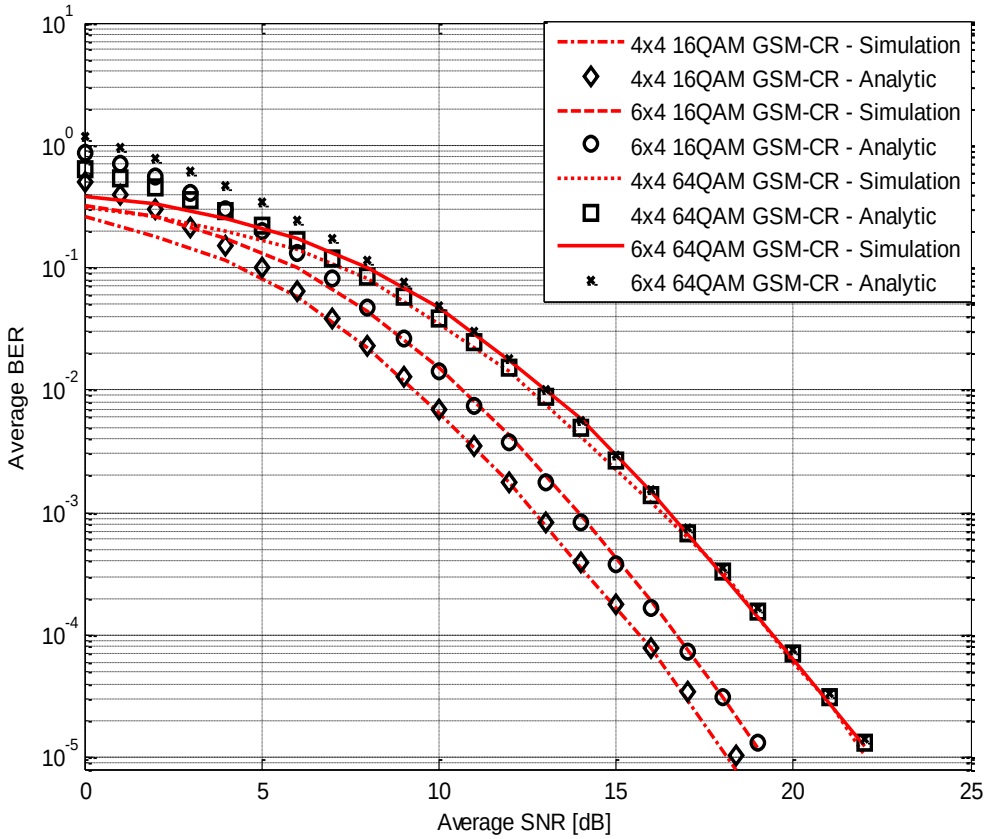

Figure A.4 Analytic and Simulated Average BER

5.2 Performance Comparison

Figures A.5 and A.6 show the average BER of GSM-CR, GSM and SM schemes for various configurations. In all cases, GSM-CR demonstrates superior BER performance, as compared to GSM and SM. In addition, GSM exhibits degraded BER performance as compared to SM. This particular trend was also observed in [8].

Figure A.5, presents the average BER for 6 bits/s/Hz and 8 bits/s/Hz transmissions. At 6 bits/s/Hz, GSM-CR achieves gains of 2.5 dB and 1.5 dB, at a BER of 10^{-5}, as compared to GSM and SM, respectively. Furthermore at 8 bits/s/Hz, GSM-CR achieves gains of 4 dB and 3.5 dB, at a BER of 10^{-5}, when compared to GSM and SM, respectively.

Figure A.6, presents the average BER for 7 bits/s/Hz and 9 bits/s/Hz transmissions. At 7 bits/s/Hz, GSM-CR achieves gains of 3 dB and 2 dB, at a BER of 10^{-5}, in comparison to GSM and SM, respectively. Furthermore at 9 bits/s/Hz, GSM-CR achieves gains of 5 dB and 4 dB, at a BER of 10^{-5}, when compared to GSM and SM, respectively. Based on the enhanced BER performance offered by GSM-CR, it is evident that this scheme is a prominent alternative to both SM and GSM.

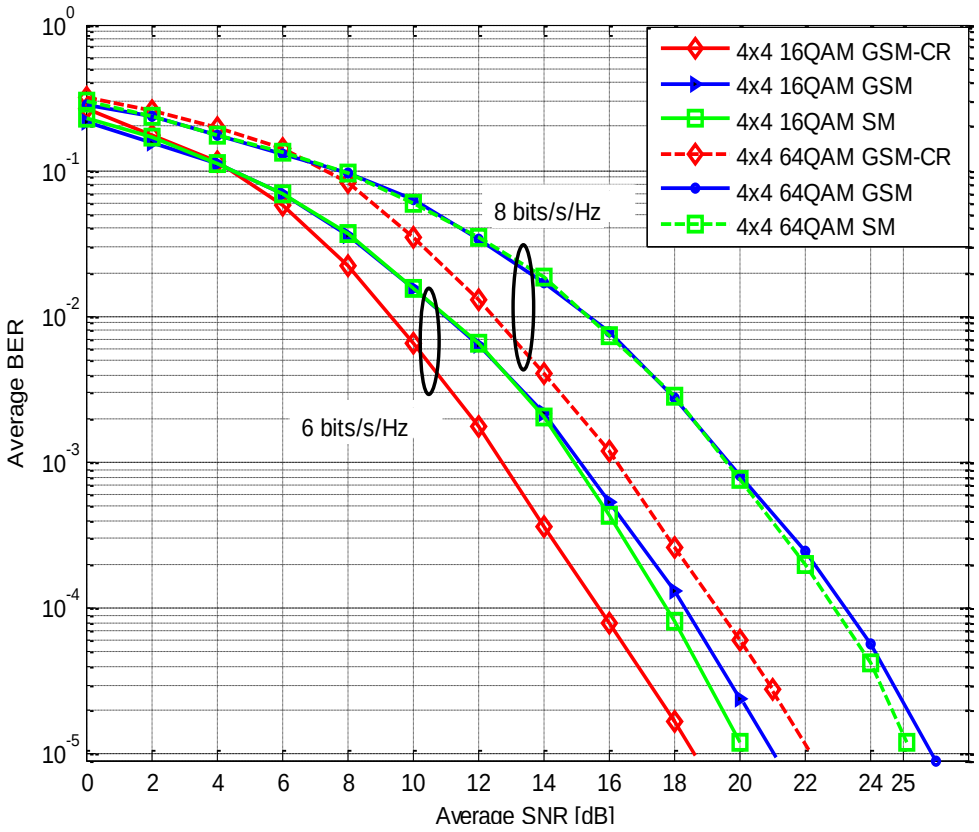

Figure A.5 Average BER - 6 bits/s/Hz and 8 bits/s/Hz Configurations

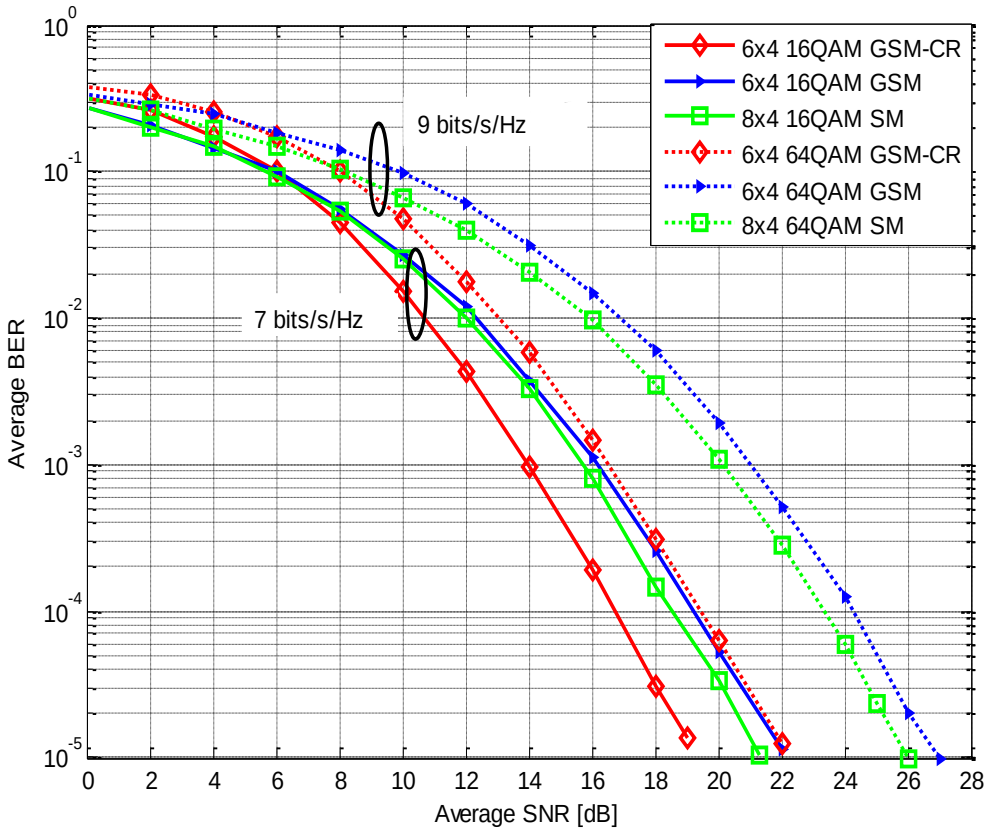

Figure A.6 Average BER - 7 bits/s/Hz and 9 bits/s/Hz Configurations

6. Conclusion

In this paper, we have proposed a BER performance enhanced GSM scheme, termed GSM-CR. Monte Carlo simulation results demonstrated that for 9 bits/s/Hz transmissions, GSM-CR was capable of achieving gains of 5 dB and 4 dB, at a BER 10^{-5}, when compared to GSM and SM, respectively. In addition, a framework for the design of GSM-CR systems was presented. An analytical bound for the average BER of GSM-CR over i.i.d. Rayleigh flat fading channels was also derived, and the accuracy of bound was verified by Monte Carlo simulation results.

Appendix A-1

Table A-1.1 $3 \times N_r$ 16QAM GSM-CR Mapping Table

Input Bits	**Spatial Symbol**		**16-QAM Symbol Pair**		
	k	**Antenna Combination**	q	x_q	$\tilde{x}_q$
00000	$k = 1$	(1,2)	$q = 0$	-3+3j	1-j
00001	$k = 1$	(1,2)	$q = 1$	-3+j	1+3j
00010	$k = 1$	(1,2)	$q = 2$	-3-3j	1+j
00011	$k = 1$	(1,2)	$q = 3$	-3-j	1-3j
00100	$k = 1$	(1,2)	$q = 4$	-1+3j	-3-j
00101	$k = 1$	(1,2)	$q = 5$	-1+j	-3+3j
00110	$k = 1$	(1,2)	$q = 6$	-1-3j	-3+j
00111	$k = 1$	(1,2)	$q = 7$	-1-j	-3-3j
01000	$k = 1$	(1,2)	$q = 8$	3+3j	-1-j
01001	$k = 1$	(1,2)	$q = 9$	3+j	-1+3j
01010	$k = 1$	(1,2)	$q = 10$	3-3j	-1+j
01011	$k = 1$	(1,2)	$q = 11$	3-j	-1-3j
01100	$k = 1$	(1,2)	$q = 12$	1+3j	3-j
01101	$k = 1$	(1,2)	$q = 13$	1+j	3+3j
01110	$k = 1$	(1,2)	$q = 14$	1-3j	3+j
01111	$k = 1$	(1,2)	$q = 15$	1-j	3-3j
10000	$k = 2$	(1,3)	$q = 0$	-3+3j	1-j
10001	$k = 2$	(1,3)	$q = 1$	-3+j	1+3j

10010	$k = 2$	(1,3)	$q = 2$	-3-3j	1+j
10011	$k = 2$	(1,3)	$q = 3$	-3-j	1-3j
10100	$k = 2$	(1,3)	$q = 4$	-1+3j	-3-j
10101	$k = 2$	(1,3)	$q = 5$	-1+j	-3+3j
10110	$k = 2$	(1,3)	$q = 6$	-1-3j	-3+j
10111	$k = 2$	(1,3)	$q = 7$	-1-j	-3-3j
11000	$k = 2$	(1,3)	$q = 8$	3+3j	-1-j
11001	$k = 2$	(1,3)	$q = 9$	3+j	-1+3j
11010	$k = 2$	(1,3)	$q = 10$	3-3j	-1+j
11011	$k = 2$	(1,3)	$q = 11$	3-j	-1-3j
11100	$k = 2$	(1,3)	$q = 12$	1+3j	3-j
11101	$k = 2$	(1,3)	$q = 13$	1+j	3+3j
11110	$k = 2$	(1,3)	$q = 14$	1-3j	3+j
11111	$k = 2$	(1,3)	$q = 15$	1-j	3-3j

Appendix A-2

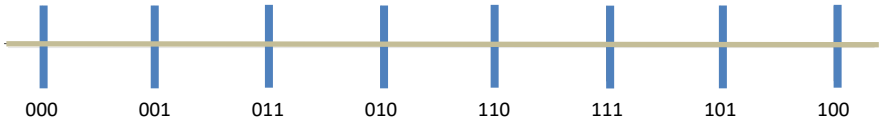

Figure A-2.1 64QAM Primary Constellation (real axis)

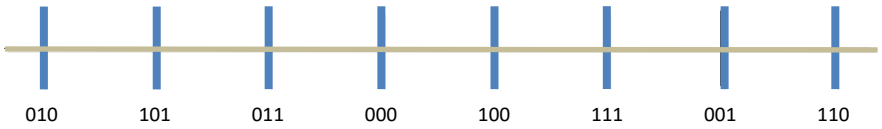

Figure A-2.2 64QAM Secondary Constellation (real axis)

Figures A-2.1 and A-2.2 show the primary and secondary constellations for 64QAM, respectively. The constellation assignment is shown only along one real axis and the same reassignment is performed along the other complex axis.

Appendix A-3

Table A-3.1 GSM-CR Transmit Antenna Pair Groupings and Rotation Angles for Various Configurations

Antenna Configuration	**Transmit Antenna Pair**	**16 QAM Rotation Angle**	**64 QAM Rotation Angle**
$4 \times N_r$	(1,3)	0	0
	(1,4)	$\pi/4$	$\pi/4$
	(2,3)	$\pi/4$	$\pi/4$
	(2,4)	0	0
$6 \times N_r$	(1,2)	0	0
	(3,4)	0	0
	(5,6)	0	0
	(2,3)	$\pi/3$	$\pi/6$
	(4,5)	$\pi/3$	$\pi/6$
	(1,6)	$\pi/3$	$\pi/6$
	(1,3)	$2\pi/3$	$\pi/3$
	(2,4)	$2\pi/3$	$\pi/3$

Appendix A-4

$$P(\boldsymbol{x}_{kq} \rightarrow \boldsymbol{x}_{k\hat{q}}|\boldsymbol{H}) = P\left(\left\|\boldsymbol{y} - \sqrt{\frac{\rho}{2}}\boldsymbol{H}\boldsymbol{x}_{k\hat{q}}\right\|_F^2 < \left\|\boldsymbol{y} - \sqrt{\frac{\rho}{2}}\boldsymbol{H}\boldsymbol{x}_{kq}\right\|_F^2\right) \quad \text{(A-4.1)}$$

Substituting $\boldsymbol{y} = \sqrt{\rho/2}\boldsymbol{H}\boldsymbol{x}_{kq} + \boldsymbol{n}$ in (A-4.1) yields:

$$P(\boldsymbol{x}_{kq} \rightarrow \boldsymbol{x}_{k\hat{q}}|\boldsymbol{H}) = P\left(\left\|\boldsymbol{n} - \sqrt{\frac{\rho}{2}}\boldsymbol{H}[\boldsymbol{x}_{k\hat{q}} - \boldsymbol{x}_{kq}]\right\|_F^2 < \|\boldsymbol{n}\|_F^2\right) \quad \text{(A-4.2)}$$

Rewriting (A-4.2) using the alternative notation $\boldsymbol{H}\boldsymbol{x}_{k\hat{q}} = \boldsymbol{h}_k'\boldsymbol{X}_{\hat{q}}$ and $\boldsymbol{H}\boldsymbol{x}_{kq} = \boldsymbol{h}_k'\boldsymbol{X}_q$ yields:

$$P(\boldsymbol{x}_{kq} \rightarrow \boldsymbol{x}_{k\hat{q}}|\boldsymbol{H}) = P\left(\left\|\boldsymbol{n} - \sqrt{\frac{\rho}{2}}\boldsymbol{h}_k'[\boldsymbol{X}_{\hat{q}} - \boldsymbol{X}_q]\right\|_F^2 < \|\boldsymbol{n}\|_F^2\right) \quad \text{(A-4.3)}$$

Treating the square of the Frobenius norm as a binomial and expanding likewise yields:

$$\begin{aligned} P(\boldsymbol{x}_{kq} \rightarrow \boldsymbol{x}_{k\hat{q}}|\boldsymbol{H}) &= P\left(\|\boldsymbol{n}\|_F^2 + \left\|\sqrt{\frac{\rho}{2}}\boldsymbol{h}_k'[\boldsymbol{X}_{\hat{q}} - \boldsymbol{X}_q]\right\|_F^2 - \right. \\ &\qquad \left. 2\left(\boldsymbol{n}, \sqrt{\frac{\rho}{2}}\boldsymbol{h}_k'[\boldsymbol{X}_{\hat{q}} - \boldsymbol{X}_q]\right) < \|\boldsymbol{n}\|_F^2\right) \\ &= P\left(\left(\boldsymbol{n}, \sqrt{\frac{\rho}{2}}\boldsymbol{h}_k'[\boldsymbol{X}_{\hat{q}} - \boldsymbol{X}_q]\right) > \frac{\left\|\sqrt{\frac{\rho}{2}}\boldsymbol{h}_k'[\boldsymbol{X}_{\hat{q}} - \boldsymbol{X}_q]\right\|_F^2}{2}\right) \end{aligned} \quad \text{(A-4.4)}$$

where $\left(\boldsymbol{n}, \sqrt{\frac{\rho}{2}}\boldsymbol{h}_k'[\boldsymbol{X}_{\hat{q}} - \boldsymbol{X}_q]\right)$ is a Gaussian random variable with 0 mean and variance $\left\|\sqrt{\frac{\rho}{2}}\boldsymbol{h}_k'[\boldsymbol{X}_{\hat{q}} - \boldsymbol{X}_q]\right\|_F^2$. Recall that for a 0 mean and unit variance Gaussian random variable Z:

$$P(Z > z) = \frac{1}{\sqrt{2\pi}}\int_z^\infty e^{\frac{-v}{2}}\,dv = Q(z) \quad \text{(A-4.5)}$$

It follows that:

$$P\left(\boldsymbol{x}_{kq} \rightarrow \boldsymbol{x}_{k\hat{q}} \middle| \boldsymbol{H}\right) = Q\left(\sqrt{\frac{\rho}{8}\left\|\boldsymbol{h}'_k\left(\boldsymbol{X}_{\hat{q}} - \boldsymbol{X}_q\right)\right\|_F^2}\right) \tag{A-4.6}$$

Appendix A-5

In accordance with [21, (19)], the bit error probability of transmit antenna pair index estimation given that the transmitted symbol pair is perfectly detected is given by:

$$P_a \leq \sum_{k=1}^{c} \sum_{q=0}^{M-1} \sum_{\hat{k}}^{c} \frac{N(k,\hat{k}) P(\boldsymbol{x}_{kq} \rightarrow \boldsymbol{x}_{\hat{k}q})}{cM} \tag{A-5.1}$$

SM systems emit a single symbol from an active transmit antenna, whereas GSM-CR emits two different symbols from a pair of active transmit antenna. This difference in configuration necessitates a reformulation of the conditional PEP $P(\boldsymbol{x}_{kq} \rightarrow \boldsymbol{x}_{\hat{k}q}|\boldsymbol{H})$ and the resulting unconditioned PEP $P(\boldsymbol{x}_{kq} \rightarrow \boldsymbol{x}_{k\hat{q}})$ in (A-5.1).

The conditional PEP for GSM-CR systems may be expressed as follows:

$$P(\boldsymbol{x}_{kq} \rightarrow \boldsymbol{x}_{\hat{k}q}|\boldsymbol{H}) = P\left(\left\|\boldsymbol{y} - \sqrt{\frac{\rho}{2}}\boldsymbol{H}\boldsymbol{x}_{\hat{k}q}\right\|_F^2 < \left\|\boldsymbol{y} - \sqrt{\frac{\rho}{2}}\boldsymbol{H}\boldsymbol{x}_{kq}\right\|_F^2\right) \tag{A-5.2}$$

Substituting $\boldsymbol{y} = \sqrt{\rho/2}\boldsymbol{H}\boldsymbol{x}_{kq} + \boldsymbol{n}$ in (A-5.2) and rearranging yields:

$$P(\boldsymbol{x}_{kq} \rightarrow \boldsymbol{x}_{\hat{k}q}|\boldsymbol{H}) = P\left(\left\|\boldsymbol{n} - \sqrt{\frac{\rho}{2}}\left[\boldsymbol{H}\boldsymbol{x}_{\hat{k}q} - \boldsymbol{H}\boldsymbol{x}_{kq}\right]\right\|_F^2 < \|\boldsymbol{n}\|_F^2\right) \tag{A-5.3}$$

Rewriting (A-5.3) using the alternative notation $\boldsymbol{H}\boldsymbol{x}_{\hat{k}q} = \boldsymbol{h}'_{\hat{k}}\boldsymbol{X}_q$ and $\boldsymbol{H}\boldsymbol{x}_{kq} = \boldsymbol{h}'_k\boldsymbol{X}_q$ yields:

$$P(\boldsymbol{x}_{kq} \rightarrow \boldsymbol{x}_{\hat{k}q}|\boldsymbol{H}) = P\left(\left\|\boldsymbol{n} - \sqrt{\frac{\rho}{2}}\left[\boldsymbol{h}'_{\hat{k}}\boldsymbol{X}_q - \boldsymbol{h}'_k\boldsymbol{X}_q\right]\right\|_F^2 < \|\boldsymbol{n}\|_F^2\right) \tag{A-5.4}$$

Treating the square of the Frobenius norm as a binomial and expanding likewise yields:

$$P(\boldsymbol{x}_{kq} \rightarrow \boldsymbol{x}_{\hat{k}q}|\boldsymbol{H}) = P\left(\left(\boldsymbol{n}, \sqrt{\frac{\rho}{2}}\left[\boldsymbol{h}'_{\hat{k}} - \boldsymbol{h}'_k\right]\boldsymbol{X}_q\right) > \frac{\left\|\sqrt{\frac{\rho}{2}}\left[\boldsymbol{h}'_{\hat{k}} - \boldsymbol{h}'_k\right]\boldsymbol{X}_q\right\|_F^2}{2}\right) \tag{A-5.5}$$

where $\left(\boldsymbol{n}, \sqrt{\frac{\rho}{2}}\left[\boldsymbol{h}'_{\hat{k}} - \boldsymbol{h}'_{k}\right]\boldsymbol{X}_q\right)$ is a Gaussian random variable with 0 mean and variance $\left\|\sqrt{\frac{\rho}{2}}\left[\boldsymbol{h}'_{\hat{k}} - \boldsymbol{h}'_{k}\right]\boldsymbol{X}_q\right\|_F^2$. Recall that for a 0 mean and unit variance Gaussian random variable Z:

$$P(Z > z) = \frac{1}{\sqrt{2\pi}}\int_z^{\infty} e^{\frac{-v}{2}}\, dv = Q(z) \tag{A-5.6}$$

It follows that:

$$P\left(\boldsymbol{x}_{kq} \rightarrow \boldsymbol{x}_{\hat{k}q} \middle| \boldsymbol{H}\right) = Q\left(\sqrt{g}\right) \tag{A-5.7}$$

g is a central Chi-square square random variable with $2N_r$ degrees of freedom and is defined by:

$$g = \frac{\rho}{8}\left\|\left(\boldsymbol{h}'_{\hat{k}} - \boldsymbol{h}'_{k}\right)\boldsymbol{X}_q\right\|_F^2 = \sum_{n=1}^{2N_r} {\alpha_n}^2 \tag{A-5.8}$$

where $\alpha_n \sim N(\mu, {\sigma_\alpha}^2)$ with $\mu = 0$ and ${\sigma_\alpha}^2 = \frac{\rho}{8}\left\|\boldsymbol{X}_q\right\|_F^2$. The probability density function of g is given by [18]:

$$p_g(v) = \frac{v^{N_r - 1}\, e^{-v/2{\sigma_\alpha}^2}}{(2{\sigma_\alpha}^2)^{N_r}(N_r - 1)!} \tag{A-5.9}$$

The unconditioned PEP $P\left(\boldsymbol{x}_{kq} \rightarrow \boldsymbol{x}_{k\hat{q}}\right)$ can therefore be formulated as:

$$P\left(\boldsymbol{x}_{kq} \rightarrow \boldsymbol{x}_{\hat{k}q}\right) = \int_0^{\infty} P\left(\boldsymbol{x}_{kq} \rightarrow \boldsymbol{x}_{\hat{k}q} \middle| \boldsymbol{H}\right) p_g(v)\, dv \tag{A-5.10}$$

$$= \int_0^{\infty} Q\left(\sqrt{v}\right) p_g(v)\, dv$$

The closed form solution for (A-5.10) is provided in [21]:

$$P\left(\boldsymbol{x}_{kq} \rightarrow \boldsymbol{x}_{\hat{k}q}\right) = \mu_{\alpha}^{N_r} \sum_{w=0}^{N_r-1} \binom{N_r - 1 + w}{w} [1 - \mu_{\alpha}]^w \qquad \text{(A-5.11)}$$

where $\mu_{\alpha} = \frac{1}{2}\left(1 - \sqrt{\frac{{\sigma_{\alpha}}^2}{1+{\sigma_{\alpha}}^2}}\right)$ with ${\sigma_{\alpha}}^2 = (\rho/8)\left|\boldsymbol{X}_q\right|^2$.

The P_a applicable to GSM-CR is therefore obtained by substituting (A-5.11) into (A-5.1) as follows:

$$P_a \leq \sum_{k=1}^{c} \sum_{q=0}^{M-1} \sum_{\hat{k}=1}^{c} \frac{N\left(k, \hat{k}\right)\mu_{\alpha}^{N_r} \sum_{w=0}^{N_r-1} \binom{N_r - 1 + w}{w} [1 - \mu_{\alpha}]^w}{cM} \qquad \text{(A-5.12)}$$

Appendix A-6

$$[\hat{k}, \hat{q}] = \underset{k, \boldsymbol{X}_q}{\text{argmax}}\, p_y\left(\boldsymbol{y} \middle| \boldsymbol{x}_{kq}, \boldsymbol{H}\right) \tag{A-6.1}$$

$$= \underset{k, \boldsymbol{X}_q}{\text{argmin}} \left\| \boldsymbol{y} - \sqrt{\frac{\rho}{2}}\, \boldsymbol{h}_k' \boldsymbol{X}_q \right\|_F^2$$

$$= \underset{k, \boldsymbol{X}_q}{\text{argmin}} \|\boldsymbol{y}\|_F^2 - \sqrt{\frac{\rho}{2}} \boldsymbol{y}^H \boldsymbol{h}_k' \boldsymbol{X}_q - \sqrt{\frac{\rho}{2}} \boldsymbol{y} \left(\boldsymbol{h}_k' \boldsymbol{X}_q\right)^H + \left\| \sqrt{\frac{\rho}{2}} \boldsymbol{h}_k' \boldsymbol{X}_q \right\|_F^2$$

$$= \underset{k, \boldsymbol{X}_q}{\text{argmin}} \|\boldsymbol{y}\|_F^2 - \left(\sqrt{\frac{\rho}{2}} \boldsymbol{y}^H \boldsymbol{h}_k' \boldsymbol{X}_q + \left(\sqrt{\frac{\rho}{2}} \boldsymbol{y}^H \boldsymbol{h}_k' \boldsymbol{X}_q \right)^H \right) + \left\| \sqrt{\frac{\rho}{2}} \boldsymbol{h}_k' \boldsymbol{X}_q \right\|_F^2$$

Using $V + V^H = 2Re(V)$

$$[\hat{k}, \hat{q}] = \underset{k, \boldsymbol{X}_q}{\text{argmin}} \|\boldsymbol{y}\|_F^2 + \left\| \sqrt{\frac{\rho}{2}} \boldsymbol{h}_k' \boldsymbol{X}_q \right\|_F^2 - 2Re\left\{ \sqrt{\frac{\rho}{2}} \boldsymbol{y}^H \boldsymbol{h}_k' \boldsymbol{X}_q \right\} \tag{A-6.2}$$

Since $\|\boldsymbol{y}\|_F^2$ is constant for all $\hat{k}$ and $\hat{q}$, (A-6.2) may be written as:

$$[\hat{k}, \hat{q}] = \underset{k, \boldsymbol{X}_q}{\text{argmin}} \sqrt{\frac{\rho}{2}} \left\| \boldsymbol{h}_k' \boldsymbol{X}_q \right\|_F^2 - 2Re\left\{ \boldsymbol{y}^H \boldsymbol{h}_k' \boldsymbol{X}_q \right\} \tag{A-6.3}$$

References

[1] R. Mesleh, H. Haas, S. Sinanovic, *et al.*, "Spatial modulation," *IEEE Trans. Veh. Technol.*, vol. 57, no. 4, pp. 2228-2241, Jul. 2008.

[2] J. Jeganathan, A. Ghrayeb and L. Szczecinski, "Spatial modulation: Optimal detection and performance analysis," *IEEE Commun. Lett.*, vol. 12, no. 8, pp. 545-547, Aug. 2008.

[3] M. D. Renzo, H. Haas and P. M. Grant, "Spatial modulation for multiple antenna wireless systems: a survey," *IEEE Commun. Mag.*, vol. 49, no. 12, pp. 182-191, Dec. 2011.

[4] G. J Foschini, "Layered space-time architecture for wireless communication in a fading environment when using multi-element antennas," *Bell Labs Technol. J.*, vol. 1, no. 2, pp. 41-59, 1996.

[5] S. M. Alamouti, "A simple transmit diversity technique for wireless communications," *IEEE J. Sel. Areas Commun.*, vol.16, no. 8, pp. 1451–1458, Oct. 1998.

[6] M. D Renzo, H. Haas, A. Ghrayeb, *et al.*, "Spatial modulation for generalized MIMO: Challenges opportunities and implementation," *Proc. IEEE*, vol. 102, no.1, pp. 56-103, Jan. 2014.

[7] P. Yang, M. D. Renzo, Y. Xiao, *et al.*, "Design guidelines for spatial modulation," *IEEE Commun. Surveys Tuts.*, vol. 17, no. 1, pp. 6-26, May 2014.

[8] A. Younis, N. Serafimovski, R. Mesleh, *et al.*, "Generalised spatial modulation," *Proc. Signals, Syst. Comput.*, pp. 1498–1502, Nov. 2010.

[9] N. Ma, A. Wang, C. Han, *et al.*, "Adaptive joint mapping generalized spatial modulation," *Proc. IEEE Int. Conf. Commun.*, pp. 520-523, Aug. 2012.

[10] Y. Zou, D. Yuan, X. Zhou, *et al.*, "Trellis coded generalised spatial modulation," *Proc. IEEE Veh. Technol. Conf.*, pp. 1-5, May 2014.

[11] K. Sundaravadivu and S. Bharathi, "STBC codes for generalized spatial modulation in MIMO systems," *Proc. Int. Conf. on Emerging Trends in Computing, Commun. and Nanotechnology*, pp. 486-490, Mar. 2013.

[12] Z. Yiğit and E. Basar, "High rate generalised spatial modulation," *Proc. IEEE. Conf. Signal Process. and Applicat.*, pp. 117-120, May 2016.

[13] K. G Seddik, A. S Ibrahim and K. J. Liu, "Trans-modulation in wireless relay networks," *IEEE Commun. Lett.*, vol. 12, no. 3, pp. 170-73, Mar. 2008.

[14] H. Samra, Z. Ding and P. Hahn, "Symbol mapping diversity design for multiple packet transmission," *IEEE Trans. on Commun.*, vol. 53, no. 5, pp. 810-807, May 2005.

[15] J. Wang, S. Jia and J. Song, "Generalised spatial modulation with multiple active antenna and low complexity detection scheme," *IEEE Trans. on Wireless Commun.*, vol. 11, no. 4, pp.1605-1615, Apr. 2012.

[16] R. Mesleh, S. Engelken, H. Haas, *et al*, "Analytical SER calculation of spatial modulation," *Proc. IEEE Int. Symp. Spread Spectrum Technol. Appl.*, pp. 272–276, Aug. 2008.

[17] M. D. Renzo and H. Haas, "Bit error probability of SM-MIMO over generalized fading channels," *IEEE Trans. Veh. Technol.*, vol. 61, no. 3, pp. 1124 – 1144, Jan. 2012.

[18] J. G. Proakis, *Digital communications*, 4th ed. New York: Mcgraw-Hill, 2001

[19] I. Al-Shahrani, "Performance of M-QAM over generalized mobile fading channels using MRC diversity," M.S thesis King Saud University, Riya, Saudi Arabia, Feb. 2007.

[20] M. K Simon and M. S Alouni, *Digital communication of fading channels – A unified approach to performance analysis*,1st ed. New York: John Wiley and Sons, 2000.

[21] N. R. Naidoo, H. Xu and T. Quazi, “Spatial modulation: Optimal detector asymptotic performance and multiple-stage detection,” *IET Commun.*, vol. 5, no. 5, pp. 1368-1376, Aug. 2011.

Paper B

A Low Complexity Detection Scheme for Generalised Spatial Modulation with Constellation Reassignment

Nigel Naidoo and Hongjun Xu

Prepared for submission to *IET Communications Journal*

Abstract

Generalised spatial modulation with constellation reassignment (GSM-CR) is a recently proposed multiple-input multiple-output (MIMO) technique which exhibits significantly enhanced bit error rate (BER) performance over conventional generalised spatial modulation (GSM). In this paper, we propose a low complexity GSM-CR detection scheme called zero-forcing maximum likelihood (ZF-ML). The ZF-ML detector is capable of attaining near-ML BER performance and has computational complexity that is independent of the order of digital modulation employed. Performance and complexity comparisons between the ZF-ML GSM-CR detector and popular GSM and GSM-CR detectors reveals that for the $N_t \times 4$ 64QAM configuration: i) the ZF-ML GSM-CR detector reduces computational complexity at the receiver by up to 60% and exhibits similar BER performance when compared to the ML GSM-CR detection scheme; ii) ZF-ML configured with two candidate symbols per initial symbol estimate reduces the receiver complexity by up to 60% whilst ZF-ML configured with eight candidate symbols per initial symbol estimate achieves gains of up to 5 dB, at a BER of 10^{-5}, when compared to the ML GSM detector; iii) for systems that encode more than one information bit in the spatial domain, certain ZF-ML configurations operate at a higher computational complexity of up to 235% when compared to the signal vector GSM (SV GSM) detector. However, the higher computational complexity imposed by the ZF-ML GSM-CR detector is traded-off by significant gains of up to 5 dB, at a BER of 10^{-5}, when compared to the SV GSM detection scheme.

1. Introduction

Multiple-input multiple-output (MIMO) digital communication techniques are key enablers for future applications that require higher data rates, enhanced quality of service and improved spectral efficiencies [1, 2]. Spatial modulation (SM) is a relatively new MIMO technique proposed in [3, 4], which overcomes the inter-antenna synchronisation and inter-channel interference challenges confronting popular MIMO schemes such as the vertical bell layered space-time (V-BLAST) architecture [5]. SM ushered in a novel approach to MIMO transmission where the location of the transmit antenna active during a particular timeslot and a conventional M-ary quadrature amplitude modulation symbol (MQAM) are both used to convey information. The use of the transmit antenna location as an information bearing unit is a key feature of SM, which increases the overall spectral efficiency by the base-two logarithm of the number of transmit antennas [4].

Despite its favourable properties, the spectral efficiency attainable by SM is limited since only one active transmit antenna is employed in a particular timeslot. This led to the development of generalised spatial modulation (GSM) in [6], which is basically an extension of the SM scheme that permits multiple active transmit antennas. Therefore, GSM increases the overall spectral efficiency by the base-two logarithm of the number of transmit antenna combinations, as compared to SM employing the same number of transmit antennas [6]. However, for identical configurations, the bit error rate (BER) performance of GSM is limited and degraded compared to SM [6].

Several GSM schemes, with enhanced error performance, have been developed to date. Relevant examples to mention are: i) generalised spatial modulation with constellation reassignment (GSM-CR) in [7] that employs the constellation reassignment (CR) [8] technique in conjunction with GSM in order to maximise the minimum Euclidean distance between transmitted symbol pairs, thereby improving BER performance; ii) space-time block coded generalised spatial modulation (STBC-GSM) in [9] that exploits the advantages of space-time block coding in order to deliver improved BER performance as compared to conventional GSM; iii) a new high-rate generalised spatial modulation (HR-GSM) scheme in [10] that encodes additional information through simultaneous transmission of different symbols. HR-GSM was demonstrated

to outperform conventional GSM and SM, in terms of BER and iv) the optimisation of the signal-spatial constellation of GSM in [11] in order to deliver improved BER performance.

This paper focusses on the GSM-CR scheme, which is deemed particularly favourable due to its inherent ability to provide gains of up to 5 dB, at a BER of 10^{-5}, when compared to GSM [7]. Moreover, it will be shown that GSM-CR achieves the aforementioned gains while maintaining computational complexity equivalent to that of GSM. In GSM-CR, a pair of transmitted symbols and the index of the active transmit antenna pair are both used to convey information. The ML GSM-CR detector in [7] performs an exhaustive search over all possible combinations of transmitted symbol and transmit antenna pair. This leads to a highly complex receiver structure, particularly when, *inter alia*, high order digital modulation techniques are employed. The ML GSM detector, similarly, performs an exhaustive search over all possible combinations of transmitted symbols and transmit antenna groupings and is therefore also prone to the highly complex receiver structure.

Several low complexity GSM detection schemes have been proposed to address the computational complexity constraint imposed by the ML detector. A non-exhaustive account of notable developments in this regard include, *inter alia*: i) the signal vector (SV) based detector in [12] that operates over two stages. In the first stage the most likely transmit antenna pair indices are determined based on the minimum Hermitian angle between the received signal vector and the combined channel vector. Thereafter in the second stage, the modulated symbol is estimated by computing the difference between the normalised projection of the received symbol in the direction of combined channel and the actual transmitted symbols [12]. The SV GSM detector was shown to operate with much lower complexity as compared to the ML GSM detector and exhibited near-ML BER performance in both the high and low signal-to-noise ratio (SNR) regions; ii) enhanced Bayesian compressive sensing (EBCS) in [13] that formulates GSM detection as a sparse recovery problem with a fixed sparsity constraint. Despite its low complexity detection properties, EBCS performs sub-optimally in the low SNR region. Moreover, the scheme is only applicable under special circumstances in which the number of receive antennas must be less than the

square of the number of transmit antennas; iii) ordered block minimum-mean-squared-error (OB-MMSE) in [14], which uses an ordering algorithm to sort possible transmit antenna combinations and then applies the minimum-mean-square-error equaliser for the recovery of the signal vector. OB-MMSE results in much lower complexity than the ML GSM detector but performs sub-optimally in the low SNR region; iv) a maximum receive ratio combining (MRRC) scheme proposed in [15] for the detection of the active transmit antenna combination and modulated symbol. However, this scheme is only applicable under certain special channel assumptions; v) an iterative zero forcing (I-ZF) detection scheme for GSM was proposed in [16]. The I-ZF detector significantly reduced complexity in comparison to the ML detector but at the expense of poor BER performance [16].

Of the aforementioned techniques, the SV GSM detector is deemed particularly favourable due to its ability to significantly reduce computational complexity, its flexibility to operate under conventional channel conditions with various antenna configurations and its demonstrable near-ML BER performance across the entire SNR range [12]. Despite its favourable application in conventional GSM, the SV detector cannot be utilised in GSM-CR. In particular, the minimum Hermitian angle metric, which is the basis for active transmit antenna pair detection in the SV scheme, is not applicable to GSM-CR systems.

The infeasible implementation of the ML detector and the fact that low complexity GSM-CR detectors are yet to be investigated, serve as motivating factors for the development of a low complexity detection scheme for GSM-CR. In this paper, we propose a novel low complexity GSM-CR detection scheme, termed zero-forcing maximum likelihood (ZF-ML). The proposed scheme implements both zero-forcing (ZF) and ML with a view of inheriting the desirable properties of its constituent detectors, namely the low complexity of ZF [17] and the optimal BER performance of ML [17]. With regard to the selection of constituent detectors in the proposed scheme, ZF was specifically chosen since it is the simplest MIMO detector [17] and ML due to its ability to provide optimal BER performance.

The proposed ZF-ML scheme employs a two-stage process for the detection of the active transmit antenna pair index and transmitted symbol pair. Stage one utilises the

ZF detector in order to obtain initial estimates of symbol pairs that may have been transmitted by each transmit antenna pair. In order to improve the probability of correct detection, additional candidate symbol pairs in the neighbourhood of the initial symbol estimates are generated, where the number of additional candidate symbol pairs selected presents a trade-off between the complexity and BER performance of the ZF-ML detector. Stage two then applies the ML detector over a reduced search space comprising combinations of transmit antenna pair and most probable transmitted symbol pair estimates obtained from stage one.

The conventional ML GSM-CR detector performs an exhaustive search over all possible combinations of transmit antenna pair and transmitted symbol pair, whereas the ZF-ML scheme operates over a reduced search space due to its two stage operation. As a result, the ZF-ML detector is capable of operating at a lower computational complexity. Moreover, the computational complexity of ZF-ML is only a function of the number of candidate symbol pairs selected in stage one, the number of transmit antenna combinations and the number of receive antennas, and is therefore independent of the order of digital modulation technique used in GSM-CR. Note that this paper discusses the ZF-ML detector specifically in the context of 64QAM GSM-CR systems, however ZF-ML may be applied to any GSM-CR configuration.

The rest of this paper is structured as follows: Sections 2 and 3 review the GSM-CR and GSM system models and various detection schemes, respectively. The novel ZF-ML GSM-CR detector is proposed in section 4. Section 5 analyses the computational complexity of the ZF-ML detector and existing GSM-CR and GSM detection schemes. Section 6 presents average BER and complexity comparisons of the various GSM and GSM-CR detection schemes, including the proposed ZF-ML detector. Finally, section 7 concludes the paper.

1.1 Notation

Bold italics upper/lower case symbols denote matrices/vectors, while regular letters represent scalar quantities. We use $\lfloor\cdot\rfloor$, $(\cdot)^T$, $(\cdot)^H$, $E[\cdot]$, $|\cdot|$, $\|\cdot\|_F$, $arccos(\cdot)$ for the floor, transpose, Hermitian, expectation, Euclidean norm, Frobenius norm and arccosine operations, respectively.

2. System Models

2.1 Generalised Spatial Modulation with Constellation Reassignment

Consider the $N_t \times N_r$ MQAM GSM-CR system proposed in [7] that utilises $c = 2^{\left\lfloor log_2\binom{N_t}{2} \right\rfloor}$ transmit antenna pairs, where N_t is the number of transmit antennas, N_r the number of receive antennas and M refers to the order of the quadrature amplitude modulation scheme employed. The basic idea behind GSM-CR is to map a stream of $m_T = log_2 c + log_2 M$ input bits such that the first $\log_2 c$ input bits determine the active transmit antenna pair identified by the index $k \in [1:c]$. The remaining $log_2 M$ input bits are assigned to a pair of MQAM symbols x_q and $\tilde{x}_q$, where $q \in [0: M-1]$ is the decimal equivalent of the $log_2 M$ input bit sequence and the index identifying the transmitted symbol pair.

The symbol pair $[x_q \ \tilde{x}_q]^T$ originates from what is termed primary and secondary MQAM signal constellations, where the primary constellation $\boldsymbol{X}^{Prm}$ is a conventional Gray-coded signal constellation and the secondary constellation $\boldsymbol{X}^{Sec}$ is generated by assigning symbols with adjacent points in the primary constellation to non-adjacent points in the secondary constellation and *vice versa*, in accordance with the CR technique [8]. The application of the CR technique increases the minimum Euclidean distance between the transmitted symbol pairs in GSM-CR as compared to conventional GSM. This is the principal reason for GSM-CR exhibiting improved BER performance when compared to conventional GSM. Secondary signal constellation design for 16QAM and 64QAM GSM-CR systems is covered in [7].

Given that GSM-CR utilises two active transmit antennas in a given timeslot, the transmitted signal vector can be expressed as follows [7]:

$$\boldsymbol{x}_{kq} = \underset{\substack{\uparrow \\ k_1{}^{th}\ position}}{0} \ \underset{\substack{\uparrow \\ 1^{st}\ position}}{x_q} \ \ldots\ldots \ \underset{\substack{\uparrow \\ k_2{}^{th}\ position}}{\tilde{x}_q} \ \ldots\ldots 0 \ \underset{\substack{\uparrow \\ N_t{}^{th}\ position}}{0}\Big]^T e^{j\theta_k} \qquad \text{(A.1)}$$

where k_1 and $k_2 \in [1:N_t]$ are active transmit antennas from the k^{th} transmit antenna pair. $E\left\{|x_q|^2\right\} = E\left\{|\tilde{x}_q|^2\right\} = 1$. θ_k denotes the rotation angle applied to the transmitted symbol pair $\left[x_q\ \tilde{x}_q\right]^T$, emitted from the k^{th} transmit antenna pair. The process for selecting appropriate rotation angles is addressed in [7].

After the mapping process, antennas k_1 and k_2 from the k^{th} transmit antenna pair simultaneously transmit the respective symbols x_q and $\tilde{x}_q$ over the $N_r \times N_t$ MIMO wireless channel $\boldsymbol{H}$. The received signal vector is given by [7]:

$$\boldsymbol{y} = \sqrt{\frac{\rho}{2}}\boldsymbol{H}\boldsymbol{x}_{kq} + \boldsymbol{n} \tag{B.2}$$

where $\boldsymbol{y}$ is the $N_r \times 1$ dimensional received signal vector. $\boldsymbol{H} = [\boldsymbol{h}_1\ \boldsymbol{h}_2 \ldots \boldsymbol{h}_a \ldots \boldsymbol{h}_{N_t}]$ and $\boldsymbol{h}_a$ is the $N_r \times 1$ dimensional vector corresponding to transmit antenna a. ρ is the average SNR at each receive antenna. $\boldsymbol{n}$ represents the $N_r \times 1$ dimensional additive white Gaussian noise (AWGN). $\boldsymbol{n}$ and $\boldsymbol{H}$ have independent and identically distributed (i.i.d.) entries according to the complex Gaussian distribution $CN(0,1)$.

An alternative but equivalent representation of the received signal vector is as follows [7]:

$$\boldsymbol{y} = \sqrt{\frac{\rho}{2}}\boldsymbol{h}'_k\boldsymbol{X}_q + \boldsymbol{n} \tag{B.3}$$

where $\boldsymbol{X}_q = \left[x_q \quad \tilde{x}_q\right]^T e^{j\theta_k}$ is the transmitted symbol pair subjected to a predefined rotation angle θ_k. $\boldsymbol{h}'_k = \left[\boldsymbol{h}_{k_1}\ \boldsymbol{h}_{k_2}\right]$ is an $N_r \times 2$ dimensional channel matrix comprising $N_r \times 1$ dimensional channel vectors $\boldsymbol{h}_{k_1}$ and $\boldsymbol{h}_{k_2}$, which correspond to the active transmit antennas k_1 and k_2, respectively.

2.2 Generalised Spatial Modulation

GSM configured with two active transmit antennas and GSM-CR differ in one aspect in that the former transmits the same symbols within a particular timeslot, whereas the latter transmits different symbols. The system model presented in section 2.1 can therefore be used to describe GSM configurations with two active transmit antennas, with the exception that the transmitted symbol pair is redefined as $\left[x_q \quad x_q\right]^T$.

3. Current Detection Schemes

3.1 Maximum Likelihood GSM and GSM-CR Detector

The optimal detector, which is based on the ML principle, performs a joint detection of the active transmit antenna pair and the transmitted symbol pair in accordance with the following rule [7]:

$$\left[\hat{k},\hat{q}\right] = \underset{k,\boldsymbol{X}_q}{argmax}\, p_y\left(\boldsymbol{y}|\boldsymbol{x}_{kq},\boldsymbol{H}\right) \tag{B.4}$$

$$= \underset{k,\boldsymbol{X}_q}{argmin}\left(\left\|\boldsymbol{h}_k'\boldsymbol{X}_q\right\|_F^2 - 2Re\left\{\boldsymbol{y}^{\boldsymbol{H}}\boldsymbol{h}_k'\boldsymbol{X}_q\right\}\right)$$

where $p_y\left(\boldsymbol{y}|\boldsymbol{x}_{kq},\boldsymbol{H}\right) = \pi^{-N_r} exp\left(\left\|\boldsymbol{y} - \sqrt{\frac{p}{2}}\boldsymbol{h}_k'\boldsymbol{X}_q\right\|_F^2\right)$ is the probability density function of $\boldsymbol{y}$ conditioned on $\boldsymbol{H}$ and $\boldsymbol{x}_{kq}$, $\hat{k}$ is the estimated active transmit antenna pair index and $\hat{q}$ is the estimated transmitted symbol pair index. Note that $\boldsymbol{X}_q = \begin{bmatrix} x_q & x_q \end{bmatrix}^T$ in the case of GSM schemes and $\boldsymbol{X}_q = \begin{bmatrix} x_q & \tilde{x}_q \end{bmatrix}^T e^{j\theta_k}$ for GSM-CR.

3.2 Signal Vector GSM Detector

The SV detector in [12] is characterised by low computational complexity and near-ML BER performance. Consider an $N_t \times N_r$ MQAM GSM system with two active transmit antennas. The SV detector determines the most likely estimates of the active transmit antenna pair based on the minimum Hermitian angle between the combined channel vector $\boldsymbol{h}_k'' = \boldsymbol{h}_{k_1} + \boldsymbol{h}_{k_2}$ and received signal vector $\boldsymbol{y}$. It should be noted that in the absence of noise, the received signal vector $\boldsymbol{y}$ and combined channel vector $\boldsymbol{h}_k''$ lie in the same direction, which corresponds to a Hermitian angle of zero.

The SV detector first determines the most probable active transmit antenna pair estimates in accordance with the following [12]:

$$\boldsymbol{\Gamma} = [j_1\, j_2 \ldots . j_\ell \ldots j_c] = argsort(\emptyset) \text{ with } \emptyset = \left[\emptyset_1\ \emptyset_2 \ldots \emptyset_j \ldots \emptyset_c\right] \tag{B.5}$$

$$\emptyset_j = arccos\ \left|\delta_j\right| \text{ with } \delta_j = \frac{\langle \boldsymbol{h}_j'', \boldsymbol{y}\rangle}{\left\|\boldsymbol{h}_j''\right\|_F \|\boldsymbol{y}\|_F} \tag{B.6}$$

where **Γ** denotes an ordered list of transmit antenna pair indices ranging in probability of occurrence from most to least. j_1 and j_c correspond to the indices of the respective minimum and maximum values in $\emptyset$ and $argsort$ is a function that arranges inputs in ascending order. $\boldsymbol{h}_j'' = [\boldsymbol{h}_{a_1} + \boldsymbol{h}_{a_2}]$ is the combined channel vector for the transmit antenna pair $j \in [1: c]$ with corresponding transmit antennas a_1 and $a_2 \in [1: N_t]$ and $\emptyset_j$ represents the Hermitian angle between the combined channel vector $\boldsymbol{h}_j''$ and received signal vector $\boldsymbol{y}$.

The transmitted symbol associated with each of the ℓ most likely estimates of active transmit antenna pair is computed as follows [12]:

$$\hat{x}_q^{j_{can}} = \min_{x_q} \left| \omega_{j_{can}} - x_q \right|^2 \tag{B.7}$$

where $\omega_{j_{can}} = \frac{\langle \boldsymbol{h}_{j_{can}}'', \boldsymbol{y} \rangle}{\left\| \boldsymbol{h}_{j_{can}}'' \right\|_F^2}$ and $\hat{x}_q^{j_{can}}$ is the symbol associated with transmit antenna pair $j_{can} \in [j_1\ j_2 \ldots . j_\ell]$.

The final estimates of the active transmit antenna pair and transmitted symbol are obtained by computing the following detection rule, which considers ℓ possible combinations of transmit antenna pair and transmitted symbol as inputs [12]:

$$[\hat{k}, \hat{q}\,] = \min_{j_{can}, \hat{x}_q^{j_{can}}} \left\| \boldsymbol{y} - \boldsymbol{h}_{j_{can}}'' \hat{x}_q^{j_{can}} \right\|_F^2 \tag{B.8}$$

where $\hat{k}$ is the estimated index of the active transmit antenna pair and $\hat{q}$ is the estimated index of the transmitted symbol.

Despite its favourable application in conventional GSM, the SV scheme is not appropriate for GSM-CR systems. This can be attributed to the fact that GSM-CR transmits different symbols from each transmit antenna, thus yielding a received signal vector of the form $y = \boldsymbol{h}_{k_1} x_q + \boldsymbol{h}_{k_2} \tilde{x}_q$. The received signal vector $\boldsymbol{h}_{k_1} x_q + \boldsymbol{h}_{k_2} \tilde{x}_q$ does not lie in the same direction as the combined channel vector $\boldsymbol{h}_k'' = \boldsymbol{h}_{k_1} + \boldsymbol{h}_{k_2}$ and therefore the minimum Hermitian angle metric, which is the basis for active transmit antenna pair detection in the SV scheme, is not applicable in the context of GSM-CR systems.

4. Proposed Zero-Forcing Maximum Likelihood Detector

The ML GSM-CR detector performs a brute force search over all possible cM combinations of transmit antenna pair index and transmitted symbol pair. The search space increases rapidly with the order of modulation, thereby resulting in a highly complex receiver structure. The proposed ZF-ML detection scheme has been developed such that the computational complexity of the receiver is independent of the order of modulation, thereby addressing the complexity constraint imposed by high order MQAM GSM-CR schemes that employ the ML detector.

The ZF-ML detector follows a two-stage process: Stage one utilises the low complexity ZF detector as a basis for generating a reduced search space, comprising the most probable candidate symbol pairs associated with each transmit antenna pair. Stage two applies the ML detector to the reduced search space to obtain a final estimate of the active transmit antenna pair and transmitted symbol pair.

4.1 Stage One: Zero-Forcing

In stage one, the zero forcing detector is applied in order to obtain initial estimates of the primary and secondary symbols that may have been emitted by each transmit antenna pair, as follows:

$$\boldsymbol{r}_j = \boldsymbol{h}_j{}^{\dagger}\boldsymbol{y} = \begin{bmatrix} r_j^{a_1} & r_j^{a_2} \end{bmatrix}^T \tag{B.9}$$

where $\boldsymbol{r}_j$ is a 2×1 dimensional vector comprising a pair of equalised symbols and $\boldsymbol{h}_j{}^{\dagger} = \left(\boldsymbol{h}_j'^{H}\boldsymbol{h}_j'\right)^{-1}\boldsymbol{h}_j'^{H}$ is the pseudo inverse matrix. $r_j^{a_1}$ and $r_j^{a_2}$ are equalised symbols associated with respective transmit antennas a_1 and $a_2 \in [1:N_t]$ from transmit antenna pair $j \in [1:c]$.

The equalised symbols are then demodulated, thus yielding the following initial primary and secondary symbol estimates associated with a particular transmit antenna pair j:

$$\left[x_{q_{1,1}}^{a_1}\, x_{q_{2,1}}^{a_2}\right] = \left[\mathcal{D}_P\left(r_j^{a_1}\right)\mathcal{D}_S\left(r_j^{a_2}\right)\right] \tag{B.10}$$

where the subscripts in $x_{a,b}^{a_1}$ denote the index identifying a primary symbol and (a) and candidate symbol number (b). The subscripts in $x_{c,d}^{a_2}$ denote the index identifying a secondary symbol and (c) and candidate symbol number (d). $\mathcal{D}_P(\cdot)$ and $\mathcal{D}_s(\cdot)$ are the constellation demodulator functions that map $r_j^{a_1}$ and $r_j^{a_2}$ to symbols in the respective primary and secondary signal constellations. It should be noted that the equalised symbols in (B.9) and the resulting demodulated symbols in (B.10) are generated independently. Therefore, the initial symbol estimate $\left[x_{q_{1,1}}^{a_1}\, x_{q_{2,1}}^{a_2}\right]^T$ may not necessarily be a valid CR mapping of primary to secondary symbol and *vice-versa*, as defined in [8].

The multiplication of the received signal vector $\boldsymbol{y}$ by the pseudo inverse matrix $\boldsymbol{h}_j{}^{\dagger}$ amplifies the noise term $\boldsymbol{n}$, which may compromise the integrity of the initial primary and secondary symbol estimates. Therefore, in order to enhance the probability of correct symbol detection, both the initial primary and secondary symbol estimates as well as n_c of their nearest neighbouring symbols in their respective signal constellations are considered as potential candidates.

An illustrative example of candidate symbol selection in a primary 64QAM signal constellation, for varying values of n_c, based on an initial symbol estimate that falls within the first quadrant, is depicted in Figure B.1. As shown in Figure B.1, stage one of the ZF-ML detector may employ $n_c \in [2, 4, 8]$. A description of the varying n_c configurations for the 64QAM GSM-CR configuration follows:

i. For $n_c = 2$, two candidate symbols located at a Euclidean distance of $\frac{2}{\sqrt{42}}$ relative to the initial symbol estimate are selected. For a given initial symbol estimate there may exist four possible candidate symbols that meet the Euclidean distance criterion; however only two candidates located vertically or horizontally relative to the initial symbol estimate are selected.

ii. For $n_c = 4$, four candidate symbols located at a Euclidean distance of $\frac{2}{\sqrt{42}}$ relative to the initial symbol estimate are selected. These candidate symbols will typically be located horizontally and vertically relative to the initial symbol estimate.

iii. For $n_c = 8$, eight candidate symbols that are located within a circle of radius $\frac{\sqrt{8}}{\sqrt{42}}$ emanating from the initial symbol estimate are selected.

It will be shown in section 6 that, for the $N_t \times 4$ 64QAM configuration, larger values of n_c yield improved BER performance at the cost of increased computational complexity. Moreover, the results presented in section 6 show that $n_c = 8$ yields near-ML BER performance and therefore there is no benefit in using larger values of n_c.

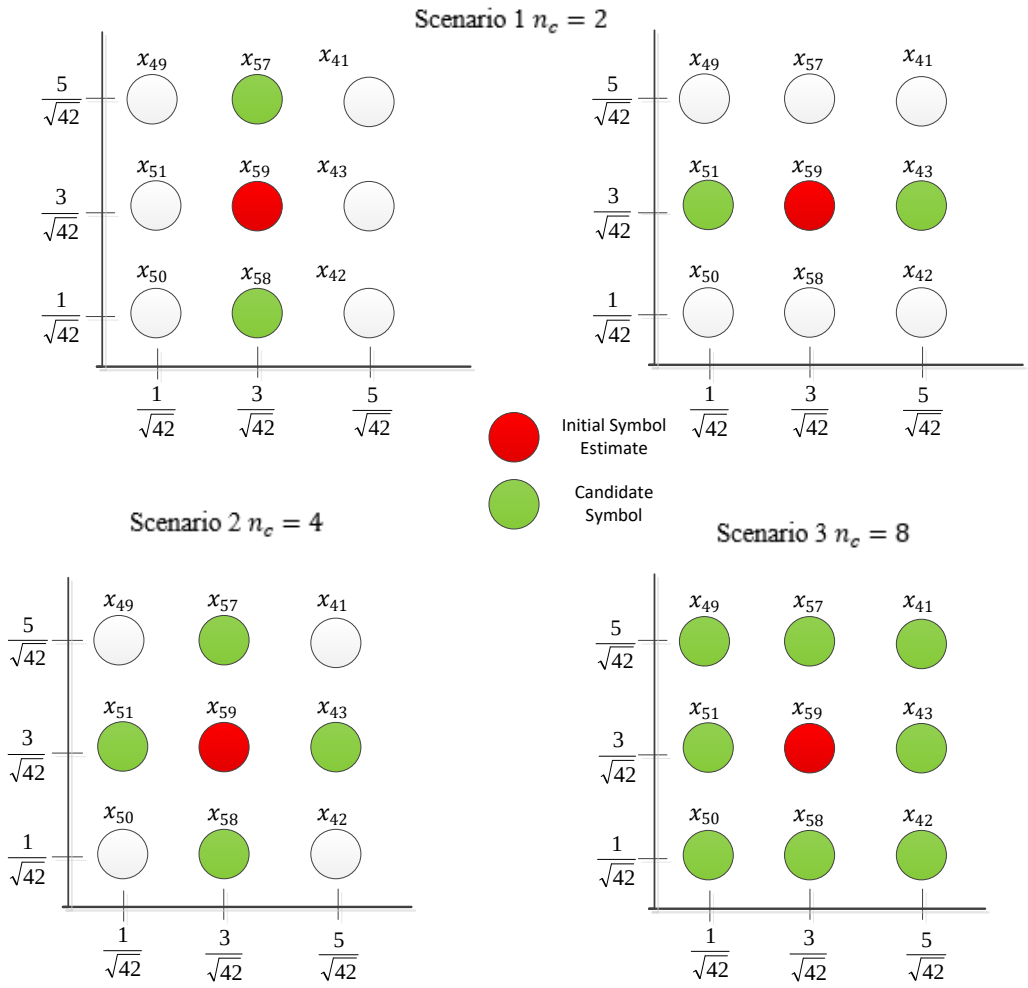

Figure B.1 Generating Candidate Symbols Based on the Initial Symbol Estimate

The initial primary and secondary symbol estimates and their associated n_c candidate symbols are generated for each transmit antenna pair j and may be represented as follows:

$$\boldsymbol{z}_j^{a_1} = \left[x_{q_{1.1}}^{a_1}\ x_{q_{1.2}}^{a_1} \quad \dots \quad x_{q_{1.n_c+1}}^{a_1}\right]^T \tag{B.11}$$

$$\boldsymbol{z}_j^{a_2} = \left[x_{q_{2.1}}^{a_1}\, x_{q_{2.2}}^{a_2} \quad \ldots \quad x_{q_{2.n_c+1}}^{a_2}\right]^T$$

where $\boldsymbol{z}_j^{a_1}$ and $\boldsymbol{z}_j^{a_2}$ are $(n_c+1)\times 1$ dimensional symbol vectors comprising the initial primary and secondary symbol estimates and their associated candidate symbols. The candidate symbols associated with $x_{q_{1,1}}^{a_1}$ and $x_{q_{2,1}}^{a_2}$ that stem from the primary and secondary constellations, respectively, are obtained from lookup tables $LT^{Prm}(\cdot)$ and $LT^{Sec}(\cdot)$. The aforementioned lookup tables will return a null value in instances where potential candidate symbols that do not meet the prescribed Euclidean distance criterion and these null values will be ignored in the subsequent application of the detection algorithm.

Thereafter, the entries in symbol vectors in $\boldsymbol{z}_j^{a_1}$ and $\boldsymbol{z}_j^{a_2}$ undergo a CR mapping process in order to generate valid primary and secondary symbol pairs. These $2(n_c+1)$ symbol pairs are considered the most probable estimates of the symbol pair, emitted from the transmit antenna pair j, and are represented as follows:

$$\begin{aligned}\boldsymbol{X}_j^{a_1} &= \left[\left\{x_{q_{1.1}}^{a_1}\, \omega^{Sec}\left(x_{q_{1.1}}^{a_1}\right)\right\} \quad \ldots \quad \left\{x_{q_{1.n_c+1}}^{a_1}\, \omega^{Sec}\left(x_{q_{1.n_c+1}}^{a_1}\right)\right\}\right] \\ \boldsymbol{X}_j^{a_2} &= \left[\left\{\omega^{Prm}\left(x_{q_{2.2}}^{a_2}\right) x_{q_{2.1}}^{a_2}\right\} \quad \ldots \quad \left\{\omega^{Prm}\left(x_{q_{2.n_c+1}}^{a_2}\right) x_{q_{2.n_c+1}}^{a_2}\right\}\right]\end{aligned} \tag{B.12}$$

where $\boldsymbol{X}_j^{a_1}$ and $\boldsymbol{X}_j^{a_2}$ each contain n_c+1 candidate symbol pairs, $\omega^{Sec}(\cdot)$ maps a primary input symbol to the corresponding secondary symbol and $\omega^{Prm}(\cdot)$ maps a secondary input symbol to the corresponding primary symbol.

4.2 Stage Two: Maximum Likelihood Detection

In stage 2, the ML detector in (B.4) is employed over the reduced search space of $2c(n_c+1)$ combinations of transmit antenna pair and most probable transmitted symbol pair estimates in order to yield a final estimate as follows:

$$\left[\hat{k}, \hat{q}\right] = \underset{k,\boldsymbol{W}_j}{argmin}\left(\left\|\boldsymbol{h}_k'\boldsymbol{W}_j\right\|_F^2 - 2Re\left\{\boldsymbol{y}^H\boldsymbol{h}_k'\boldsymbol{W}_j\right\}\right) \tag{B.13}$$

where $\boldsymbol{W}_j \in \left[\boldsymbol{X}_{\boldsymbol{j}}^{a_1} e^{j\theta_j} \cup \boldsymbol{X}_{\boldsymbol{j}}^{a_2} e^{j\theta_j}\right]$.

5. Computational Complexity Analysis

The computational complexity of the proposed ZF-ML GSM-CR detection scheme, ML GSM-CR, ML GSM and SV GSM detectors are computed in this section. The computational complexity will be formulated in terms of the number of complex additions and multiplications required for the detection of the active transmit antenna pair and transmitted symbol pair, similar to the approach adopted in [18, 19].

5.1 Maximum Likelihood GSM-CR Detector

The computational complexity of the ML GSM-CR detector was not addressed in [7], however this issue will be thoroughly investigated in this paper. Considering the ML detection rule in (B.4), the first term $\left\|\boldsymbol{h'}_k \boldsymbol{X}_q\right\|_F^2$ may be expressed as $\|\boldsymbol{h'}_k\|_F^2 \left\|\boldsymbol{X}_q\right\|_F^2$. The $\|\boldsymbol{h'}_k\|_F^2$ operation requires $2N_r$ complex multiplications and zero complex additions, and is evaluated for $k \in [1:c]$. Therefore, the computational complexity of the operation $\|\boldsymbol{h'}_k\|_F^2$ over all possible iterations is $2cN_r$ complex multiplications and zero complex additions. Moreover, the $\left\|\boldsymbol{X}_q\right\|_F^2$ operation entails 2 complex multiplications and zero complex additions. Evaluating for $q \in [0: M-1]$ yields $2M$ complex multiplications and zero complex additions. The multiplication of $\|\boldsymbol{h'}_k\|_F^2$ by $\left\|\boldsymbol{X}_q\right\|_F^2$ involves the multiplication of real values and is therefore neglected in this complexity analysis. As a result, the computational complexity of the first term in (B.4) is given by:

$$\delta_{ML\_term1} = 2cN_r + 2M \tag{B.14}$$

The computational complexity of the second term in (B.4) is obtained by first assessing $\boldsymbol{y}^H \boldsymbol{h'}_k$. This operation involves $2N_r$ complex multiplications and $2(N_r - 1)$ complex additions. Evaluating over $k \in [1:c]$ requires $4cN_r - 2c$ complex operations.

Thereafter, the multiplication of $\boldsymbol{y}^H \boldsymbol{h'}_k$ by $\boldsymbol{X}_q$ can be observed to require two complex multiplications and one complex addition. Computing $\boldsymbol{y}^H \boldsymbol{h'}_k \boldsymbol{X}_q$ over $k \in [1:c]$ and $q \in [0: M-1]$ yields a complexity of $3cM$. Therefore, the computational complexity of the second term in (B.4) can be expressed as:

$$\delta_{ML\_term2} = 4cN_r - 2c + 3cM \quad \text{(B.15)}$$

Summing (B.14) and (B.15) yields the total computational complexity of ML-based GSM-CR detection:

$$\delta_{GSM-CR\,ML} = 6cN_r + 2M - 2c + 3cM \quad \text{(B.16)}$$

5.2 Maximum Likelihood GSM Detector

The ML detection rule for GSM and GSM-CR is given by the common expression in (B.4). Therefore, the complexity formulated in (B.16) is also applicable to ML GSM schemes. It should be noted that (B.16) differs from the complexity expression presented in [6]. This can be attributed to the fact that [6] formulates the computational complexity based on alternate non-simplified representation of the GSM ML detection rule, which differs in comparison to (B.4).

5.3 Signal Vector GSM Detector

The SV GSM detector was described in section 3.2. The generation of the ℓ most likely estimates of transmit antenna pair in (B.5) and (B.6) is first considered. As in [18, 19], the complexity associated with the $argsort$ operation in (B.5) is ignored. Inspecting the computation of δ_j in (B.6), the vector dot product operation $\langle \boldsymbol{h}_j'', \boldsymbol{y} \rangle$ requires N_r complex multiplications and $N_r - 1$ complex additions, the $\left\| \boldsymbol{h}_j'' \right\|_F$ operation involves N_r complex multiplications and zero complex additions, and the calculation of $\|\boldsymbol{y}\|_F$ requires N_r complex multiplications and zero complex additions. Therefore, evaluating δ_j for $j \in [1\colon c]$ yields a computational complexity of $4cN_r - c$. Note that the $\|\boldsymbol{y}\|_F$ and $\left\| \boldsymbol{h}_j'' \right\|_F$ operations produce real value outputs and therefore the complexity of multiplying $\|\boldsymbol{y}\|_F$ by $\left\| \boldsymbol{h}_j'' \right\|_F$ is not considered. Moreover, it follows that the product $\|\boldsymbol{y}\|_F \left\| \boldsymbol{h}_j'' \right\|_F$ is a real value and therefore the complexity associated with dividing $\langle \boldsymbol{h}_j'', \boldsymbol{y} \rangle$ by this real value quantity is not considered.

The computation of $\emptyset_j$ in (B.6) for $j \in [1\colon c]$ can be shown to entail c complex multiplications and zero complex additions, where the complexity of the $arccos$ function is ignored. Summing all the aforementioned complexity contributions yields

the total complexity associated with the generating the ℓ most likely estimates of transmit antenna pair:

$$\delta_{\ell\_ant} = 4cN_r \tag{B.17}$$

The complexity of transmitted symbol estimation in (B.7) is considered next. The complexity associated with the calculation of $\omega_{j_{can}}$ is ignored in view of the fact that $\langle \boldsymbol{h}''_{j_{can}}, \boldsymbol{y} \rangle$ and $\left\| \boldsymbol{h}''_{j_{can}} \right\|_F$ were previously computed in (B.6), and that the division by the real quantity $\left\| \boldsymbol{h}''_{j_{can}} \right\|_F^{\mathbf{2}}$ does not contribute to the complexity. The evaluation of (B.7) for ℓ symbol estimates over $q \in [0: M-1]$ requires ℓM complex mutiplications and ℓM complex additions. Therefore, the complexity associated with the generation of ℓ symbol estimates is given by:

$$\delta_{\ell\_sym} = 2\ \ell M \tag{B.18}$$

Lastly, we assess the complexity associated with obtaining the final estimate of transmit antenna pair and transmitted symbol in (B.8). The evaluation of $\left\| \boldsymbol{y} - \boldsymbol{h}''_{j_{can}} \hat{x}_q^{j_{can}} \right\|_F$ for one combination of estimated transmit antenna pair and transmitted symbol entails $2N_r$ complex multiplications and N_r complex additions. It follows that the evaluation of (B.8) over ℓ combinations of estimated transmit antenna pair and transmitted symbol carries an associated complexity of:

$$\delta_{Final} = 3\ell N_r \tag{B.19}$$

Summing (B.17), (B.18) and (B.19) yields the total computational complexity of SV-based GSM detection:

$$\delta_{GSM\ SV} = 4cN_r + 2\ell M + 3\ell N_r \tag{B.20}$$

5.4 Zero-Forcing Maximum Likelihood GSM-CR Detector

The computational complexity of the zero-forcing detector applied in stage one of the ZF-ML scheme is first assessed. Consider the formulation of the pseudo inverse matrix $\boldsymbol{h}_j{}^{\dagger} = \left(\boldsymbol{h}_j'^{H} \boldsymbol{h}'_j \right)^{-1} \boldsymbol{h}_j'^{H}$ in (B.9). The $\boldsymbol{h}_j'^{H} \boldsymbol{h}'_j$ operation requires $4N_r$ complex

multiplications and $2N_r - 2$ complex additions. The outcome of the $\boldsymbol{h}_j'^H \boldsymbol{h}_j'$ operation is a 2×2 matrix of the following form:

$$\boldsymbol{h}_j'^H \boldsymbol{h}_j' = \begin{bmatrix} a & b \\ c & d \end{bmatrix} \tag{B.21}$$

where a and d represent real numbers and b and c are complex numbers.

Taking into account the structure of (B.21) and applying the well-known identity $\begin{bmatrix} a & b \\ c & d \end{bmatrix}^{-1} = \frac{1}{ad-bc}\begin{bmatrix} d & -b \\ -c & a \end{bmatrix}$, it can be shown that the matrix inverse operation $\left(\boldsymbol{h}_j'^H \boldsymbol{h}_j'\right)^{-1}$ operation requires three complex multiplications and zero complex additions. Assessing the multiplication of $\left(\boldsymbol{h}_j'^H \boldsymbol{h}_j'\right)^{-1}$ by $\boldsymbol{h}_j'^H$, which is the last step in calculating the pseudo inverse matrix, reveals that $4N_r$ complex multiplications and $2N_r$ complex additions are needed. Summing the aforementioned complexity contributions yields the following complexity for generating a single pseudo inverse matrix:

$$\delta_{pseudo} = 12N_r + 1 \tag{B.22}$$

Finally, the $\boldsymbol{h}_k{}^{\dagger}\boldsymbol{y}$ operation in (B.9) is considered, which entails $2N_r$ complex multiplications and $2N_r - 2$ complex additions. Summing these complexity contributions with (B.22) yields a complexity of $16N_r - 1$ for one iteration of (B.9). The rule in (B.9) is evaluated for $j \in [1:c]$ and therefore the total computational complexity of the zero-forcing operation is given by:

$$\delta_{ZF} = 16cN_r - c \tag{B.23}$$

The mapping operations utilised in (B.10), (B.11) and (B.12) represent one-to-one mappings and do not impose any additional complexity [19]. Therefore, the computational complexity of the first stage of ZF-ML is given by (B.23).

The second stage detection rule described in (B.13) is considered next. It is noted that the computational complexity of the ML GSM-CR detector has already been evaluated in (B.16). Therefore, the complexity of the second stage can be attained by replacing

M in (B.16) with the reduced transmitted symbol pair search space, of size $2(n_c + 1)$, derived from stage one. This yields the following:

$$\delta_{ML} = 6cN_r + 4n_c + 6cn_c + 4c + 4 \quad \text{(B.24)}$$

Summing (B.23) and (B.24) yields the total computational complexity of the ZF-ML GSM-CR detector:

$$\delta_{ZF-ML} = 22cN_r + 4n_c + 3c + 6cn_c + 4 \quad \text{(B.25)}$$

The expression in (B.25) clearly shows that the computational complexity of ZF-ML is independent of the order of digital modulation technique employed in GSM-CR.

6. Performance and Computational Complexity Comparison

The trade-off between the computational complexity and BER performance of the various detection schemes is assessed in this section.

6.1 Computational Complexity

In this section, the computational complexity of the various GSM and GSM-CR detection schemes will be compared. The complexity expressions derived in sections 5.1 to 5.4 are evaluated for the $N_t \times 4$ 64QAM configuration and a graphical and numerical representation of results are presented in Figure B.2 and Table B.1, respectively.

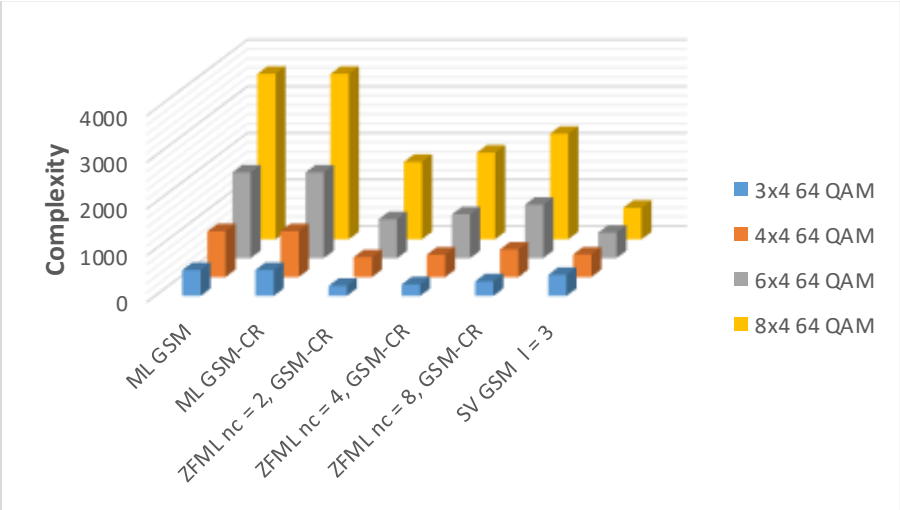

Figure B.2 Computational Complexity of Various Detection Schemes

Table B.1: Computational Complexity Comparison of Various Detection Schemes

	ML GSM	ML GSM-CR	ZFML $n_c = 2$ GSM-CR	ZFML $n_c = 4$ GSM-CR	ZFML $n_c = 8$ GSM-CR	SV GSM $l = 3$
3×4 64QAM	556	556	218	250	314	452
4×4 64QAM	984	984	424	480	592	484
6×4 64QAM	1840	1840	836	940	1148	548
8×4 64QAM	3552	3552	1660	1860	2266	676

Table B.1 shows that the proposed ZF-ML GSM-CR detector operates at a significantly lower complexity as compared to the ML GSM and ML GSM-CR detection schemes. In particular, for the 3×4 64QAM configuration, computational complexity reductions of up to 60%, 55% and 43% are observed when the ZF-ML detector, with respective n_c configurations of 2, 4 and 8, is compared to both the ML GSM and ML GSM-CR detectors. Understandably, the complexity of the ZF-ML GSM-CR detector increases with higher values of n_c. It will be demonstrated in section 6.2 that the lower complexity obtained by smaller values of n_c is offset by reduced BER performance.

Table B.1 also shows that for certain configurations, ZF-ML operates at a lower computational complexity as compared to the SV GSM detector. It should be noted that the SV GSM detector with $\ell = 3$ has been selected based on its low complexity and near-ML BER performance capabilities, which were demonstrated in [12]. For the 3×4 64QAM configuration, computational complexity reductions of 51%, 44% and 30% are observed when the ZF-ML detector with respective n_c values of 2, 4 and 8 is compared to the SV GSM detector. On the other hand, for the 8×4 64QAM configuration, increased computational complexity by 145%, 175% and 235% is observed when the ZF-ML detector with respective n_c values of 2, 4 and 8 is compared to the SV GSM detector.

In order to investigate the circumstances under which ZF-ML operates at a higher computational complexity than SV GSM, the following inequality corresponding to (B.25) being greater than (B.20) may be constructed as follows:

$$22cN_r + 4n_c + 3c + 6cn_c + 4 \; > \; 4cN_r + 2\ell M + 3\ell N_r \qquad \text{(B.26)}$$

Considering the specific system parameters of Table B.1 with $l = 3, N_r = 4$ and $M = 64$ and substituting these in (B.26) yields:

$$75c + 4n_c + 6cn_c > 416 \qquad \text{(B.27)}$$

From (B.27) it can be deduced that for the $N_t \times 4$ 64QAM GSM-CR system, the ZF-ML detector configured with $n_c = 8$ will function at a higher computational complexity in instances where more than one information bit is conveyed in the spatial domain. This outcome is confirmed by the results presented in Table B.1. It will be demonstrated in section 6.2 that the increased computational complexity of the ZF-ML detector under the aforementioned circumstances is traded-off by its far superior BER performance as compared to the SV GSM detection scheme.

Another notable observation from Table B.1 is that the SV GSM detector operates at a lower complexity as compared to the ML GSM and ML GSM-CR detectors. In particular, for the 8×4 64QAM configuration, the SV GSM detector reduces computational complexity by 81% when compared to the ML GSM and ML GSM-CR detection schemes.

6.2 Performance Comparison

In this section, the average BER of the various GSM and GSM-CR detection schemes will be compared. Monte Carlo simulations were performed under the following assumptions: i.i.d. Rayleigh flat fading channel with AWGN, as defined in section 2.1; full channel knowledge at the receiver; antennas at the transmitter and receiver are separated wide enough to avoid correlation and the total transmit power is the same for all transmissions.

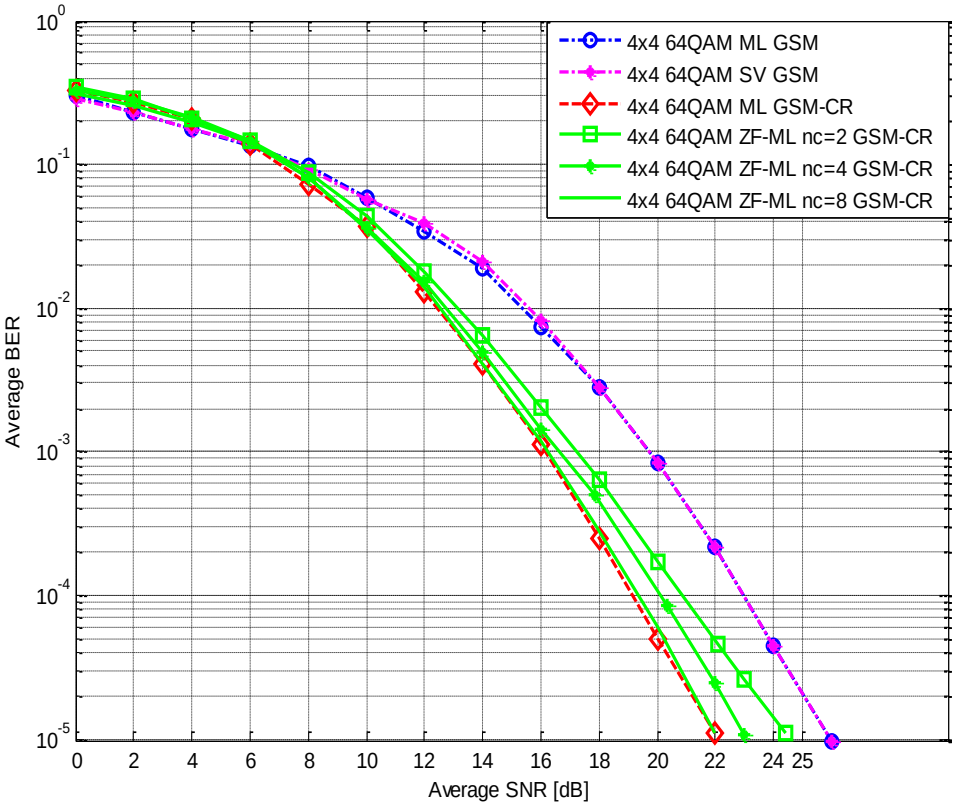

Figure B.3 Average BER - 4x4 64QAM GSM and GSM-CR Configurations

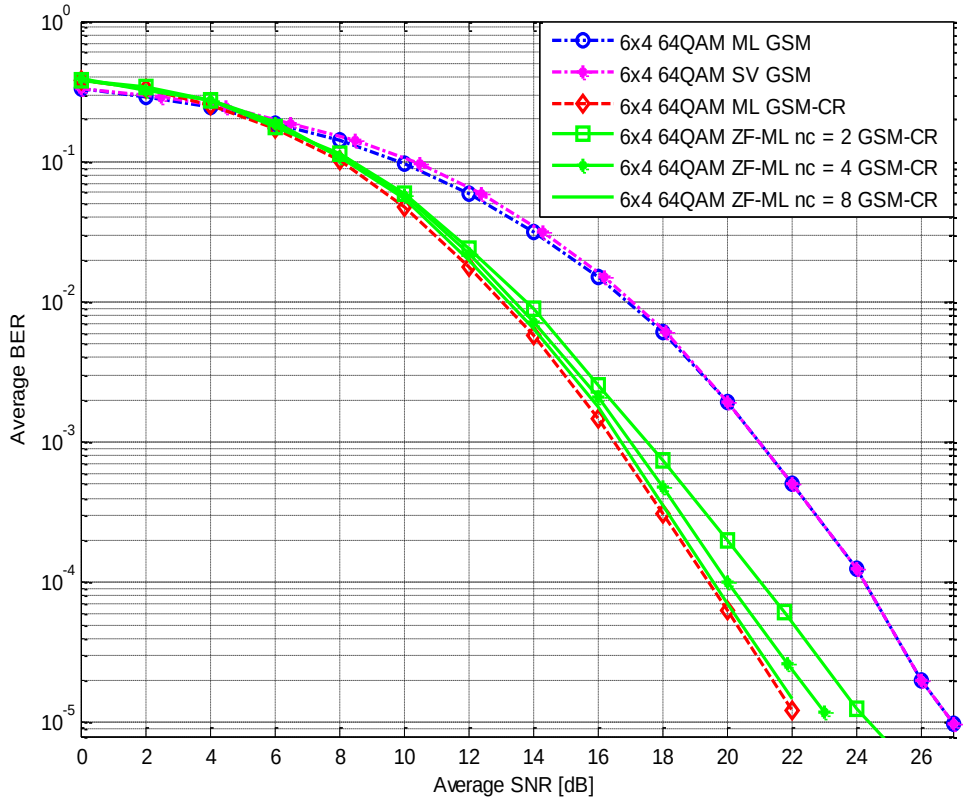

Figure B.4. Average BER - 6x4 64QAM GSM and GSM-CR Configurations

Figures B.3 and B.4 show the average BER of various GSM and GSM-CR detection schemes for the 4×4 64QAM and 6×4 64QAM configurations, respectively. Both Figures B.3 and B.4 demonstrate that for 4×4 64QAM and 6×4 64QAM, ML GSM-CR outperforms ML GSM by 4 dB and 5 dB, respectively, at a BER of 10^{-5}. This outcome is in accordance with the trends observed in [7]. Moreover, Figures B.3 and B.4 reconfirm trends observed in [12] where the SV GSM detector closely matches the average BER of ML GSM over the entire range of SNR values.

Figures B.3 and B.4 also demonstrate that the average BER of the ZF-ML GSM-CR detector is linked to the value of n_c, where larger values of n_c yield improved BER performance. In particular, the ZF-ML GSM-CR detector configured with n_c = 8 obtains near-ML BER performance. The value of n_c utilised in ZF-ML determines the number of most probable transmitted symbol pair candidates, which are input to the ML detector in the second stage of ZF-ML. The consideration of a greater number of most probable transmitted symbol pair candidates enhances the probability of correct detection in the second stage of ZF-ML, which leads to improved BER performance. However, the utilisation of higher values of n_c and the subsequent attainment of improved BER performance is traded-off by increased computational complexity, as highlighted in section 6.1.

Another notable observation from Figures B.3 and B.4 is that for the 4×4 64QAM and 6×4 64QAM configurations, ZF-ML with n_c = 8 achieves gains of 4 dB and 5 dB, respectively, at a BER of 10^{-5}, when compared to ML GSM. Based on the aforementioned BER performance characteristics and computational complexity results presented in section 6.1, it is evident that the ZF-ML GSM-CR detector, configured with n_c = 8, offers a two-fold benefit of enhanced BER performance and reduced computational complexity when compared to the ML GSM detection scheme.

Moreover, Figures B.3 and B.4 show that for the 4×4 64QAM and 6×4 64QAM configurations, the ZF-ML GSM-CR detector, configured with n_c = 8, offers gains of 4 dB and 5 dB, respectively, at a BER of 10^{-5}, when compared to the SV GSM detection scheme. However, these significant gains are traded-off by higher computational complexity, as shown in section 6.1

7. Conclusion

In this paper, we have proposed the ZF-ML GSM-CR detector, which has low computational complexity that is independent of the order of digital modulation employed. Complexity and performance comparisons between the ZF-ML GSM-CR detector and popular GSM and GSM-CR detection schemes revealed that for the $N_t \times 4$ 64QAM configuration: i) the ZF-ML GSM-CR detector reduced the computational complexity at the receiver by up to 60% and achieved similar BER performance in comparison to the ML GSM-CR detection scheme; ii) the ZF-ML GSM-CR detector demonstrated a two-fold benefit of reduced computational complexity at the receiver and significant gains, as compared to the ML GSM detection scheme. In particular, ZF-ML configured with two candidate symbols per initial symbol estimate reduces the receiver complexity by up to 60% whilst ZF-ML configured with eight candidate symbols per initial symbol estimate achieves gains of up to 5 dB, at a BER of 10^{-5}, when compared to the ML GSM detector; iii) the ZF-ML GSM-CR detection scheme achieved gains of up to 5 dB, at a BER of 10^{-5}, as compared to the SV GSM detector, at the expense of increased computational complexity. In particular, for configurations that encoded more than one information bit in the spatial domain, the ZF-ML GSM-CR detector was found to increase computational complexity at the receiver by up to 235% as compared to the SV GSM detection scheme.

References

[1] E. Telatar, "Capacity of multi-antenna Gaussian channels," *Eur. Trans. Telecommun.*, vol. 10, no. 6, pp. 558–595, Nov. 1999.

[2] G. J. Foschini and M. J. Gans, "On limits of wireless communications in a fading environment when using multiple antennas," *Wireless Pers. Commun.*, vol. 6, no. 3, pp. 311–335, Mar. 1998.

[3] R. Mesleh, H. Haas, C. W. Ahn, *et al.*, "Spatial modulation - A new low complexity spectral efficiency enhancing technique," *Proc. ChinaCOM*, pp. 1–5, Oct. 2006.

[4] R. Mesleh, H. Haas, S. Sinanovic, *et al.*, "Spatial modulation," *IEEE Trans. Veh. Technol.*, vol. 57, no. 4, pp. 2228-2241, Jul. 2008.

[5] P. Wolniansky, G. Foschini, G. Golden, *et al.*, "V-BLAST: An architecture for realizing very high data rates over the richscattering wireless channel," *Proc. URSI Int. Symp. on Signals, Syst. and Electron.*, pp. 295–300, Oct. 1998.

[6] A. Younis, N. Serafimovski, R. Mesleh, *et al.*, "Generalised spatial modulation," *Proc. 2010 Signals, Syst. Comput.*, pp. 1498–1502, Nov. 2010.

[7] N. R Naidoo, H. Xu and N. Pillay, "Generalised spatial modulation with constellation reassignment," [under review *IET Commun.*]

[8] K. G Seddik, A. S Ibrahim and K. J. Liu, "Trans-modulation in wireless relay networks," *IEEE Commun. Lett.*, vol. 12, no. 3, pp. 170-73, Mar. 2008.

[9] K. Sundaravadivu and S. Bharathi, "STBC codes for generalized spatial modulation in MIMO systems," *Proc. Int. Conf. on Emerging Trends in Computing, Commun. and Nanotechnology*, pp. 486-490, Mar. 2013.

[10] Z. Yiğit and E. Basar, "High rate generalised spatial modulation," *Proc. IEEE. Conf. Signal Process. and Applicat.*, pp. 117-120, May 2016.

[11] W. Wang and R. Y. Chang, "Signal space optimisation for generalised spatial modulation," *Proc. IEEE 79th Veh. Technol. Conf.*, pp. 1-5, May 2014.

[12] Y. Jiang, Y. Xu, Y. Xie, *et al.*, "Low complexity detection scheme for generalised spatial modulation," *J. of Commun.*, vol. 11, no. 8, pp. 726-732, Aug. 2016.

[13] C. Wang, P. Cheng, Z. Chen, *et al.*, "Near-ML low-complexity detection for generalized spatial modulation," *IEEE Commun. Lett.*, vol. 20, no. 3, pp. 618–621, Jan. 2016.

[14] Y. Xiao, Z. Yang, L. Dan, *et al.*, "Low complexity signal detection for generalized spatial modulation," *IEEE Commun. Lett.*, vol. 18, no. 3, pp. 403–406, Apr. 2014.

[15] J. Fu, C. Hou, W. Xiang, et al., "Generalised spatial modulation with multiple active transmit antennas," *Proc. IEEE Global Commun. Conf*, pp. 839-844, Dec. 2010.

[16] Y. Sun, J. Wang and L. He, "Iterative zero forcing detection scheme for generalised spatial modulation," *IEEE Int. Symp Broadband Multimedia Syst. and Broadcast.*, pp. 1-4, Jun. 2016.

[17] S. Verdu, *Multiuser Detection*, 1st ed., United Kingdom: Cambridge University Press, 1998.

[18] N. R. Naidoo, H. Xu and T. Quazi, "Spatial modulation: Optimal detector asymptotic performance and multiple-stage detection," *IET Commun.*, vol. 5, no. 5, pp. 1368-1376, Aug. 2011.

[19] H. Xu and N. Pillay, "A simple near-ML low complexity detection scheme for Alamouti space-time block coded spatial modulation," *IET Commun.*, vol. 8, no. 15, pp. 2611-2618, Oct. 2014.

Paper C

Generalised Spatial Modulation with Dual Constellation Reassignment

Nigel Naidoo and Hongjun Xu

Prepared for submission to *IET Communications Journal*

Abstract

This paper proposes a generalised spatial modulation with dual constellation reassignment (GSM-DCR) technique, which is geared towards improving the overall spectral efficiency of generalised spatial modulation with constellation reassignment (GSM-CR). By encoding an additional information bit in the signal domain, GSM-DCR effectively increases the overall spectral efficiency by 1 bit/s/Hz when compared to equivalent GSM-CR and GSM schemes. A framework for the design of GSM-DCR is presented. Moreover, an analytical bound for the average bit error rate (BER) of GSM-DCR over independent and identically distributed (i.i.d.) Rayleigh flat fading channels is derived, and the accuracy of this bound is verified by Monte Carlo simulation results. A comparison between various GSM-DCR, GSM-CR and generalised spatial modulation (GSM) schemes, which employ equivalent system configurations, reveals the following: i) in all cases, GSM-DCR improves spectral efficiency by 1 bits/s/Hz as compared to both GSM-CR and GSM; ii) for the 6×4 64QAM configuration, GSM-DCR exhibits reduced performance of 2 dB, at a BER of 10^{-5}, as compared to GSM-CR. However, this performance degradation is traded-off by the enhanced spectral efficiency of 1 bit/s/Hz attained by the GSM-DCR scheme; iii) for the 6×4 64QAM configuration, GSM-DCR can achieve gains of 2.5 dB, at a BER of 10^{-5}, when compared to GSM.

1. Introduction

Multiple-input multiple-output (MIMO) techniques offer significant enhancements in data rate, quality of service and spectral efficiency, as compared to single antenna systems [1]-[4]. As a result, MIMO techniques have been incorporated into several next generation wireless communication standards such as IEEE 802.11n, IEEE 802.16e, and 3GPP long-term evolution (LTE) [5, 6]. Amongst the plethora of proposed MIMO techniques, spatial modulation (SM) has emerged as an excellent candidate due to its ability to convey information in both the spatial and signal domains [7]-[9]. Moreover, SM employs a single active transmit antenna within a particular timeslot, and is therefore not prone to the inter-antenna synchronisation (IAS) and inter-channel interference (ICI) issues that plague conventional MIMO schemes [7]-[9].

The single active transmit antenna architecture of SM poses a limitation to the number of information bits that can be encoded in the spatial domain, and ultimately the achievable spectral efficiency. Generalised spatial modulation (GSM) [10] is an extension to the SM scheme, which employs multiple active transmit antennas in order to improve the achievable spectral efficiency. However, for configurations with the same number of transmit antennas, the bit error rate (BER) performance of GSM is limited and degraded as compared to SM [10].

Significant research has been conducted towards improving the error performance of GSM systems. Notable recent developments include, *inter alia*: i) generalised spatial modulation with constellation reassignment (GSM-CR) in [11] that employs the constellation reassignment (CR) [12] technique in conjunction with GSM. The CR technique maximises the minimum Euclidean distance between transmitted symbol pairs, thereby improving BER performance; ii) heuristic methods for antenna combination selection in GSM systems are proposed in [13] in order to improve the symbol error rate (SER) performance; iii) GSM signal constellations based on multiplicative groups of Eisenstein integers are proposed in [14], where the proposed constellations yield improved BER performance; iv) a BER performance enhanced high-rate generalised spatial modulation (HR-GSM) scheme, which is tailored for M-ary phase shift keying (MPSK) signal constellations, is proposed in [15].

The GSM-CR scheme is particularly promising due to its inherent ability to achieve gains of up to 5 dB, at a BER of 10^{-5}, when compared to GSM, whilst maintaining computational complexity equivalent to that of GSM [11, 16]. However, GSM-CR only permits two active transmit antennas during a particular timeslot. This limits the number of bits that can be encoded in the spatial domain, and therefore the overall spectral efficiency attainable.

In this paper, we propose a generalised spatial modulation with dual constellation reassignment (GSM-DCR) technique, which is geared towards improving the overall spectral efficiency of GSM-CR. The GSM-DCR technique can be viewed as an extension to conventional GSM-CR. Similar to the GSM-CR scheme, GSM-DCR uses the CR technique [12] to maximise the minimum Euclidean distance between transmitted symbol pairs. However, a key difference between GSM-CR and GSM-DCR is that the former generates a transmitted symbol pair based on a single pair of signal constellations, whereas the latter uses one of two possible signal constellation pairs in order to generate a transmitted symbol pair. The GSM-DCR technique uses an additional information bit to select between the two possible signal constellation pairs, thus improving spectral efficiency by 1 bit/s/Hz when compared to GSM-CR. As a result, GSM-DCR improves the spectral efficiency of GSM-CR without requiring the use of higher order digital modulation techniques or imposing additional transmit antenna requirements. To the best of the author's knowledge, utilising the active signal constellation pair as an information bearing unit is a novel concept, which has yet to be explored within the context of either GSM or CR systems.

Note, the following important differences exist between GSM-CR and the proposed GSM-DCR technique: In conventional GSM-CR, the active transmit antenna pair index and transmitted symbol pair are used to convey information. GSM-DCR on the other hand utilises the active transmit antenna pair index, the active signal constellation pair and the transmitted symbol pair as information bearing units. Moreover, in GSM-CR there exists a single pair of bit-to-signal constellation mappers, whilst in GSM-DCR two pairs of bit-to-signal constellation mappers are employed.

The remainder of the paper is structured as follows: Section 2 presents the GSM-DCR system model. Section 3 outlines design principles for GSM-DCR. Section 4

formulates an analytical bound for the average BER of GSM-DCR over independent and identically distributed (i.i.d.) Rayleigh flat fading channels. Section 5 presents Monte Carlo simulation results and discussion. Finally, the paper is concluded in section 6.

1.1 Notation

Bold italics upper/lower case symbols denote matrices/vectors, while regular letters represent scalar quantities. We use $\lfloor\cdot\rfloor$, $(\cdot)^T$, $(\cdot)^H$, $E[\cdot]$, $|\cdot|$ and $\|\cdot\|_F$ for the floor, transpose, Hermitian, expectation, Euclidean norm and Frobenius norm operations, respectively.

2. System Model

The basic idea behind GSM-DCR is to map a stream of input bits to a pair of transmit antenna (spatial domain) and a pair of symbols emanating from one of two possible signal constellation pairs (signal domain). The spatial domain mapping is equivalent to that performed in conventional GSM-CR or GSM configured with two active transmit antennas.

The signal domain mapping on the other hand, is a two-stage process. Stage one entails selecting one of two possible signal constellation pairs. A particular signal constellation pair comprises either primary and secondary or primary and dual signal constellations. The primary constellation, denoted by $\boldsymbol{X}^{Prm}$, corresponds to a Gray-coded M-ary quadrature amplitude modulation (MQAM) signal constellation, and the secondary constellation, denoted by $\boldsymbol{X}^{Sec}$, is generated by assigning symbols with adjacent points in the primary constellation to non-adjacent points in the secondary constellation and *vice versa*, in accordance with the CR technique [12].

The dual constellation, denoted by $\boldsymbol{X}^{Dual}$, is generated by rotating the secondary signal constellation by 180 degrees. Given that the dual constellation is merely a rotated version of the secondary signal constellation, the minimum Euclidean distance between transmitted symbol pairs emanating from either the primary and secondary or primary and dual signal constellations is identical. The primary, secondary and dual signal constellations for 16QAM and 64QAM GSM-DCR configurations are

contained in Appendix C-1. It should be noted that the primary and secondary signal constellations of GSM-DCR are equivalent to those used in GSM-CR.

In stage two of the signal domain mapping process, a pair of MQAM symbols is generated based on the signal constellation pair obtained from stage one. Thereafter, the selected transmit antenna pair simultaneously transmits the pair of MQAM symbols over a wireless channel. At the receiver, a maximum likelihood (ML) detector is utilised for the joint detection of the following three information bearing units: the active transmit antenna pair, signal constellation pair and transmitted symbol pair. Thereafter, a de-mapping process is undertaken for the recovery of the original input bits.

2.1 Transmission

Consider an $N_t \times N_r$ MQAM GSM-DCR system model shown in Figure C.1, where N_t refers to the number of transmit antennas, N_r is the number of receive antennas and M is the order of the QAM employed. The GSM-DCR scheme conveys information via the spatial and signal domains. The spatial domain comprises all possible combinations of transmit antenna pairs. The number of usable transmit antenna pair combinations within the spatial domain must be a power of two and is given by $c = 2^{ml}$, where $ml = \left\lfloor log_2 \binom{N_t}{2} \right\rfloor$. The signal domain on the other hand consists of two subsets of M symbol pairs, namely $(\omega_1\ \omega_2 | \omega_1 \in \boldsymbol{X}^{Prm}, \omega_2 \in \boldsymbol{X}^{Sec})$ and $(\omega_1\ \omega_3 | \omega_1 \in \boldsymbol{X}^{Prm}, \omega_3 \in \boldsymbol{X}^{Dual})$, $\omega_i, i \in [1:3]$, are the component MQAM symbols of a particular symbol pair. It therefore follows that the signal domain contains a total of 2M possible symbol pair combinations.

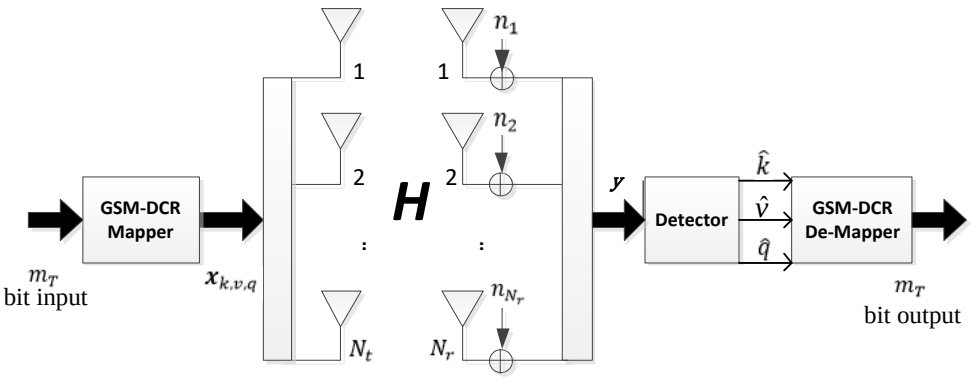

Figure C.1 GSM-DCR System Model

Initially, a stream of $m_T = log_2 c + log_2 M + 1$ random bits are input to the GSM-DCR mapper, which performs a mapping function in accordance with a predefined table known at both the transmitter and receiver. A sample mapping table for a $3 \times N_r$ 16QAM GSM-DCR system is provided in Appendix C-2. The first $log_2 c$ input bits are mapped to a transmit antenna pair index k, and the next input bit to the constellation index v, which determines whether the primary and secondary or the primary and dual signal constellation pair is utilised.

The remaining log_2M bits are assigned to a pair of MQAM symbols x_q and $\tilde{x}_{v,q}$, where $q \in [0: M-1]$ is the decimal equivalent of the log_2M input bit sequence and the index identifying the transmitted symbol pair, and $\tilde{x}_{v,q} \in \boldsymbol{X}^{Sec}$ for $v = 0$ or $\tilde{x}_{v,q} \in \boldsymbol{X}^{Dual}$ for $v = 1$.

The outcome of the spatial and signal mapping processes can be expressed as follows:

$$\boldsymbol{x}_{k,v,q} = \underset{\substack{\uparrow \\ k_1{}^{th}\ position}}{[0} \; x_q \; \ldots\ldots \underset{\substack{\downarrow \\ k_2{}^{th}\ position}}{\tilde{x}_{v,q}} \ldots\ldots 0 \; \underset{\substack{\uparrow \\ N_t{}^{th}\ position}}{0}] e^{j\theta_k} \qquad \text{(C.1)}$$

where k_1 and $k_2 \in [1: N_t]$ are active transmit antennas from the k^{th} transmit antenna pair. $E\left\{|x_q|^2\right\} = E\left\{|\tilde{x}_{v,q}|^2\right\} = 1$. θ_k denotes the rotation angle applied to the symbol pair $[x_q \;\; \tilde{x}_{v,q}]^T$ that is emitted from transmit antenna pair k. The process for generating appropriate rotation angles will be described in section 3.3.

The symbols x_q and $\tilde{x}_{v,q}$ are then simultaneously transmitted from their respective transmit antennas k_1 and k_2 over the $N_r \times N_t$ MIMO channel $\boldsymbol{H}$, and are subjected to N_r dimensional additive white Gaussian noise (AWGN) $\boldsymbol{n}$. The received signal vector is therefore given by:

$$\boldsymbol{y} = \sqrt{\frac{\rho}{2}} \boldsymbol{H} \boldsymbol{x}_{k,v,q} + \boldsymbol{n} \qquad \text{(C.2)}$$

where $\boldsymbol{y}$ is the $N_r \times 1$ dimensional received signal vector. $\boldsymbol{H} = [\boldsymbol{h}_1\ \boldsymbol{h}_2 \ldots \boldsymbol{h}_a \ldots \boldsymbol{h}_{N_t}]$ and $\boldsymbol{h}_a$ is the $N_r \times 1$ dimensional vector corresponding to transmit antenna a. ρ is the average signal-to-noise ratio (SNR) at each receive antenna. $\boldsymbol{n}$ and $\boldsymbol{H}$ have i.i.d. entries according to the complex Gaussian distribution $CN(0,1)$.

Alternatively, the received signal vector may be represented as follows:

$$\boldsymbol{y} = \sqrt{\frac{\rho}{2}}\boldsymbol{h}'_k \boldsymbol{X}_{v,q} + \boldsymbol{n} \tag{C.3}$$

where $\boldsymbol{X}_{v,q} = \begin{bmatrix} x_q & \tilde{x}_{v,q} \end{bmatrix}^T e^{j\theta_k}$ is the transmitted symbol pair subjected to a predefined rotation angle θ_k and $\boldsymbol{h}'_k = \begin{bmatrix} \boldsymbol{h}_{k_1} & \boldsymbol{h}_{k_2} \end{bmatrix}$ is an $N_r \times 2$ dimensional channel matrix corresponding to the active transmit antenna pair k.

2.2 Maximum Likelihood Detector

The following ML rule is applied for the joint detection of the active transmit antenna pair, the signal constellation pair and transmitted symbol pair:

$$\begin{aligned} [\hat{k}, \hat{v}, \hat{q}] &= \underset{k,v,q}{argmax}\ p_y(\boldsymbol{y}|\boldsymbol{x}_{k,v,q}, \boldsymbol{H}) \\ &= \underset{k,\boldsymbol{X}_{v,q}}{argmin}\left(\left\|\boldsymbol{h}'_k \boldsymbol{X}_{v,q}\right\|_F^2 - 2Re\{\boldsymbol{y}^{\boldsymbol{H}} \boldsymbol{h}'_k \boldsymbol{X}_{v,q}\}\right) \end{aligned} \tag{C.4}$$

where $p_y(\boldsymbol{y}|\boldsymbol{x}_{k,v,q}, \boldsymbol{H}) = \pi^{-N_r} exp\left(\left\|\boldsymbol{y} - \sqrt{\frac{\rho}{2}}\boldsymbol{h}'_k \boldsymbol{X}_{v,q}\right\|_F^2\right)$ is the probability density function of $\boldsymbol{y}$ conditioned on $\boldsymbol{H}$ and $\boldsymbol{x}_{k,v,q}$, $\hat{k}$ is the estimated active transmit antenna pair index, $\hat{v}$ is the estimated signal constellation index, and $\hat{q}$ is the estimated transmitted symbol pair index.

The estimates $\hat{k}, \hat{v}$ and $\hat{q}$ are then input to the GSM-DCR demapper, which uses a mapping table to reproduce the corresponding m_T input bit sequence.

3. System Design

The principal objective of GSM-DCR system design is to maximise the minimum distance between transmitted signal vectors, and in so doing improve BER

performance. The three dimensional constellation space of GSM-DCR warrants the adoption of a hybrid distance metric that reflects both the spatial and signal domain. Due to their similarities in terms of system models, the following hybrid minimum distance metric proposed for GSM-CR in [11] is also applicable in the context of GSM-DCR:

$$d_{min} = \underset{\substack{k,v,q \\ \hat{k},\hat{v},\hat{q} \\ q \neq \hat{q}}}{\operatorname{argmin}} \left\{ \sqrt{\delta_{k\hat{k}}{}^2 + \left| x_q e^{j\theta_k} - x_{\hat{q}} e^{j\theta_{\hat{k}}} \right|^2 + \left| \tilde{x}_{v,q} e^{j\theta_k} - \tilde{x}_{\hat{v},\hat{q}} e^{j\theta_{\hat{k}}} \right|^2} \right\} \quad \text{(C.5)}$$

where d_{min} is the minimum distance between transmitted between signal vectors $\boldsymbol{x}_{k,v,q}$ and $\boldsymbol{x}_{\hat{k},\hat{v},\hat{q}}$ and $\boldsymbol{x}_{k,v,q} \neq \boldsymbol{x}_{\hat{k},\hat{v},\hat{q}}$. $\delta_{k\hat{k}}$ is defined as the number of non-overlapping indices between antenna pairs k and $\hat{k}$. For example, consider a $4 \times N_r$ GSM-DCR configuration with $\binom{4}{2}$ possible transmit antenna pair groupings $\varepsilon_1 = (1\ 1\ 0\ 0), \varepsilon_2 = (1\ 0\ 1\ 0)$, $\varepsilon_3 = (1\ 0\ 0\ 1)$, $\varepsilon_4 = (0\ 1\ 1\ 0)$, $\varepsilon_5 = (0\ 1\ 0\ 1)$ and $\varepsilon_6 = (0\ \ 0\ 1\ 1)$, where 1 and 0 represent the respective active and idle state of a particular transmit antenna. Then we have $\delta_{1,4}(\varepsilon_1, \varepsilon_4) = 2$ and $\delta_{1,6}(\varepsilon_1, \varepsilon_6) = 4$.

3.1 Spatial Constellation Optimisation

The maximisation of d_{min} in (C.5) may be attained by maximising, *inter alia*, the term $\delta_{k\hat{k}}{}^2$. The maximisation of $\delta_{k\hat{k}}{}^2$ is implemented by selecting transmit antenna pairs such that overlapping transmit antenna indices are avoided to the greatest extent possible. Selecting transmit antenna pairs with overlapping indices is not desirable as it leads to an increase of the linear dependence probability of channel space, which is the principal cause of active transmit antenna pair index detection error [11, 17]. Practical examples demonstrating the design of optimised spatial constellations are provided in [11]. It should be noted that GSM-CR and GSM-DCR systems employ identical spatial constellations and therefore all design principles and examples presented in section 3.1 of [11] are directly applicable to the GSM-DCR scheme. The optimised transmit antenna pair groupings for various GSM-DCR configurations are provided in Appendix C-3.

3.2 MQAM Signal Constellation Optimisation

The maximisation of d_{min} in (C.5) is also underpinned by the ability to maximise the terms $\left|x_q e^{j\theta_k} - x_{\hat{q}} e^{j\theta_{\hat{k}}}\right|^2 + \left|\tilde{x}_{v,q} e^{j\theta_k} - \tilde{x}_{\hat{v},\hat{q}} e^{j\theta_{\hat{k}}}\right|^2$. The CR technique generates a secondary signal constellation by assigning symbols with adjacent points in the primary constellation to non-adjacent points in the secondary constellation and *vice versa* [12]. This maximises the minimum Euclidean distance between transmitted symbol pairs emanating from the primary and secondary signal constellations, and therefore maximises the expression $\left|x_q e^{j\theta_k} - x_{\hat{q}} e^{j\theta_{\hat{k}}}\right|^2 + \left|\tilde{x}_{v,q} e^{j\theta_k} - \tilde{x}_{\hat{v},\hat{q}} e^{j\theta_{\hat{k}}}\right|^2$, by specifically maximising the term $\left|\tilde{x}_{v,q} e^{j\theta_k} - \tilde{x}_{\hat{v},\hat{q}} e^{j\theta_{\hat{k}}}\right|^2$.

The dual constellation is generated by rotating the secondary signal constellation by 180 degrees. In light of the fact that the dual constellation is merely a rotated version of the secondary signal constellation, the minimum Euclidean distance between symbol pairs emanating from either the primary and secondary or primary and dual signal constellations is identical. Therefore, maximisation of the term $\left|\tilde{x}_{v,q} e^{j\theta_k} - \tilde{x}_{\hat{v},\hat{q}} e^{j\theta_{\hat{k}}}\right|^2$ and the subsequent maximisation of $\left|x_q e^{j\theta_k} - x_{\hat{q}} e^{j\theta_{\hat{k}}}\right|^2 + \left|\tilde{x}_{v,q} e^{j\theta_k} - \tilde{x}_{\hat{v},\hat{q}} e^{j\theta_{\hat{k}}}\right|^2$ is ensured.

Generating a transmitted symbol pair based on a primary and secondary or primary and dual signal constellation pair, yields a minimum Euclidean distance between transmitted symbol pairs which is greater than that attained in conventional GSM. This is the foremost reason why GSM-DCR exhibits enhanced BER performance as compared to conventional GSM. However, the introduction of the dual constellation in GSM-DCR, and the subsequent utilisation of two possible signal constellation pairs, has a negative impact on BER performance. As a result, GSM-DCR exhibits reduced performance when compared to GSM-CR, which only utilises a single constellation pair comprising primary and secondary signal constellations. An illustrative example will be used to substantiate the aforementioned. Consider the 16QAM GSM-DCR configuration that uses signal constellations associated with the same spatial constellation point and where no rotation angle is applied, as shown in Figures C.2a and C.2b.

Figure C.2a shows that for the adjacent symbol pair $[x_0\ \tilde{x}_{v,0}]$ and $[x_4\ \tilde{x}_{v,4}]$, a minimum Euclidean distance of $d_{pri} = \frac{2}{\sqrt{10}}$ occurs between x_0 and x_4 in the primary signal constellation. With regard to the secondary signal constellations, it can observed that $\tilde{x}_{0,0}$ and $\tilde{x}_{0,4}$ are separated by $d_{sec} = \frac{4}{\sqrt{10}}$. For the dual constellation, it can be seen that and $\tilde{x}_{1,0}$ and $\tilde{x}_{1,4}$ are separated by $d_{dual} = \frac{4}{\sqrt{10}}$. However, closer inspection of Figure C.2b reveals that the use of the secondary constellation in conjunction with the dual constellation creates an additional likely source of error, where a symbol $\tilde{x}_{0,q}$ in the secondary constellation may be incorrectly decoded as its counterpart $\tilde{x}_{1,q}$ in the dual constellation and *vice versa*. In this specific example $\tilde{x}_{0,0}$ in the secondary constellation and its counterpart $\tilde{x}_{1,0}$ in the dual constellation are separated by a Euclidean distance of $d_{\mathrm{sec}\_dual} = \frac{\sqrt{8}}{\sqrt{10}} = 0.89$, which is smaller as compared to both d_{sec} and d_{dual}. Therefore, the effective minimum Euclidean distance between adjacent symbol pairs can be considered to be $d_{pri} + d_{\mathrm{sec}\_dual} = \frac{2+\sqrt{8}}{\sqrt{10}} = 1.53$. Note that in the case of GSM-CR which only employs primary and secondary signal constellations, the minimum Euclidean distance between adjacent symbol pairs will be given by $d_{pri} + d_{\mathrm{sec}} = \frac{6}{\sqrt{10}} = 1.90$.

In section 3.2 of [11] it was demonstrated that for GSM, the minimum Euclidean distance of $\frac{4}{\sqrt{10}} = 1.26$ occurs between adjacent symbol pairs, whereas the minimum Euclidean distance between adjacent symbol pairs in the case of GSM-CR is $\frac{6}{\sqrt{10}} = 1.90$. Hence, it can be concluded for systems with identical antenna configurations, order of modulation and spatial constellation, GSM-DCR would exhibit improved and reduced BER performance when compared to GSM and GSM-CR, respectively.

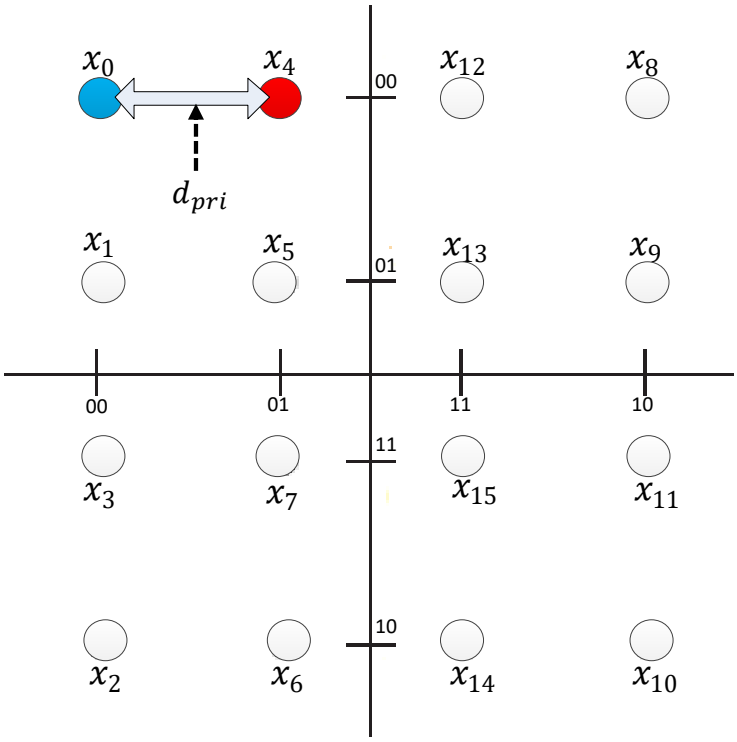

Figure C.2a 16QAM Primary Signal Constellation

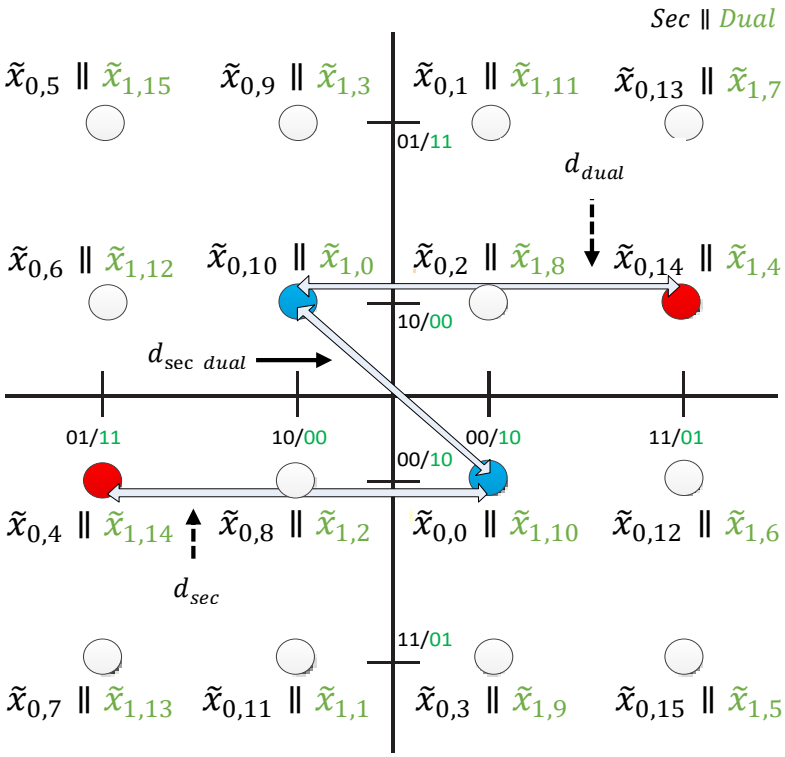

Figure C.2b 16QAM Secondary and Dual Signal Constellations

3.3 Rotation Angle Optimisation

An inspection of the terms $\left|x_q e^{j\theta_k} - x_{\hat{q}} e^{j\theta_{\hat{k}}}\right|^2 + \left|\tilde{x}_{v,q} e^{j\theta_k} - \tilde{x}_{\hat{v},\hat{q}} e^{j\theta_{\hat{k}}}\right|^2$ in (C.5) reveals that d_{min} may also be maximised through the application of suitable rotation angles θ_k and $\theta_{\hat{k}}$ to either the primary and secondary or primary and dual signal constellation pairs. The hybrid distance metric in (C.5) does not permit the derivation rotation angles for MQAM systems with $M > 4$ and therefore an exhaustive search via computer simulation will be employed [17].

The following high level process for generating rotation angles, via computer simulation, was proposed for GSM-CR in [11] and is also applicable in the context of GSM-DCR systems:

i. Given that c possible transmit antenna pair groupings have been generated, select a subset $\boldsymbol{c}_{nov}$ of transmit antenna pairs that contain non-overlapping entries. Note that transmit antenna pairs contained in $\boldsymbol{c}_{nov}$ should satisfy the criterion $\delta_{k\hat{k}}{}^2 = 4$.
ii. Set the rotation angle $\theta_i = 0$ for $i \in \boldsymbol{c}_{nov}$.
iii. Generate a subset $\boldsymbol{c}_{ov}$ comprising all valid transmit antenna pairs not contained in $\boldsymbol{c}_{nov}$.
iv. Determine the rotation angles θ_i for $i \in \boldsymbol{c}_{ov}$ by computing the maximisation problem $d_{max} = \underset{0 < \boldsymbol{\theta}_{\boldsymbol{c}_{ov}} < 2\pi}{argmax\{d_{min}\}}$, where $\boldsymbol{\theta}_{\boldsymbol{c}_{ov}}$ is the set of rotation angles to be optimised and d_{min} has been defined in (C.5).

The rotation angles applicable to the primary, secondary and dual signal constellations for various GSM-DCR configurations are contained in Appendix C-3.

4. BER Performance Analysis

In this section, an analytical bound for the average BER of GSM-DCR over i.i.d. Rayleigh flat fading channels is presented. In general, GSM-DCR comprises an active transmit antenna pair index detection process and a transmitted symbol pair detection process. For the purpose of this analysis we assume that the transmitted symbol pair detection process entails the implicit detection of the signal constellation pair.

In accordance with the approaches adopted in [7, 11, 18], the transmit antenna pair index and transmitted symbol pair detection processes are considered to be independent. Therefore, the average BER of GSM-DCR may be approximated by [11, (A.6)]:

$$P_e \cong P_a + P_d - P_a P_d \tag{C.6}$$

where $P_c = (1 - P_a)(1 - P_d)$ is the probability that correct input bits are detected. P_a is the bit error probability of estimating the active transmit antenna pair index given that the transmitted symbols are correctly detected. P_d is the bit error probability of symbol pair estimation given that the active transmit antenna pair index is correctly detected.

4.1 Analytical BER of Symbol Pair Estimation

The bit error probability of symbol pair estimation, given that the transmit antenna pair index is perfectly detected, was derived for GSM-CR in [11, (A.16)]. The GSM-CR and GSM-DCR systems are identical except for their signal domains, where the former utilises M possible symbol pair combinations and the later employs 2M possible symbol pair combinations. Taking into consideration the aforementioned difference in signal domains, the expression in [11, (A.16)] may be adapted to predict the P_d performance of GSM-DCR as follows:

$$P_d \leq \sum_{r=0}^{2M-1} \sum_{\substack{\hat{r}=0 \\ \hat{r} \neq r}}^{2M-1} \frac{N(r,\hat{r}) \left[\frac{1}{4n} M\left(\frac{1}{2}\right) + \frac{1}{2n} \sum_{c=1}^{n-1} M\left(\frac{1}{2\sin^2(c\pi/2n)}\right) \right]}{2M\,(log_2 M + 1)} \tag{C.7}$$

where $\mathbf{Z}_r \in \left[\boldsymbol{X}_{0,0} \ldots \boldsymbol{X}_{0,q} \ldots \boldsymbol{X}_{0,M-1}\right]$ for $r \in [0: M-1]$ and $\mathbf{Z}_r \in \left[\boldsymbol{X}_{1,0} \ldots \boldsymbol{X}_{1,q} \ldots \boldsymbol{X}_{1,M-1}\right]$ for $r \in [M: 2M-1]$. $N(r, \hat{r})$ is the number of bits in error between $\mathbf{Z}_r$ and $\mathbf{Z}_{\hat{r}}$. $M(s) = \int_0^\infty \frac{e^{-sv} v^{N_r - 1} e^{-v/2\sigma_\alpha{}^2}}{(2\sigma_\alpha{}^2)^{N_r}(N_r-1)!}\, dv = \int_0^\infty e^{-sv} p_k(v)\, dv = \left(\frac{1}{1+2\sigma_\alpha{}^2 s}\right)^{N_r}$ and $\sigma_\alpha{}^2 = \frac{p}{8} \left\| \left(\boldsymbol{X}_{\hat{v},\hat{q}} - \boldsymbol{X}_{v,q} \right) \right\|_F^2$. The application of $n > 10$ is necessary to ensure convergence between the actual Gaussian Q-function and its trapezoidal approximation [19].

4.2 Analytical BER of Transmit Antenna Pair Index Estimation

The bit error probability of transmit antenna pair index estimation, given that the transmitted symbol pair is perfectly detected, was derived for GSM-CR in [11, (A.16)].

Since GSM-CR and GSM-DCR employ identical spatial constellations, the analytical BER expression in [11, (A.16)] may be used to predict the P_a performance of GSM-DCR as follows:

$$P_a \leq \sum_{k=1}^{c} \sum_{r=0}^{2M-1} \sum_{\hat{k}=1}^{c} \frac{N(k,\hat{k})\mu_\alpha^{N_r} \sum_{w=0}^{N_r-1} \binom{N_r-1+w}{w} [1-\mu_\alpha]^w}{2cM} \qquad \text{(C.8)}$$

where $N(k,\hat{k})$ is the number of bits in error between transmit antenna pair k and $\hat{k}$ and $\mu_\alpha = \frac{1}{2}\left(1 - \sqrt{\frac{\sigma_\alpha{}^2}{1+\sigma_\alpha{}^2}}\right)$ with $\sigma_\alpha{}^2 = (\rho/8)\,|\mathbf{Z}_r|^2$.

5. Simulation Results

In this section, the analytical framework presented in section 4 is validated by comparing the analytical average BER to the simulated average BER obtained from Monte Carlo simulations. Moreover, a BER performance comparison between various GSM, GSM-CR and GSM-DCR schemes, with equivalent configurations, is presented. The system models for GSM, GSM-CR and GSM-DCR are consistent with those defined in [10], [11] and section 2, respectively.

To ensure a fair comparison, identical spatial domain mappings were used for GSM, GSM-CR and GSM-DCR. In particular, the following transmit antenna pair groupings were used for the $4 \times N$r and $6 \times N_r$ configurations:

- $4 \times N_r$ – (1,3); (1,4); (2,3) and (2,4)
- $6 \times N_r$ – (1,2); (3,4); (5,6); (2,3); (4,5); (1,6); (1,3) and (2 4)

where the numbers within brackets denote transmit antenna indices.

The Monte Carlo simulations were performed over an i.i.d. Rayleigh flat fading channel with AWGN, where the parameters pertaining to the channel and AWGN are consistent with those defined in section 2. Furthermore, the Monte Carlo simulations were conducted under the following assumptions: full channel knowledge at the receiver; antennas at the transmitter and receiver are separated wide enough to avoid correlation and the total transmit power is the same for all transmissions.

5.1 Analytic and Simulated Average BER Comparison

Figures C.3 and C.4 show the analytic and simulated average BER for the 4x4 GSM-DCR and 6x4 GSM-DCR configurations, respectively. In both Figures C.3 and C.4, the analytic average BER is observed to closely estimate the simulated average BER in the high SNR region. Moreover, the analytic bound for the average BER is observed to overestimate the average simulated BER in the low SNR region. This can be attributed to the fact that (C.7) and (C.8) are derived based on the union bound technique, which is well-known to be inaccurate in the low SNR region.

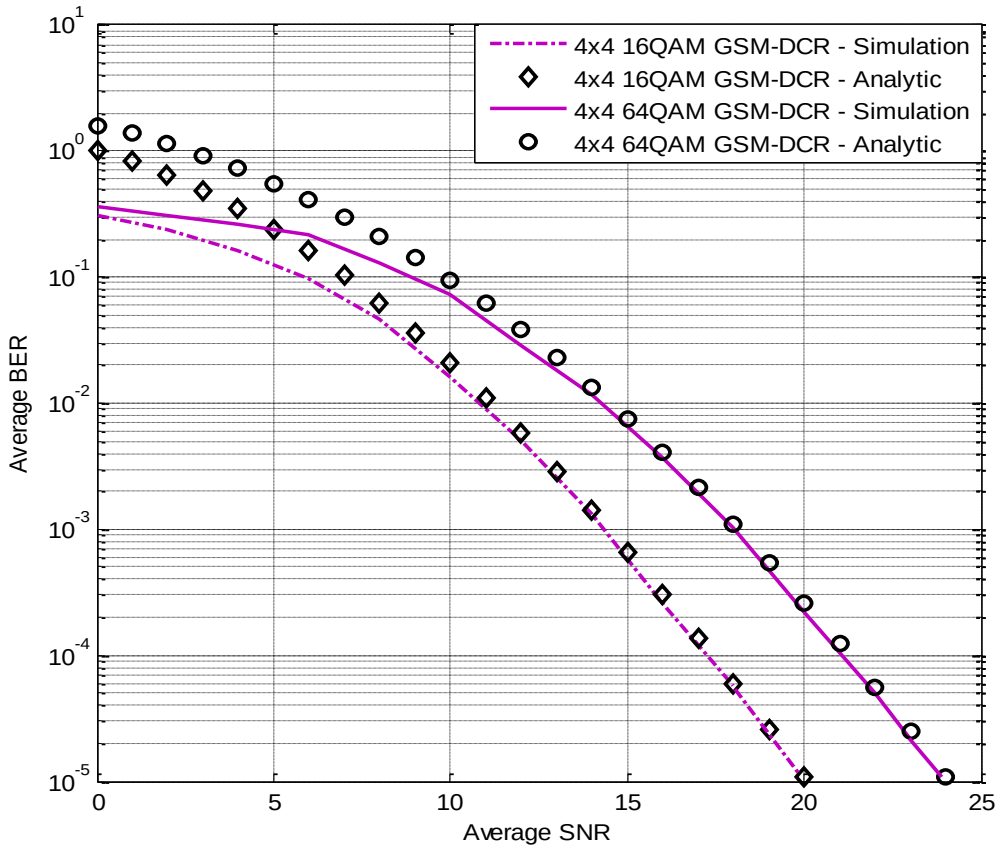

Figure C.3 Analytic and Simulated Average BER – 4x4 GSM-DCR

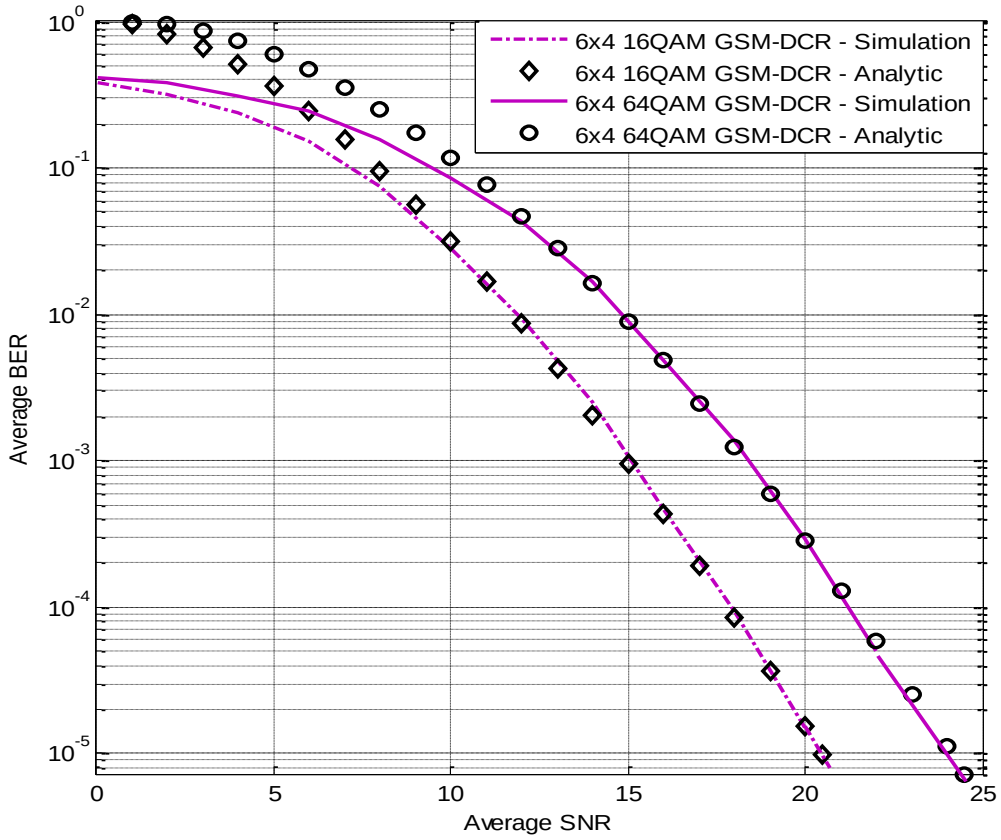

Figure C.4 Analytic and Simulated Average BER – 6x4 GSM-DCR

5.2 Performance Comparison

Figures C.5 and C.6 show the average BER of GSM, GSM-CR and GSM-DCR for various configurations. It can be seen that for systems with identical antenna configurations, order of modulation and spatial constellation, GSM-DCR exhibits improved BER performance as compared to GSM and degraded BER performance as compared to GSM-CR. This can be attributed to the fact that the minimum Euclidean distance between transmitted symbol pairs in GSM-DCR is greater as compared to GSM and smaller in comparison to GSM-CR. A detailed description of this phenomenon was presented in section 3.2. Another notable observation is that for equivalent configurations, GSM-DCR is capable of attaining a higher spectral efficiency when compared to both GSM and GSM-CR. In particular, GSM-DCR improves the overall spectral efficiency by 1 bit/s/Hz as compared to GSM and GSM-CR, without requiring the use of higher order modulation or imposing additional transmit antenna requirements.

Figure C.5 shows that GSM-DCR achieves gains of 1.5 dB and 2 dB, at a BER of 10^{-5}, when compared to the 4×4 16QAM GSM and 4×4 64QAM GSM configurations, respectively. Figure C.6 also demonstrates the enhanced performance of GSM-DCR in comparison to GSM, where gains of 1.5 dB and 2.5 dB, at a BER of 10^{-5}, are observed for the 6x4 16QAM and 6x4 64QAM configurations, respectively. Based on the spectral efficiency and performance characteristics of GSM-DCR, it is evident that the proposed scheme is a prominent alternative to GSM.

Moreover, Figure C.5 shows that GSM-DCR offers degraded performance of 1 dB and 1.5 dB, at a BER of 10^{-5}, when compared to the 4×4 16QAM GSM-CR and 4×4 64QAM GSM-CR configurations, respectively. The degraded performance of GSM-DCR in relation to GSM-CR is also demonstrated in Figure C.6. When compared to GSM-CR, GSM-DCR exhibits degraded performance of 1 dB and 2 dB, at a BER of 10^{-5}, for the 6×4 16QAM and 6×4 64QAM configurations, respectively. This degradation in performance is traded-off by the higher spectral efficiency attained by the GSM-DCR technique.

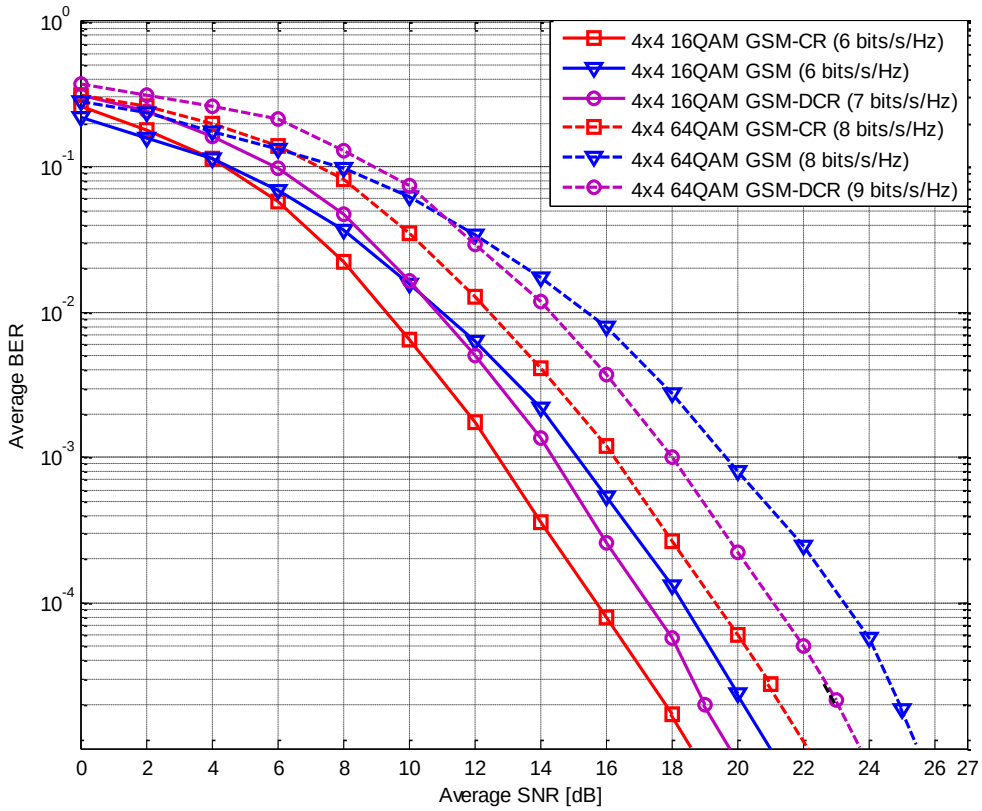

Figure C.5 Average BER – 4x4 Configuration

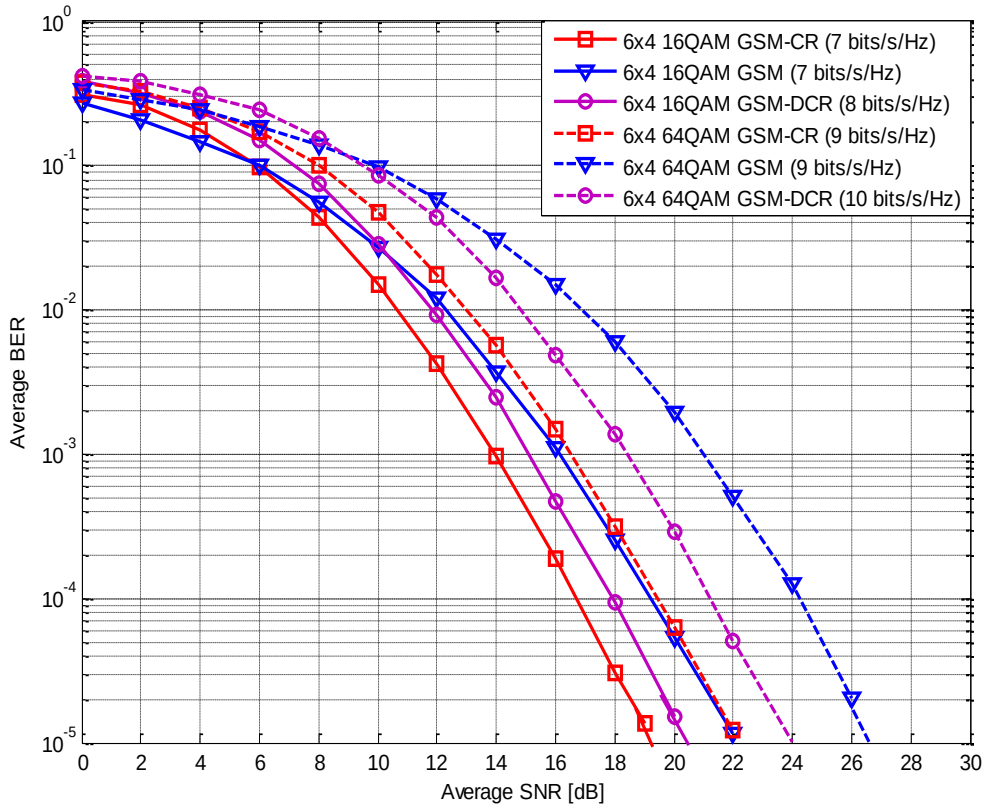

Figure C.6 Average BER – 6x4 Configuration

6. Conclusion

In this paper, we have proposed a GSM-CR scheme with enhanced spectral efficiency, termed GSM-DCR. GSM-DCR improves the overall spectral efficiency of equivalent GSM-CR and GSM schemes by 1 bit/s/Hz through encoding an additional information bit in the signal domain. A framework for the design of GSM-DCR systems was presented. Moreover, an analytical bound for the average BER of GSM-DCR over i.i.d. Rayleigh flat fading was derived, and the accuracy of the bound was verified by Monte Carlo simulation results. A comparison between various GSM-DCR, GSM-CR and GSM schemes, which employed equivalent system configurations, led to the following findings: i) GSM-DCR improved spectral efficiency by 1 bits/s/Hz as compared to GSM-CR. This spectral efficiency improvement was traded-off by the reduced performance of GSM-DCR in relation to GSM-CR. In particular, for the 6×4 64QAM configuration, GSM-DCR exhibited reduced performance of 2 dB, at a BER of 10^{-5}, as compared to GSM-CR; ii) GSM-DCR offered a two-fold benefit of increased spectral efficiency of 1 bit/s/Hz and significant gains when compared to

GSM. In particular, for the 6×4 64QAM configuration, GSM-DCR achieved gains of 2.5 dB, at a BER of 10^{-5}, as compared to GSM.

Appendix C-1

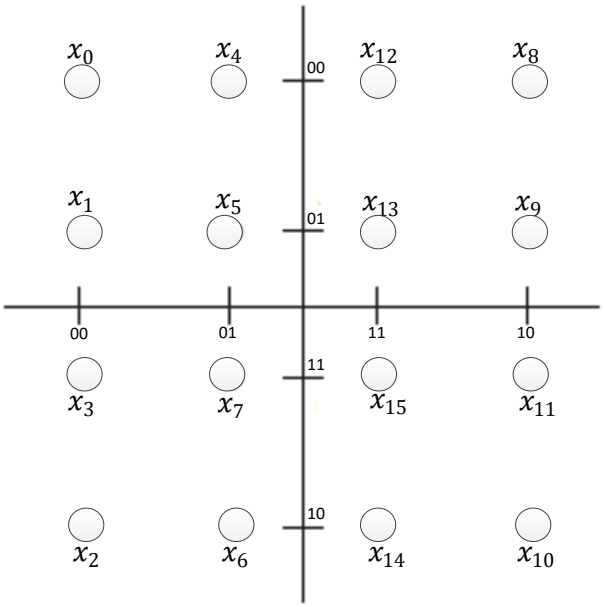

Figure C-1.1 16QAM GSM-DCR Primary Signal Constellation

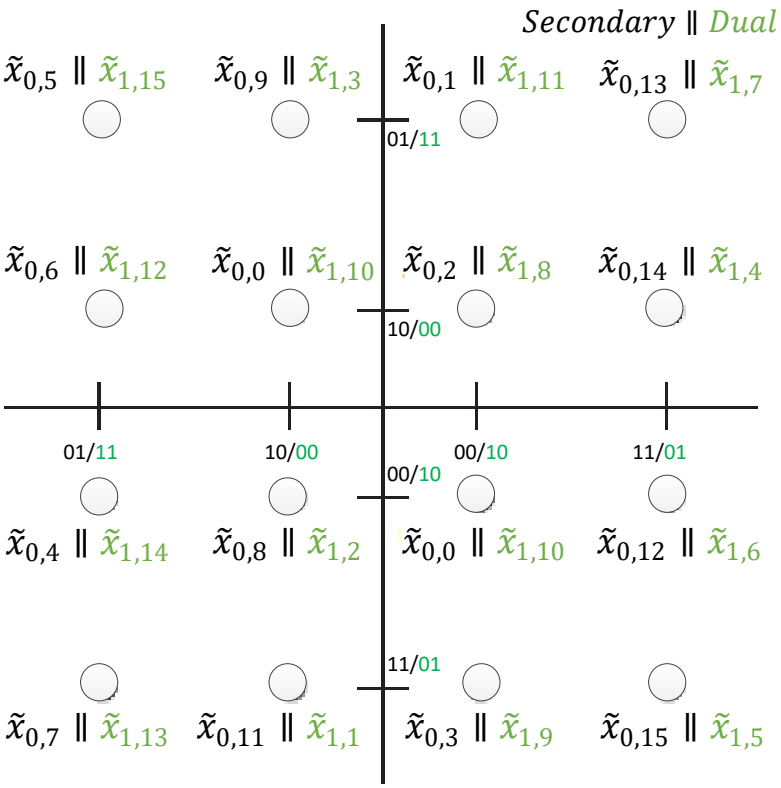

Figure C-1.2 16QAM GSM-DCR Secondary and Dual Signal Constellations

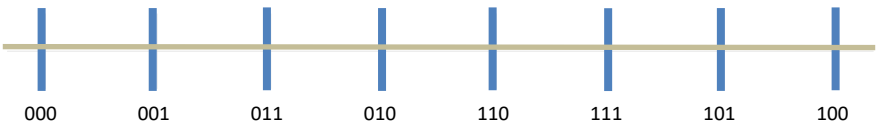

Figure C-1.3 64QAM Primary Signal Constellation (real axis)

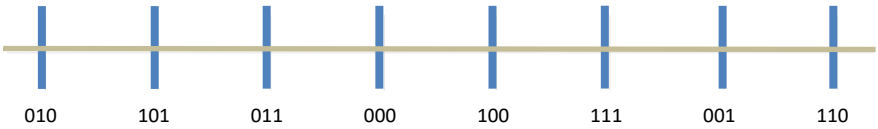

Figure C-1.4 64QAM Secondary Signal Constellation (real axis)

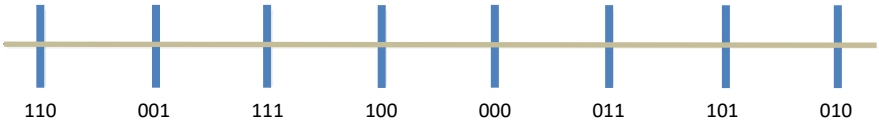

Figure C-1.5 64QAM Dual Signal Constellation (real axis)

Figures C-1.3, C-1.4 and C-1.5 show the primary, secondary and dual signal constellations for 64QAM, respectively. The constellation assignment is shown only along one real axis and the same reassignment is performed along the other complex axis.

Appendix C-2

Table C-2.1 $3 \times N_r$ 16QAM GSM-DCR Mapping Table

Input Bits	k	Spatial Symbol: Transmit Antenna Pair	v	Constellation Pair: (P,S) – Primary, Secondary (P,D) – Primary, Dual	Symbol Pair: q	x_q	$\tilde{x}_q$
0 0 0 0 0 0	1	(1,2)	0	(P,S)	0	-3+3j	1-j
0 0 0 0 0 1	1	(1,2)	0	(P,S)	1	-3+j	1+3j
0 0 0 0 1 0	1	(1,2)	0	(P,S)	2	-3-3j	1+j
0 0 0 0 1 1	1	(1,2)	0	(P,S)	3	-3-j	1-3j
0 0 0 1 0 0	1	(1,2)	0	(P,S)	4	-1+3j	-3-j
0 0 0 1 0 1	1	(1,2)	0	(P,S)	5	-1+j	-3+3j
0 0 0 1 1 0	1	(1,2)	0	(P,S)	6	-1-3j	-3+j
0 0 0 1 1 1	1	(1,2)	0	(P,S)	7	-1-j	-3-3j
0 0 1 0 0 0	1	(1,2)	0	(P,S)	8	3+3j	-1-j
0 0 1 0 0 1	1	(1,2)	0	(P,S)	9	3+j	-1+3j
0 0 1 0 1 0	1	(1,2)	0	(P,S)	10	3-3j	-1+j
0 0 1 0 1 1	1	(1,2)	0	(P,S)	11	3-j	-1-3j
0 0 1 1 0 0	1	(1,2)	0	(P,S)	12	1+3j	3-j
0 0 1 1 0 1	1	(1,2)	0	(P,S)	13	1+j	3+3j
0 0 1 1 1 0	1	(1,2)	0	(P,S)	14	1-3j	3+j
0 0 1 1 1 1	1	(1,2)	0	(P,S)	15	1-j	3-3j
0 1 0 0 0 0	1	(1,2)	1	(P,D)	0	-3+3j	-1+j
0 1 0 0 0 1	1	(1,2)	1	(P,D)	1	-3+j	-1-3j
0 1 0 0 1 0	1	(1,2)	1	(P,D)	2	-3-3j	-1-j
0 1 0 0 1 1	1	(1,2)	1	(P,D)	3	-3-j	-1+3j
0 1 0 1 0 0	1	(1,2)	1	(P,D)	4	-1+3j	3+1j
0 1 0 1 0 1	1	(1,2)	1	(P,D)	5	-1+j	3-3j

0	1	0	1	1	0	1	(1,2)	1	(P,D)	6	-1-3j	3-j
0	1	0	1	1	1	1	(1,2)	1	(P,D)	7	-1-j	3+3j
0	1	1	0	0	0	1	(1,2)	1	(P,D)	8	3+3j	1+j
0	1	1	0	0	1	1	(1,2)	1	(P,D)	9	3+j	1-3j
0	1	1	0	1	0	1	(1,2)	1	(P,D)	10	3-3j	1-j
0	1	1	0	1	1	1	(1,2)	1	(P,D)	11	3-j	1+3j
0	1	1	1	0	0	1	(1,2)	1	(P,D)	12	1+3j	-3+j
0	1	1	1	0	1	1	(1,2)	1	(P,D)	13	1+j	-3-3j
0	1	1	1	1	0	1	(1,2)	1	(P,D)	14	1-3j	-3-j
0	1	1	1	1	1	1	(1,2)	1	(P,D)	15	1-j	-3+3j
1	0	0	0	0	0	2	(1,3)	0	(P,S)	0	-3+3j	1-j
1	0	0	0	0	1	2	(1,3)	0	(P,S)	1	-3+j	1+3j
1	0	0	0	1	0	2	(1,3)	0	(P,S)	2	-3-3j	1+j
1	0	0	0	1	1	2	(1,3)	0	(P,S)	3	-3-j	1-3j
1	0	0	1	0	0	2	(1,3)	0	(P,S)	4	-1+3j	-3-j
1	0	0	1	0	1	2	(1,3)	0	(P,S)	5	-1+j	-3+3j
1	0	0	1	1	0	2	(1,3)	0	(P,S)	6	-1-3j	-3+j
1	0	0	1	1	1	2	(1,3)	0	(P,S)	7	-1-j	-3-3j
1	0	1	0	0	0	2	(1,3)	0	(P,S)	8	3+3j	-1-j
1	0	1	0	0	1	2	(1,3)	0	(P,S)	9	3+j	-1+3j
1	0	1	0	1	0	2	(1,3)	0	(P,S)	10	3-3j	-1+j
1	0	1	0	1	1	2	(1,3)	0	(P,S)	11	3-j	-1-3j
1	0	1	1	0	0	2	(1,3)	0	(P,S)	12	1+3j	3-j
1	0	1	1	0	1	2	(1,3)	0	(P,S)	13	1+j	3+3j
1	0	1	1	1	0	2	(1,3)	0	(P,S)	14	1-3j	3+j
1	0	1	1	1	1	2	(1,3)	0	(P,S)	15	1-j	3-3j
1	1	0	0	0	0	2	(1,3)	1	(P,D)	0	-3+3j	-1+j
1	1	0	0	0	1	2	(1,3)	1	(P,D)	1	-3+j	-1-3j
1	1	0	0	1	0	2	(1,3)	1	(P,D)	2	-3-3j	-1-j
1	1	0	0	1	1	2	(1,3)	1	(P,D)	3	-3-j	-1+3j
1	1	0	1	0	0	2	(1,3)	1	(P,D)	4	-1+3j	3+1j

1	1	0	1	0	1	2	(1,3)	1	(P,D)	5	-1+j	3-3j
1	1	0	1	1	0	2	(1,3)	1	(P,D)	6	-1-3j	3-j
1	1	0	1	1	1	2	(1,3)	1	(P,D)	7	-1-j	3+3j
1	1	1	0	0	0	2	(1,3)	1	(P,D)	8	3+3j	1+j
1	1	1	0	0	1	2	(1,3)	1	(P,D)	9	3+j	1-3j
1	1	1	0	1	0	2	(1,3)	1	(P,D)	10	3-3j	1-j
1	1	1	0	1	1	2	(1,3)	1	(P,D)	11	3-j	1+3j
1	1	1	1	0	0	2	(1,3)	1	(P,D)	12	1+3j	-3+j
1	1	1	1	0	1	2	(1,3)	1	(P,D)	13	1+j	-3-3j
1	1	1	1	1	0	2	(1,3)	1	(P,D)	14	1-3j	-3-j
1	1	1	1	1	1	2	(1,3)	1	(P,D)	15	1-j	-3+3j

Appendix C-3

Table C-3.1 GSM-DCR Transmit Antenna Pair Groupings and Rotation Angles for Various Configurations

		Rotation angles applicable to primary and secondary or primary and dual signal constellation pairs	
Antenna Configuration	**Transmit Antenna Pair**	16QAM	64QAM
$4 \times N_r$	(1,3)	0	0
	(1,4)	$\pi/4$	$\pi/4$
	(2,3)	$\pi/4$	$\pi/4$
	(2,4)	0	0
$6 \times N_r$	(1,2)	0	0
	(3,4)	0	0
	(5,6)	0	0
	(2,3)	$\pi/3$	$\pi/6$
	(4,5)	$\pi/3$	$\pi/6$
	(1,6)	$\pi/3$	$\pi/6$
	(1,3)	$2\pi/3$	$\pi/3$
	(2,4)	$2\pi/3$	$\pi/3$

References

[1] E. Telatar, "Capacity of multi-antenna Gaussian channels," *Eur. Trans. Telecommun.*, vol. 10, no. 6, pp. 558–595, Nov. 1999.

[2] J. Mietzner, R. Schober, L. Lampe, *et al.*, "Multiple-antenna techniques for wireless communications—A comprehensive literature survey," *IEEE Commun. Surveys Tuts.*, vol. 11, no. 2, pp. 87–105, Jun. 2009.

[3] G. J. Foschini and M. J. Gans, "On limits of wireless communications in a fading environment when using multiple antennas," *Wireless Pers. Commun.*, vol. 6, no. 3, pp. 311–335, Mar. 1998.

[4] V. Tarokh, N. Seshadri, and A. R. Calderbank, "Space–time codes for high data rate wireless communication: Performance criterion and code construction," *IEEE Trans. Inf. Theory*, vol. 44, no. 2, pp. 744–765, Mar. 1998.

[5] Q. Li, G. Li, W. Lee, *et al.*, "MIMO techniques in WiMAX and LTE: A feature overview," *IEEE Commun. Mag.*, vol. 48, no. 5, pp. 86–92, May 2010.

[6] F. Boccardi, B. Clerckx, A. Ghosh, *et al.*, "Multiple-antenna techniques in LTE-advanced," *IEEE Commun. Mag.*, vol. 50, no. 3, pp. 114–121, Mar. 2012.

[7] R. Mesleh, H. Haas, S. Sinanovic, *et al.*, "Spatial modulation," *IEEE Trans. Veh. Technol.*, vol. 57, no. 4, pp. 2228-2241, Jul. 2008.

[8] J. Jeganathan, A. Ghrayeb and L. Szczecinski, "Spatial modulation: Optimal detection and performance analysis," *IEEE Commun. Lett.*, vol. 12, no. 8, pp. 545-547, Aug. 2008.

[9] M. D. Renzo, H. Haas and P. M. Grant, "Spatial modulation for multiple antenna wireless systems: a survey," *IEEE Commun. Mag.*, vol. 49, no. 12, pp. 182-191, Dec. 2011.

[10] A. Younis, N. Serafimovski, R. Mesleh, *et al.*, "Generalised spatial modulation," *Proc. 2010 Signals, Syst. Comput.*, pp. 1498–1502, Nov. 2010.

[11] N. R Naidoo, H. Xu and N. Pillay, "Generalised spatial modulation with constellation reassignment," [under review *IET Commun.*]

[12] K. G Seddik, A. S Ibrahim and K. J. Liu, "Trans-modulation in wireless relay networks," *IEEE Commun. Lett.*, vol. 12, no. 3, pp. 170-73, Mar. 2008.

[13] Y. Sun, J. Wang, L. He, *et al.*, "Heuristic antenna combination selection in generalised spatial modulation," *Proc. Wireless Commun. and Mobile Computing Conf*, pp. 1024 – 1029, Sep. 2016.

[14] J. Freudenberger and S. Shavguildze, "Signal constellations based on Eisenstein integers for generalised spatial modulation," *IEEE Commun. Lett,*, vol. 21, no. 3, pp. 556-559, Mar. 2017.

[15] Z. Yiğit and E. Basar, "High-rate generalised spatial modulation," *Proc. IEEE. Conf. Signal Process. and Applicat.*, pp. 117-120, May 2016.

[16] N. R Naidoo and H. Xu, "A low complexity detection scheme for generalised spatial modulation with constellation reassignment," [Prepared for submission to *IET Commun.*]

[17] J. Wang, S. Jia and J. Song, "Generalised spatial modulation with multiple active antenna and low complexity detection scheme," *IEEE Trans. on Wireless Commun.*, vol. 11, no. 4, pp.1605-1615, Apr. 2012.

[18] R. Mesleh, S. Engelken, H. Haas, *et al*, "Analytical SER calculation of spatial modulation," *Proc. IEEE Int. Symp. Spread Spectrum Technol. Appl.*, pp. 272–276, Aug. 2008.

[19] I. Al-Shahrani, "Performance of M-QAM over generalized mobile fading channels using MRC diversity," M.S thesis King Saud University, Riya, Saudi Arabia, Feb. 2007.

Part III

Conclusion and Future Work

1. Conclusion and Future Work

1.1 Conclusion

The principal contributions and outcomes presented in this thesis may be summarised as follows:

Paper A proposed a BER performance enhanced GSM scheme, termed GSM-CR. Monte Carlo simulation results demonstrated that for 9 bits/s/Hz transmissions, GSM-CR was capable of achieving gains of 5 dB and 4 dB, at a BER 10^{-5}, when compared to GSM and SM, respectively. In addition, a framework for the design of GSM-CR systems was presented. An analytical bound for the average BER of GSM-CR over i.i.d. Rayleigh flat fading was also derived, and the accuracy of bound was verified by Monte Carlo simulation results.

Paper B proposed a ZF-ML GSM-CR detection scheme, which has low computational complexity that is independent of the order of digital modulation technique employed. Complexity and performance comparisons between the ZF-ML GSM-CR detector and popular GSM and GSM-CR detection schemes revealed that for the $N_t \times 4$ 64QAM configuration: i) the ZF-ML GSM-CR detector reduced the computational complexity at the receiver by up to 60% and achieved similar BER performance in comparison to the ML GSM-CR detection scheme; ii) the ZF-ML GSM-CR detector demonstrated a two-fold benefit of reduced computational complexity at the receiver and significant gains, as compared to the ML GSM detection scheme. In particular, certain ZF-ML configurations reduced receiver complexity by up to 60% or achieved gains of up to 5 dB, at a BER of 10^{-5}, when compared to the ML GSM detector; iii) the ZF-ML GSM-CR detection scheme achieved gains of up to 5 dB, at a BER of 10^{-5}, as compared to the SV GSM detector, at the expense of increased computational complexity. In particular, for configurations that encoded more than one information bit in the spatial domain, the ZF-ML GSM-CR detector was found to increase computational complexity at the receiver by up to 235% as compared to the SV GSM detection scheme.

Paper C proposed a GSM-CR scheme with enhanced spectral efficiency, termed GSM-DCR. GSM-DCR improves the overall spectral efficiency of equivalent GSM-CR and

GSM schemes by 1 bit/s/Hz through encoding an additional information bit in the signal domain. A framework for the design of GSM-DCR systems was presented. Moreover, an analytical bound for the average BER of GSM-DCR over i.i.d. Rayleigh flat fading channels was derived and the accuracy of the bound was verified by Monte Carlo simulation results. A comparison between various GSM-DCR, GSM-CR and GSM schemes, which employed equivalent system configurations, led to the following findings: i) GSM-DCR improved spectral efficiency by 1 bits/s/Hz as compared to GSM-CR. This spectral efficiency improvement was traded-off by the reduced performance of GSM-DCR in relation to GSM-CR. In particular, for the 6×4 64QAM configuration, GSM-DCR exhibited reduced performance of 2 dB, at a BER of 10^{-5}, as compared to GSM-CR; ii) GSM-DCR offered a two-fold benefit of increased spectral efficiency of 1 bit/s/Hz and significant gains when compared to GSM. In particular, for the 6×4 64QAM configuration, GSM-DCR achieved gains of 2.5 dB, at a BER of 10^{-5}, as compared to GSM.

1.2 Future Work

Future research initiatives are envisaged in the following areas:

i. Further investigate the performance of GSM-CR and GSM-DCR under generalised correlated and uncorrelated fading channel conditions.
ii. Extension of the GSM-CR and GSM-DCR schemes in order to incorporate MPSK and star QAM signal constellations.
iii. Explore the application of GSM-CR or GSM-DCR in conjunction with hierarchical QAM with a view of effectively and efficiently serving multimedia-type applications.
iv. Derive closed form average BER expressions for GSM-CR and GSM-DCR as opposed to the current analytical framework which utilises bounds.